

DUDLEY KNOX LIBRARY
NAVAL POSTGRADUATE SCHOOL
MONTEREY, CALIF.

NPG - 203

REPORT DOCUMENTATION PAGE		READ INSTRUCTIONS BEFORE COMPLETING FORM
1. REPORT NUMBER	2. GOVT ACCESSION NO.	3. RECIPIENT'S CATALOG NUMBER
4. TITLE (and Subtitle) A Comparison of Acoustic and Visual Determination of Cavitation Inception on a Model Propeller		5. TYPE OF REPORT & PERIOD COVERED THESIS
7. AUTHOR(s) PRESTERO, MARK G.		6. PERFORMING ORG. REPORT NUMBER
9. PERFORMING ORGANIZATION NAME AND ADDRESS Massachusetts Institute of Technology Cambridge, MA		8. CONTRACT OR GRANT NUMBER(s)
11. CONTROLLING OFFICE NAME AND ADDRESS CODE 031 NAVAL POSTGRADUATE SCHOOL MONTEREY, CALIFORNIA 93940		10. PROGRAM ELEMENT, PROJECT, TASK AREA & WORK UNIT NUMBERS
14. MONITORING AGENCY NAME & ADDRESS (if different from Controlling Office)		12. REPORT DATE June 1979
		13. NUMBER OF PAGES 221
		15. SECURITY CLASS. (of this report) UNCLAS
		16. DECLASSIFICATION/DOWNGRADING SCHEDULE
16. DISTRIBUTION STATEMENT (of this Report) APPROVED FOR PUBLIC RELEASE; DISTRIBUTION UNLIMITED		
17. DISTRIBUTION STATEMENT (of the abstract entered in Block 20, if different from Report)		
18. SUPPLEMENTARY NOTES		
19. KEY WORDS (Continue on reverse side if necessary and identify by block number) Naval Engineering Acoustic Detection Cavitation Noise Demodulated Analysis		
20. ABSTRACT (Continue on reverse side if necessary and identify by block number) SEE REVERSE		

ABSTRACT

Although acoustic detection of cavitation inception has been shown to agree relatively well with visual detection, acoustic methods have generally not been used to detect cavitation inception during cavitation testing of model propellers. In addition, it has been suggested that noise measurements on model propellers be made at high frequencies to more properly represent the full scale noise. In this thesis, three different methods of acoustic detection were investigated. Two of these methods, the measurement of high frequency one-third octave band levels and the analysis of the complete noise spectrum between 10 and 50 kHz, met with some success, but were not equivalent to the capability of a visual detection method. The third method used, the demodulated analysis of high frequency cavitation noise, gave excellent agreement with visually determined results.

Approved for public release;
distribution unlimited.

A COMPARISON OF
ACOUSTIC AND VISUAL DETERMINATION OF CAVITATION INCEPTION
ON A MODEL PROPELLER

by

LCDR Mark G. Prestero, USN
B.S., College of the Holy Cross
(1967)

SUBMITTED IN PARTIAL FULFILLMENT
OF THE REQUIREMENTS FOR THE
DEGREE OF

OCEAN ENGINEER

and for the degree of

MASTER OF SCIENCE IN NAVAL ARCHITECTURE
AND MARINE ENGINEERING

at the

MASSACHUSETTS INSTITUTE OF TECHNOLOGY
June 1979

© 1979 Mark G. Prestero

A COMPARISON OF
ACOUSTIC AND VISUAL DETERMINATION OF CAVITATION INCEPTION
ON A MODEL PROPELLER

by

MARK G. PRESTERO

Submitted to the Department of Ocean Engineering on 11 May 1978, in partial fulfillment of the requirements for the degrees of Ocean Engineer and Master of Science in Naval Architecture and Marine Engineering.

ABSTRACT

Although acoustic detection of cavitation inception has been shown to agree relatively well with visual detection, acoustic methods have generally not been used to detect cavitation inception during cavitation testing of model propellers. In addition, it has been suggested that noise measurements on model propellers be made at high frequencies to more properly represent the full scale noise. In this thesis, three different methods of acoustic detection were investigated. Two of these methods, the measurement of high frequency one-third octave band levels and the analysis of the complete noise spectrum between 10 and 50 kHz, met with some success, but were not equivalent to the capability of a visual detection method. The third method used, the demodulated analysis of high frequency cavitation noise, gave excellent agreement with visually determined results.

Thesis Supervisor: Professor J.E. Kerwin

Title: Professor of Naval Architecture

ACKNOWLEDGEMENTS

There is a large number of people to whom I am indebted for their assistance to me on this project. It is difficult to thank them enough. Included in this group are; CDR D.V. Burke, USN, whose project for me at NAVSEC last summer got me interested in the subject, and who subsequently helped to open many doors to me in learning about it; Dick Cumming at DTNSRDC, who kindly provided the propeller used in the experiment; Ken Remmers of DTNSRDC, who provided much of the background on the cavitation test procedure; Shirley Childers of DTNSRDC, who was always available as a point of contact and as a source of hard to find reference material; Neal Brown of Bolt, Beranek and Newman, whose enthusiasm for the experiment and continuing support enabled the most successful part of the experiment to be performed; Professors J.E. Kerwin and P. Leehey, whose knowledge and expertise with propeller testing and acoustics helped me to fill some rather glaring holes in my background, and whose words of encouragement came when they were needed the most; Dean Lewis and Sukeyuki Kobayashi, whose patience with me during the testing of the wake screen and propeller and guidance for where and how to get things done at MIT were an incredible benefit; Dave Greeley, whose knowledge of the problem I was investigating and of the equipment necessary to investigate it properly, and whose many hours of unselfish assistance, made the technical aspects of all of this experiment come together. Without the

help of this group, I would not have been able to perform this experiment. But there is one last group, my wife Linda, and Christopher, Timothy and Katherine, without whose continuing support, understanding and personal sacrifices, neither this experiment, nor any part of this education would have been successful.

TABLE OF CONTENTS

TITLE PAGE1

ABSTRACT2

ACKNOWLEDGEMENTS3

TABLE OF CONTENTS5

LIST OF FIGURES6

LIST OF TABLES7

I. INTRODUCTION8

II. BACKGROUND11

III. EXPERIMENTAL PROCEDURE16

 A. Equipment Setup16

 B. Calibration28

 C. Test Procedure29

IV. DATA REDUCTION32

V. RESULTS AND DISCUSSION43

VI. CONCLUSIONS55

VII. REFERENCES56

APPENDIX A - DETAILS OF THE WAKE SCREEN DESIGN57

APPENDIX B - RAW DATA66

 B.1 Wake Survey Data69

 B.2 One-third Octave Analysis77

 B.3 Demodulated Analysis, 20 kHz high pass105

 B.4 Demodulated Analysis, 50-63 kHz band150

 B.5 Full Spectrum, Hydrophone and Accelerometer193

 B.6 Demodulated Spectra, sensor comparison197

 B.7 $J=0.51$, Sequence of spectra for decreasing σ ...209

LIST OF FIGURES

<u>Figure Number</u>	<u>Title</u>	
1	Shaft Adapter Fittings	17
2A	Wake Screen Photograph	19
2B	Wkae Screen Photograph	19
3	Wake Profile - Looking Upstream	20
4	Wake Fraction versus Non-dimensional Radius	22
5	Hydrophone Mounting	25
6	Arrangement of Tunnel Test Section	26
7	Electronics Setup	27
8	One-third Octave Levels vs. Cavitation Index	36
9	Complete Spectrum - Non-cavitating	37
10	Complete Spectrum - Visual Inception	38
11	Complete Spectrum - Acoustic Inception	39
12	Typical Demodulated Spectrum, J = 0.395	41
13	Typical Demodulated Spectrum, J = 0.46	42
14	σ_i vs. J, Visual Determination, Unmodified	44
15	σ_i vs. J, One-third Octave Band Levels	45
16	σ_i vs. J, Visual Determination, Modified Screen ..	46
17	σ_i vs. J, Demodulated Analysis, 20 kHz High Pass ..	47
18	σ_i vs. J, Demodulated Analysis, 50-63 kHz Band ..	48
19	Demodulated Spectrum, J = 0.62, Hydrophone	50
20	Demodulated Spectrum, J = 0.62, Accelerometer.....	51
A-1	Wake Survey - Initial Wake Screen	64
A-2	Wake Survey - Final Wake Screen	64

LIST OF TABLES

<u>Table Number</u>	<u>Title</u>
1	Accelerometer Characteristics23
2	Hydrophone Characteristics24
A-1	Wake Characteristics60
A-2	Screen Characteristics62
A-3	Installed vs. Measured K Values62
A-4	Final Screen Resistance Coefficients65
B-1	Wake Survey Data - Initial Wake Screen69
B-2	Wake Survey Data - Final Wake Screen (Unmodified)71
B-3	Wake Survey Data - Final Wake Screen (Modified) 73

I. INTRODUCTION

Since the first observation of cavitation associated with marine propellers was reported by Reynolds in 1873, a number of unwanted effects, including loss of propeller efficiency, erosion of propeller surfaces, excitation of hull vibrations, and generation of noise, have been identified and studied. Because of these detrimental effects, it has been, and continues to be, desirable to predict the cavitation performance of a propeller design before the expensive full scale propeller is built. With no exact analytical approach available for predicting the full scale cavitation performance of a propeller, the testing of scale models has been used to aid in cavitation prediction in the propeller design process.

For the model test to properly represent the full scale, it is necessary for similarity conditions be satisfied. For propeller cavitation testing, this amounts to using a geometrically similar propeller operating in a flow which matches the wake where the full scale propeller operates. With these conditions met, it is assumed that cavitation performance for similar values of cavitation index,

$$\sigma = \frac{p - p_v}{\frac{1}{2}\rho U_\infty^2}$$

and advance coefficient,

$$J = \frac{V_a}{nD}$$

will be the same for the model and full scale propeller. But this assumption is not precisely correct, and scale effects, which arise from the inability to satisfy all hydrodynamic, thermodynamic and other microscopic similarity requirements, are encountered. These scale effects are usually eliminated by means of empirically or theoretically determined corrections.

In general, the procedure for conducting a model test for determining cavitation inception performance is to operate the model propeller in a variable pressure water tunnel, downstream of a device which produces the desired wake at the plane of the propeller. A water and propeller speed combination are chosen to give the desired value of advance coefficient. Water pressure is changed to change the cavitation index until cavitation is visually observed to either begin or to cease, depending upon the criterion used at the particular test facility. This process is then repeated for several different values of advance coefficient. The final result is a curve of inception cavitation index, σ_i , versus advance coefficient.

Although visual observation is the usual method for determining the presence or absence of cavitation, it is not the only available means. It is possible to use the detection of cavitation-generated noise to determine, or to assist visually determining, the inception of cavitation. Good correlation between acoustic and visual inception determination has been reported (Lehman, 1964). It has also been reported

that "numerous" facilities use an acoustic technique for this purpose (ITTC, 1978), but the details of these methods were not available. It is proposed for this investigation to consider several different schemes for detecting cavitation-generated noise as a method for inception determination, and to compare acoustically-determined inception data with visual observations of inception for a model propeller.

II. BACKGROUND

The sound generated by cavitation comes primarily from the growth and collapse of the cavitation bubbles. The theoretical energy spectrum for the sound generated by a single bubble has been shown to contain maxima at frequencies which correspond to the reciprocal of the time required for the growth and collapse of the bubble (Fitzpatrick and Strasberg, 1959). Experimental investigations into the spectrum of cavitation noise have found that the shape of the measured spectrum resembles the theoretical spectrum quite closely (Ross, 1976; Strasberg, 1977).

Strasberg also notes that the peak of the observed spectra move toward lower frequencies as the cavitation becomes more severe. The larger maximum size of the bubbles in the more developed cavitation corresponds to the observed peak at a lower frequency. Ross points out that the energy radiated per collapse is proportional to the product of the collapse pressure and the maximum bubble volume. So, when cavitation becomes more severe, and a larger number of bubbles, which also have a greater diameter, are produced, the amount of sound energy radiated becomes greater, the magnitude of the peak in the spectrum increases, and the frequency of the peak becomes lower. If the various spectra are non-dimensionalized in the manner of Fitzpatrick and Strasberg, the spectra for different degrees of cavitation intensity all agree well with the non-dimensionalized theoretical spectrum (Strasberg, 1977).

Continuing on with the scheme given by Strasberg, if the propeller diameter is used for the non-dimensionalizing length scale instead of the maximum bubble radius, a similarity condition for relating frequencies of interest between a model and a full scale propeller is obtained. For a given ratio of maximum bubble radius to propeller diameter (which can be interpreted as a measure of relative cavitation intensity), the non-dimensional frequency of the peak in the cavitation noise spectrum will remain invariant between different length scales. It should then be possible to compare cavitation noise measurements made at a given actual frequency on a full scale propeller with measurements made at the same non-dimensional frequency on a model propeller, so long as other similarity requirements are satisfied. For example, with the submarine propeller cavitation noise measurements used by Strasberg (1977), assuming that the full scale measurements were made at a submergence depth of 200 feet, the model measurements were made at an ambient pressure of 1 atmosphere, the same fluid was used in each case, and the length scale ratio was 8, the ratio between the frequency of interest with the model (f_M) to the frequency of interest with the full scale propeller (f_P) is:

$$\frac{f_M}{f_P} = \frac{D_P}{D_M} \cdot \left(\frac{P_M}{P_P} \right)^{\frac{1}{2}}$$
$$= 8 \cdot (34 \div 234)^{\frac{1}{2}} = 3.05$$

So, for cavitation noise measurements, the frequency of interest in model scale is about three times the full scale frequency for equivalent severity of cavitation in the two cases.

There are several considerations about the model cavitation noise which this concern with frequency alone does not show:

1) The size of the cavitation bubbles for the model will be one eighth the actual size of the full scale bubbles and might, consequently, be too small to see

2) At the same distance from the propeller as in model measurements (assuming the distances are large enough to avoid near field effects) the sound pressures, \tilde{p} , would have the ratio of

$$\begin{aligned} \frac{\tilde{p}_M}{\tilde{p}_P} &= \frac{P_M}{P_P} \times \frac{D_M}{D_P} \\ &= \frac{34}{234} \times \frac{1}{8} = 1.8 \times 10^{-2} \end{aligned}$$

or approximately 35 db lower for the model, if the non-dimensionalization of Strasberg (1977) is used with the same bandwidth, distance and non-dimensional frequency.

3) The actual cavitation does not, in general, occur uniformly for all angular positions for all blades.

Operation of the propeller in a non-uniform wake causes variations of inflow velocity seen by the propeller which are periodic, with a frequency that corresponds to once per revolution. This periodic flow variation causes the inception,

growth, decrease, and disappearance of cavitation to occur in a periodic fashion on a given blade. For a given average level of cavitation intensity, the amplitude of the cavitation noise will vary over one propeller revolution. This change in amplitude will have two effects - it will shift the peak frequency of the noise spectrum over the time span of one revolution of the propeller, and it will vary the amplitude of the noise spectrum.

If all blades of the propeller are the same, the amplitude modulation of the noise occurs at blade passing rate - once for each blade for each revolution of the shaft. Since the blades are generally not identical, one blade will usually begin to cavitate ahead of the others, and the modulation of the noise will occur, in addition, at the shaft rate (Strasberg, 1946; Ross, 1976).

It is intended, then, to investigate the use of these two aspects of cavitation noise, frequency scaling and amplitude modulation, either independently or together, as a means of detecting cavitation inception on a model propeller. It is expected that this approach would have certain advantages as a part of the process for predicting full scale cavitation performance:

- (1) Visual determination of inception is very dependent upon a number of conditions outside the test tunnel for repeatable results. Lighting conditions, as well as the location and visual acuity of the observer, can have a

substantial effect upon the outcome of a test. With an appropriate criteria for determining cavitation inception from acoustically obtained data, this sort of variation could be eliminated.

(2) For many ships, cavitation inception determination for the full scale propeller is accomplished using acoustic information. An acoustic method on model scale would more closely approximate the full scale test.

(3) Based upon bubble size considerations, an acoustic method might be able to detect the presence of cavitation bubbles before they are visible.

But there are disadvantages associated with using acoustic information for this purpose:

(1) The equipment to make the acoustic measurements is substantially more expensive than that needed for the visual determination of inception. For a very large length scale ratio, the frequency of interest at the model scale might become so high that the normal analysis equipment for acoustic measurements would not be usable, or the level of the acoustic signal from cavitation noise might be too low to be detected.

(2) If it is used alone, an acoustic method would appear to be less useful to the designer, since the method would not directly identify the type of cavitation causing the noise. The steps necessary to improve the cavitation performance of an unsatisfactory design would be less clear.

III. EXPERIMENTAL PROCEDURE

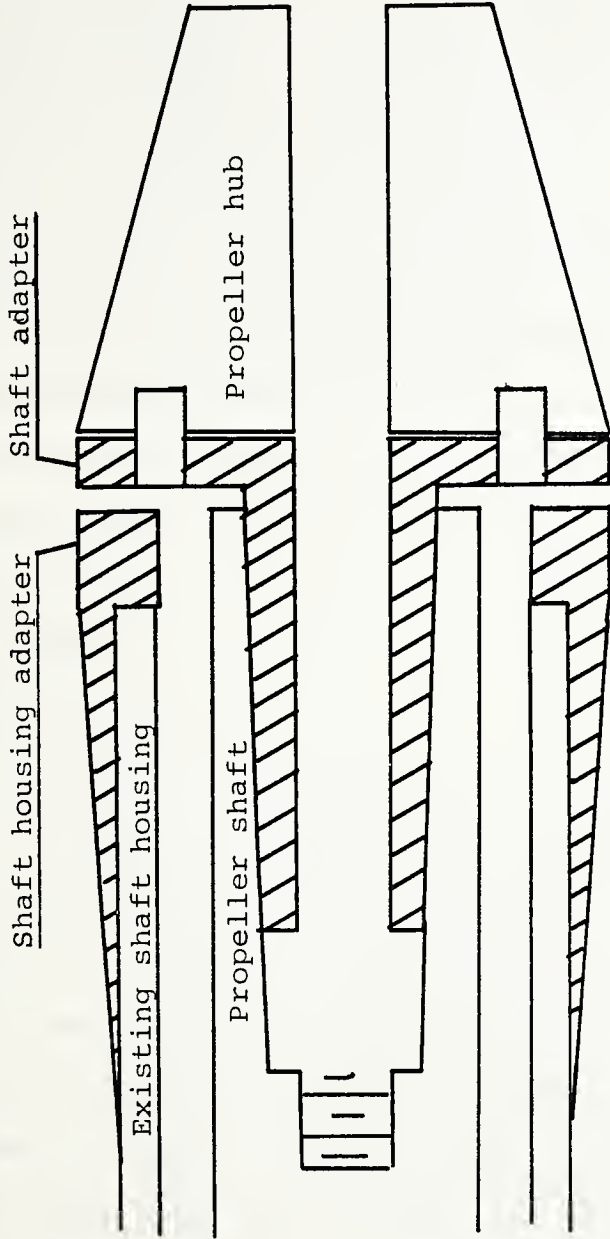
A. Equipment Setup

Experiments were conducted in the MIT Variable Pressure Water Tunnel, which has a 20 in square closed jet test section with a length of 54 in. All four walls of the test section have a 16 in by 44.5 in plexiglass viewing window insert. The propeller is located at the vertical and horizontal centerlines of the test section, and is driven by an upstream propeller shaft.

The propeller used for this test was the David Taylor Naval Ship Research and Development Center (DTNSRDC) model 3927, which had a diameter of 10.8 in and had seven blades. The tapered hub of the propeller had a maximum diameter of 2.8 in, which required the use of an adapter to provide a smooth transition between the 2.375 in diameter of the propeller shaft housing and the hub. Figure 1 shows this adapter. The propeller was installed on the shaft with no hub fairwater cap, leaving the mounting capscrew and lockwasher exposed.

Attached to the shaft housing 20 in upstream of the plane of the propeller was the holder for the screen which generated the desired wake at the propeller. The design of this screen used a scheme proposed by McCarthy (1963) as a starting point. The details of this process are given in Appendix A.

The wake prescribed for testing this propeller is

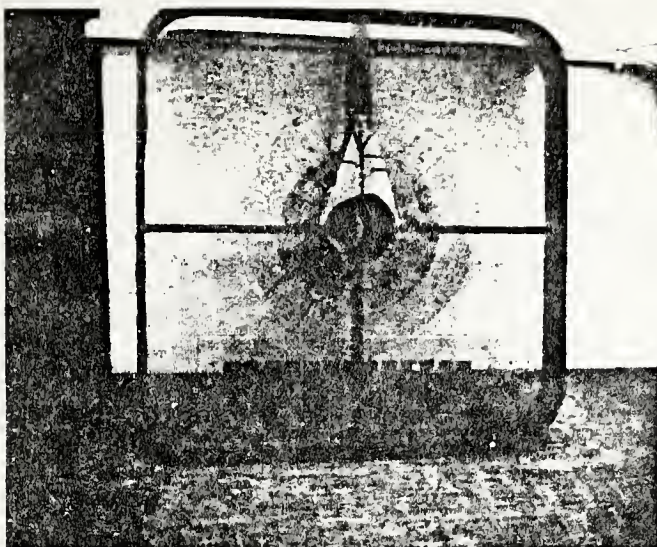


Shaft Adapter Fittings

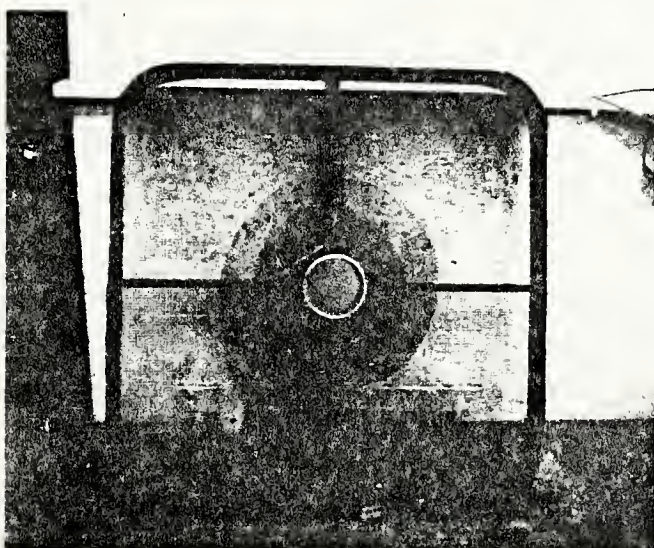
Figure 1

axisymmetric, with a specific radial distribution of longitudinal velocity. For the first variation of the wake, the velocity distribution was measured along a diameter on a diagonal, but at the radii where the values of longitudinal velocity were given. The values for the two radii were averaged and compared to the specified values. An error of less than 10-12% was considered acceptable.

During the initial testing of the propeller it was discovered that face cavitation would occur behind the supports of the wake screen holder. This indicated a velocity increase as the propeller blade entered the region downstream of the supports, and was attributed to boundary layer viscous effects as the flow passed the wake screen holder supports. At the same time it was noted that modulation of the cavitation noise for other than this face cavitation was not detectable with the equipment being used. This indicated that a severe, once per revolution, velocity defect was desirable. This defect was achieved by using screen material to make the topmost support much thicker and tapered. No effort was made to maintain the same circumferential mean wake. The final wake screen used is shown in the photographs in figures 2A and 2B. Figure 3 shows the results of the wake survey made with a 1 in square grid, in a plane 2.5 in downstream of the blade root leading edge, but with the propeller removed, after the upper support was altered. The diagonal line indicates where the initial screen velocity measurements were made, as well as the data from the final



Final Wake Screen - Looking Downstream
Figure 2A



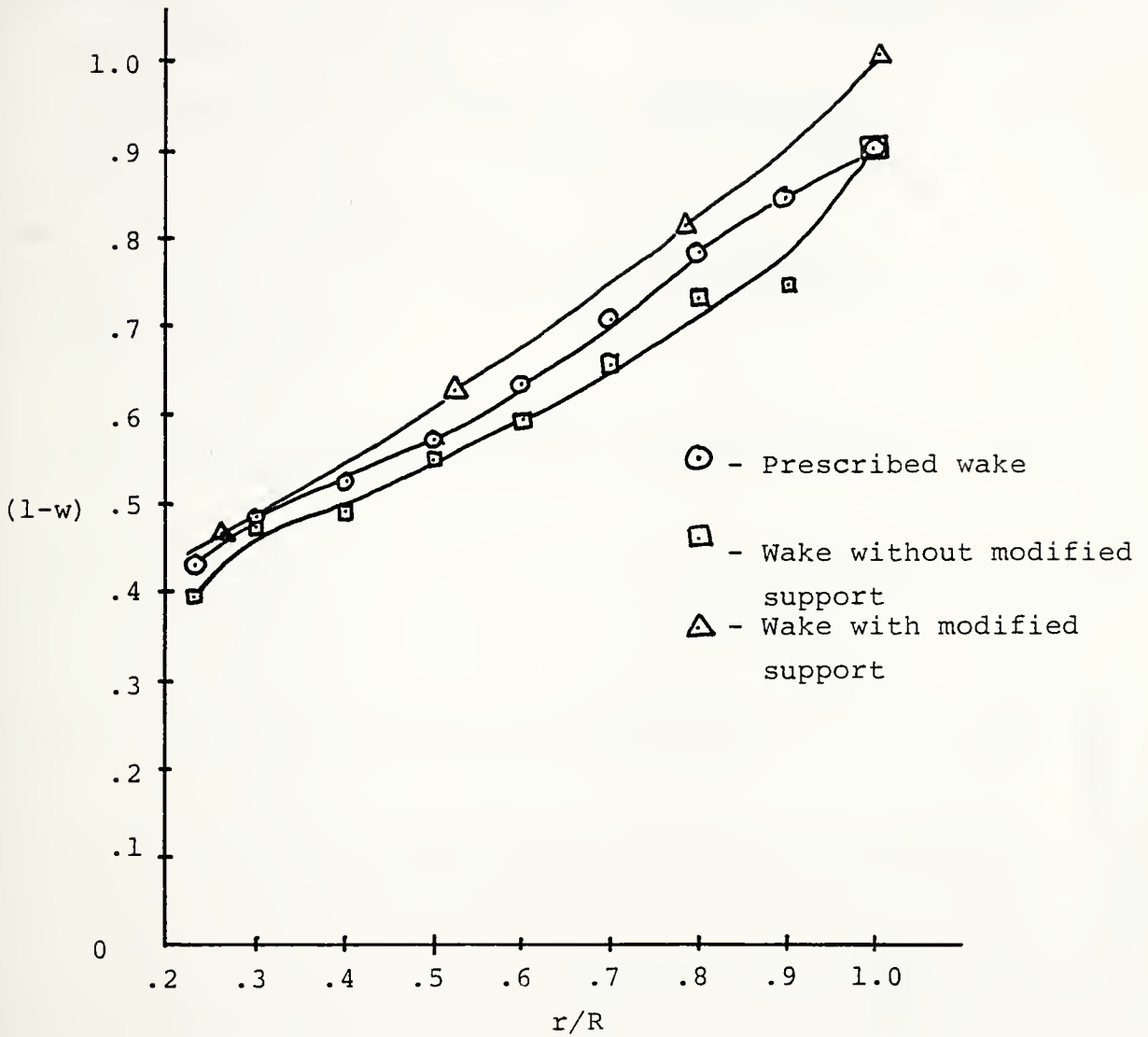
Final Wake Screen - Looking Upstream
Figure 2B

screen velocity measurements, for comparison with the prescribed wake were taken. A plot, comparing the actual and prescribed velocities is shown in figure 4.

Two sensors were used at different times to obtain the acoustic signal. The first, an accelerometer, was a Brüel & Kjaer (B&K) type 4344. The characteristics of this accelerometer are shown in table 1. The accelerometer was mounted directly to one of the viewing windows, as close to the center as possible, using a cyanoacrylate adhesive. The other sensor, a miniature hydrophone, was a B&K type 8103. The principal characteristics of this hydrophone are given in table 2. The hydrophone was mounted in the viewing window as shown in figure 5, 2.5 in downstream of the leading edges of the propeller blades. A schematic diagram of the arrangement of the test section is shown in figure 6.

The methods of processing of the signal from the sensor are shown in figures 7A and 7B. In configuration 7A, the Ithaco 4213 filter was used as a band pass filter for one-third octave bands, with the level indicated on the B&K type 2607 measuring amplifier as the output. The other configuration used a Federal Scientific Model UA-15A Ubiquitous Spectrum Analyzer coupled to a model 1015 Spectrum Averager, which, in turn, drove an X-Y plotter to provide an output.

With the spectrum analyzer providing the output, two set-ups were used. The first was to obtain the complete spectrum of the cavitation noise to 50 kHz, the upper



Wake Fraction versus Non-Dimensional Radius

Figure 4

Table 1

Accelerometer Characteristics

Type: B&K 4344

Serial Number: 475507

Reference sensitivity at 50 Hz at 23 °C and including cable capacitance of 106 pF:

Voltage sensitivity: 0.308 mV/ms⁻² or 3.02 mV/g

Charge sensitivity: 0.344 pC/ms⁻² or 3.37 pC/g

Capacitance (including cable): 1116 pF

Weight: 22 gm

Undamped natural frequency: 121 KHz

Frequency response:

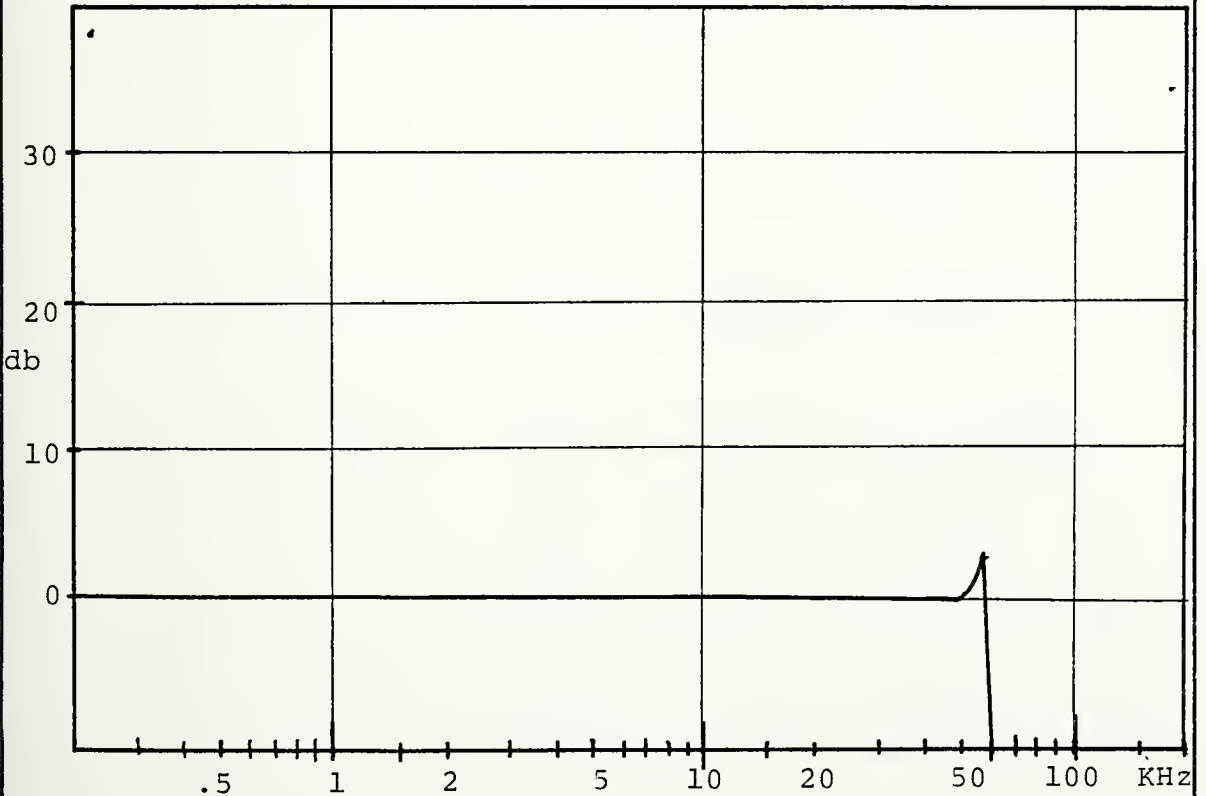


Table 2

Hydrophone Characteristics

Type: B&K 8103

Serial Number: 636764

Reference sensitivity at 250 Hz at 23 °C including 6m
integral cable:

Open circuit sensitivity:

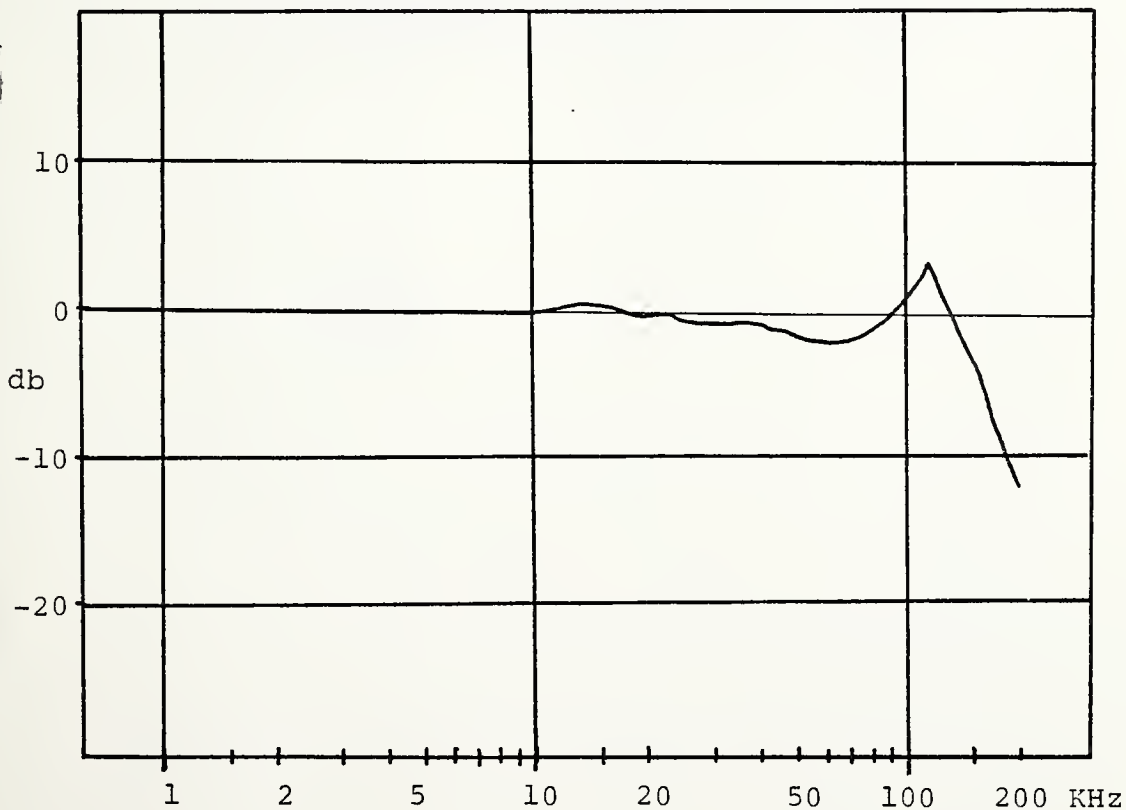
Voltage sensitivity: -211.6 db re 1V/ μ Pa
- 91.6 db re 1V/Pa or 26.3 μ V per
Pa

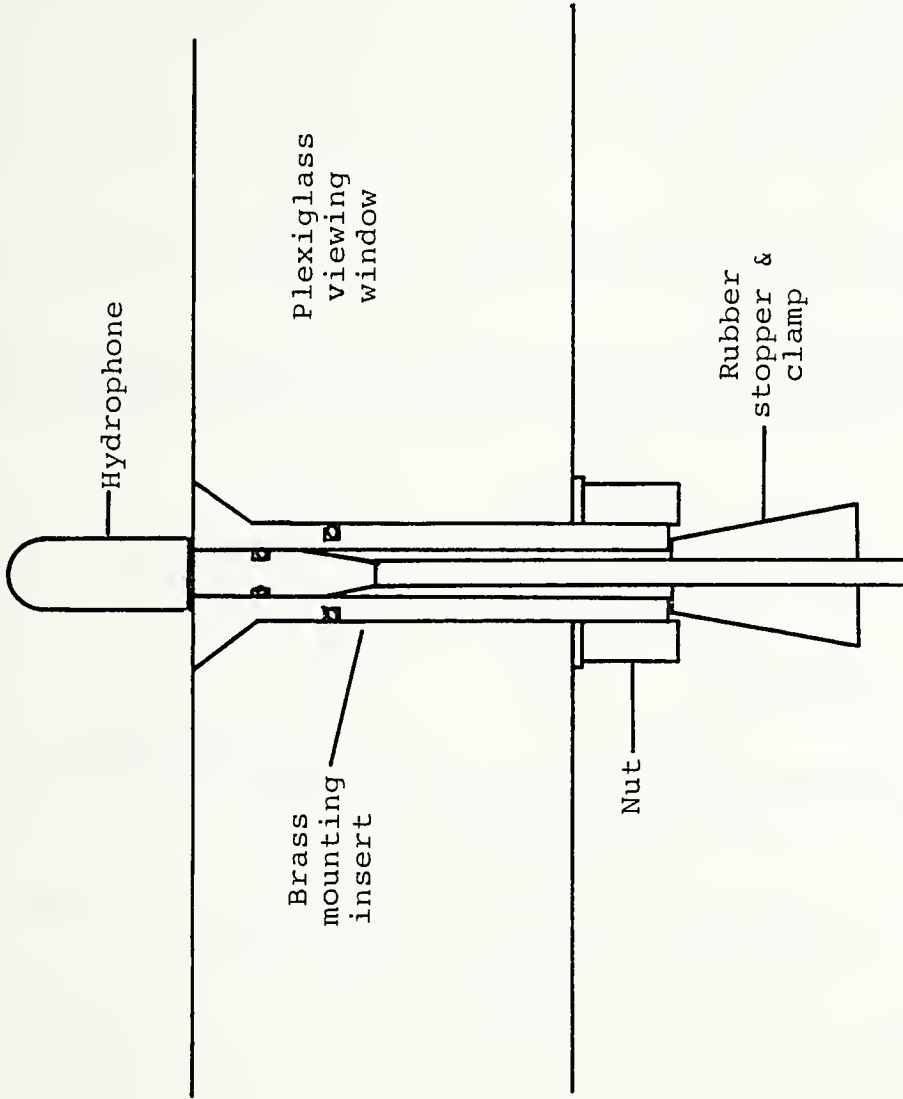
-111.6 db re 1V per μ bar

Charge sensitivity: 91.5×10^{-3} pC per Pa

Capacitance: 3480 pF

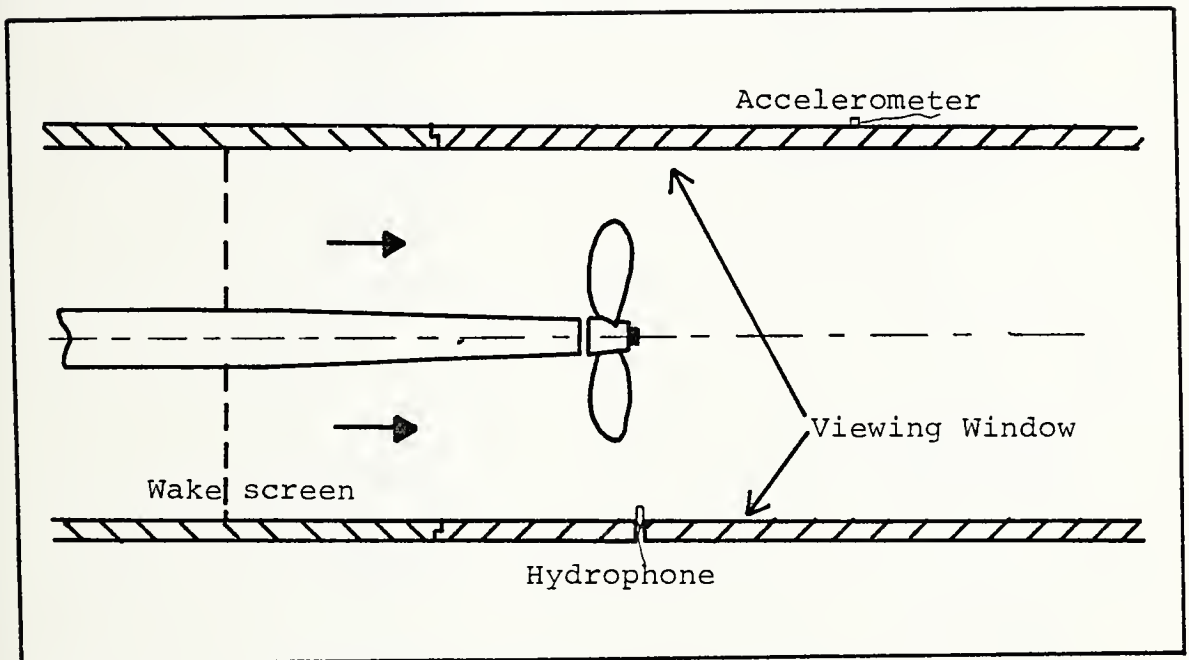
Frequency response:





Hydrophone Mounting

Figure 5



Arrangement of tunnel test section

Figure 6

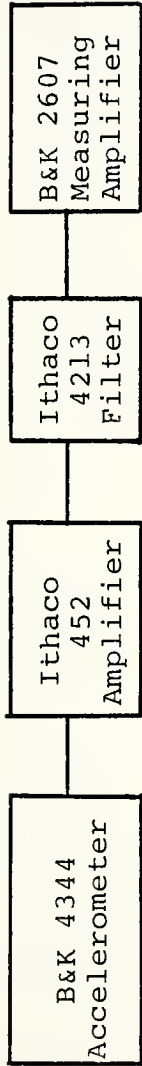


Figure 7A

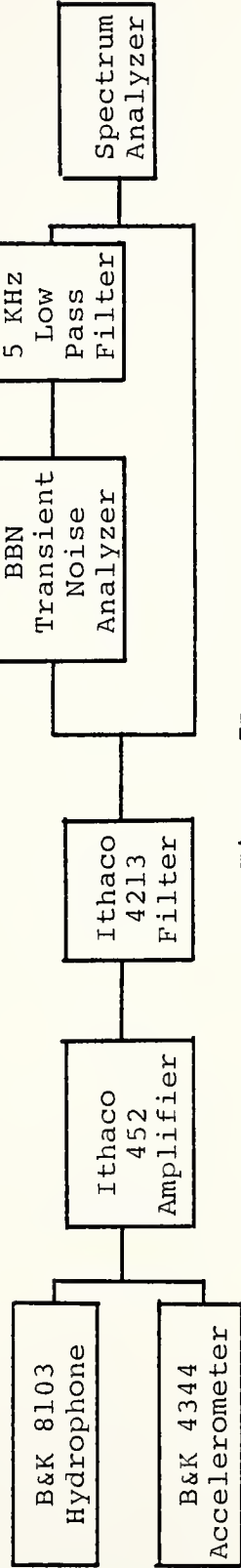


Figure 7B

frequency limit of the spectrum analyzer. In this case, the 4213 filter was used as a 10 kHz high pass filter to prevent the large amount of noise below 10 kHz, little of which was considered to be cavitation related, from overdriving the analysis equipment and preventing a good representation of the high frequency noise. For this analysis, 128 spectra were averaged to provide the output.

The second setup was intended to detect the cavitation by the presence of modulation of the high frequency noise, so that some form of demodulation was required. Demodulation of the signal was performed by passing it first through the Bolt, Beranek and Newman (BBN) Transient Signal Analyzer, which squared the signal, and then through a 5 kHz low pass filter and into the spectrum analyzer. For this setup, the 4213 filter was used either as a 20 kHz high pass filter or a 50-63 kHz band pass filter, so that only the high frequency, cavitation-related noise was being analyzed. (It was necessary to use high frequencies to obtain good results with this method of demodulation.) The spectrum analyzer was used on the 0-500 Hz range, and 32 spectra were averaged to obtain the output.

B. Calibration

It was not intended to attempt to measure the absolute levels of the cavitation noise, so a calibration of the level of the signal was not performed. In addition, a calibration of the frequency display of the spectrum analyzer was not

performed. Consequently, many of the spectra of the demodulated signal do not have peaks at the proper frequencies. But, because the peaks generally showed the proper spacing, this error in the display was not considered significant.

C. Test Procedure

The conventional test procedure of maintaining constant free stream velocity and propeller speed, and varying static pressure was used for this testing. This technique kept the frequency of interest for the demodulated analysis constant for a given test run.

Since it was not possible to determine the air content of the tunnel water, it was decided to perform the acoustic and visual cavitation inception determinations concurrently. Thus variations in air content would affect visual and acoustic results equally.

Prior to beginning data recording for a series of data points, the water was drained from the test section and the propeller was operated in air at about 1000 RPM. At this time, tare loadings for the thrust and torque load cells were recorded and the height of the manometer column was recorded as a no flow condition zero. The test section was refilled with water, an initial atmospheric pressure reading was recorded, and testing began.

For each data point, the following sequence was followed:

(1) A nominal flow speed and propeller RPM were selected to give the desired value of J , and tunnel conditions were adjusted to these values. The flow speed chosen was such that cavitation inception would occur after tunnel static pressure was reduced from atmospheric pressure, but before the pressure was so low that air coming out of solution would begin to cause absorption of the high frequency acoustic signal or to obscure the propeller from view (250-300 mm Hg).

(2) Tunnel static pressure was set to atmospheric pressure. Room air and tunnel water temperatures, and amplifier gain and filter settings were recorded, and the first set of data taken. This data included tunnel static pressure, manometer height, propeller RPM, thrust and torque readings, and the acoustic data, either the one-third octave level or the spectral analysis. A visual observation of the propeller was made using a strobe light triggered by a once per revolution signal from the propeller shaft. A variable triggering delay on the light allowed the observation of all blades at all points in the propeller rotation. The large viewing windows enabled viewing the propeller under conditions of both back and front lighting, from both up and downstream using the one strobe light.

(3) Tunnel static pressure was lowered, and another set of data recorded. This process was continued until cavitation inception had been observed both visually and acoustically.

The sequence above was then repeated at the selected

values of advance coefficient needed to produce the curve of cavitation index at inception versus advance coefficient. At the end of a day's testing, the water was drained from the test section. The propeller was operated in air, tare loadings, atmospheric pressure and no-flow manometer height were once again recorded. All raw data recorded is contained in Appendix B.

IV. DATA REDUCTION

Reduction of the data for obtaining propeller parameters was accomplished using a program written for a TI-59 programmable hand calculator. This program performed the following functions:

(1) Determined the changes in tare loadings, atmospheric pressure and no-flow manometer height between the beginning and end of a series of test runs. A linear interpolation, based upon run number of a series, was then used to determine the value of these parameters for each run.

(2) Air and water temperatures were used to determine the vapor pressure of water at the two temperatures (p_{vw} and p_{va}). The vapor pressure of water at the room air temperature was used to correct the reading of the mercury column which was used for indication of tunnel static pressure, since this reading (p) was actually static pressure minus the vapor pressure of water at room temperature. Tunnel water temperature was also used to determine its density, ρ , and kinematic viscosity, ν .

(3) Tabulated values for the conversion from manometer height to velocity for the range of values encountered in a given test were entered and stored. They were then used in a linear interpolation to determine flow speed.

(4) For each value of static pressure where data was recorded during the test, the following calculations were made:

(a) Manometer height was entered, corrected for the no-flow zero and converted to flow speed, U_{∞} , in feet per second.

(b) Static pressure reading, p , was entered. To this value the vapor pressure of water at room temperature, p_{va} , was added to give the true static pressure at the tunnel axis:

$$p_{stat} = p + p_{va}$$

(c) Propeller RPM was entered and converted to revolutions per second, n .

(d) Propeller thrust reading was entered and corrected for the tare loading. A correction for the change in thrust from the pressure differential between tunnel static pressure and atmospheric pressure acting across the 1.317 in diameter propeller shaft was then applied to give the actual thrust, T . The thrust coefficient

$$K_T = \frac{T}{\rho n^2 D^4}$$

where D is the propeller diameter, was then calculated.

(e) This value of K_t was used to determine the advance coefficient, J , from the open water test results provided for this propeller. This value was entered and stored for later use.

(f) For the first pressure increment for each test, the measured torque was then entered, where

it was corrected for the tare loading to give measured torque, Q , and a torque coefficient,

$$K_Q = \frac{Q}{\rho n^2 D^5}$$

was calculated. The open water test results were entered with this value of K_Q to verify that the J obtained in the previous step was reasonable. The value of J obtained from the thrust identity was used for the cavitation inception curve. In addition, at this step, the 0.7 radius Reynolds number,

$$R = \frac{c_{0.7} \times (V_a^2 + (0.7\pi nD)^2)^{\frac{1}{2}}}{\nu}$$

- where V_a is the average inflow velocity seen at the propeller (calculated from J) and $c_{0.7}$ was the blade chord at the 0.7 radius, was calculated.

(g) Finally, the cavitation number,

$$\sigma = \frac{p_{stat} - p_{vw}}{\frac{1}{2}\rho U_\infty^2}$$

Once the data was reduced, and a value of J and σ could be assigned to each data run, it was necessary to determine which run represented the cavitation index at inception, σ_i , for each value of J . The criteria used to define inception are as follows:

- (1) Visual observation - Hub vortex cavitation had a different criterion from all other types. For it, the

appearance of a trail of bubbles from the vicinity of the hub was used as the criterion. For other types of cavitation, the criterion was to have a steady occurrence of that type of cavitation on more than one blade. Steady occurrence meant that the cavitation was present on each revolution of the propeller at one location, but not necessarily throughout the entire revolution.

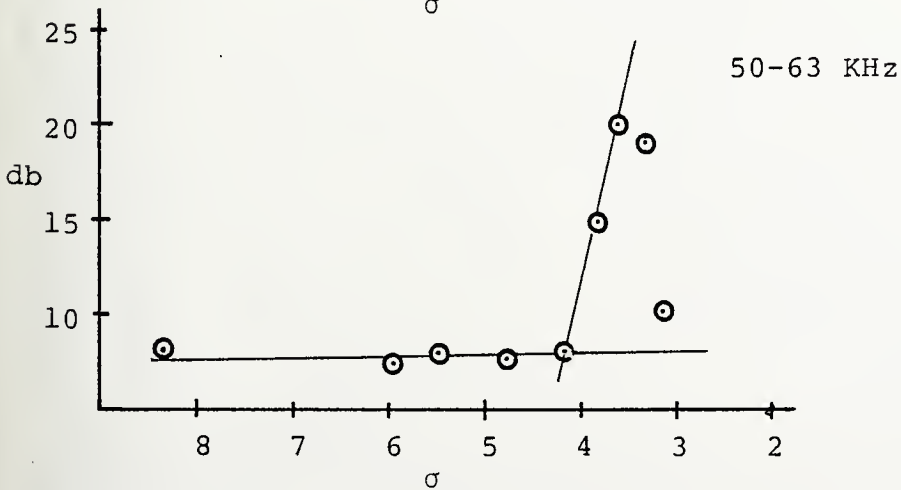
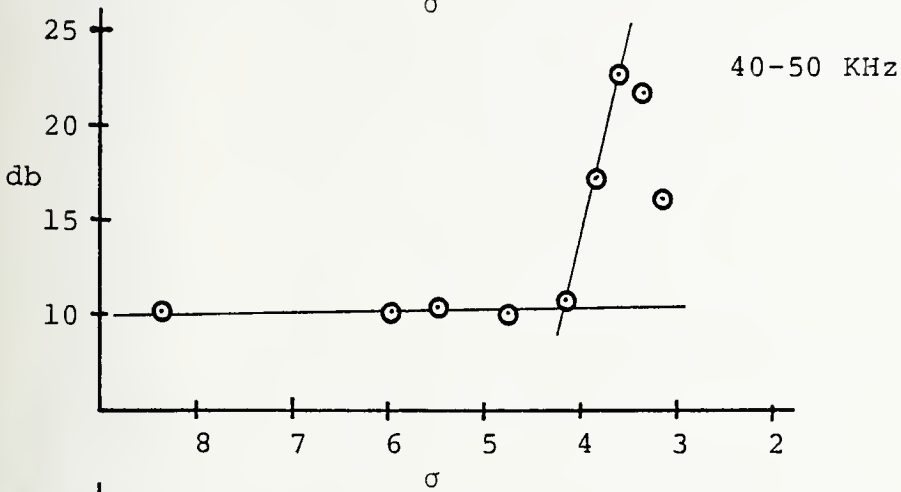
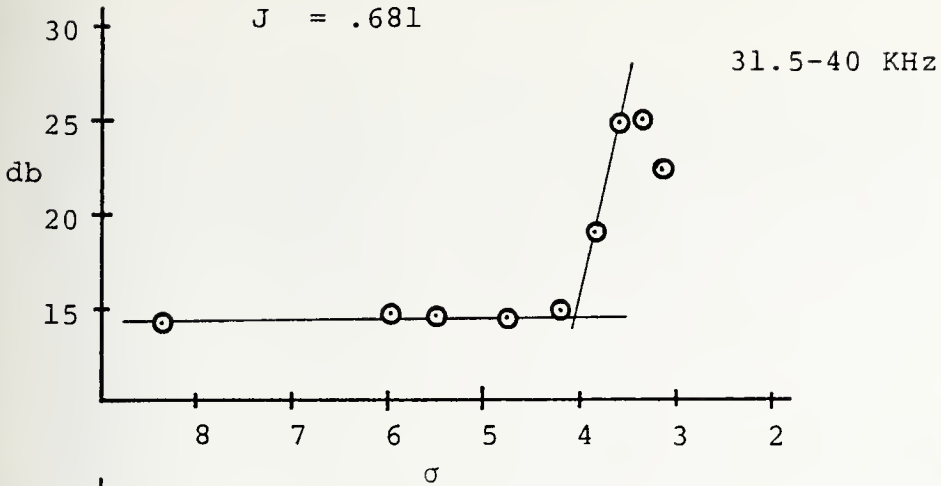
(2) One third octave band level - the arbitrary db level displayed on the measuring amplifier meter was plotted against decreasing cavitation index as shown in figure 8. The value of σ which corresponded to the curve after the "knee" being 3 db above the extension of the curve before the knee was taken as σ_i .

(3) Spectral analysis, complete spectrum - an increase of 3 db from the level at atmospheric pressure across the 40-50 kHz portion of the spectrum was taken as the criteria. The three spectra in figures 9, 10 and 11 correspond to a fixed J, 0.51, and three different values of σ : that for atmospheric pressure, σ_i for acoustically determined inception and σ_i for acoustically determined inception, respectively. The differences between these spectra are very slight and tend to make the determination of inception difficult and rather arbitrary. For this reason, this method was abandoned in favor of using the demodulated analysis.

(4) Spectral analysis, demodulated signal - it was assumed that the presence of a sharp peak ("line") at shaft rate frequency indicated one blade cavitating, and that a

$U_\infty \approx 16$ fps -36-
1150 rpm

$J = .681$



Typical One-Third Octave Band Levels vs. Cavitation Index
Figure 8

461510

K-E 10 X 10 TO THE CENTIMETER 18 X 25 CM
KUFFEL & ESSER CO. MADE IN U.S.A.

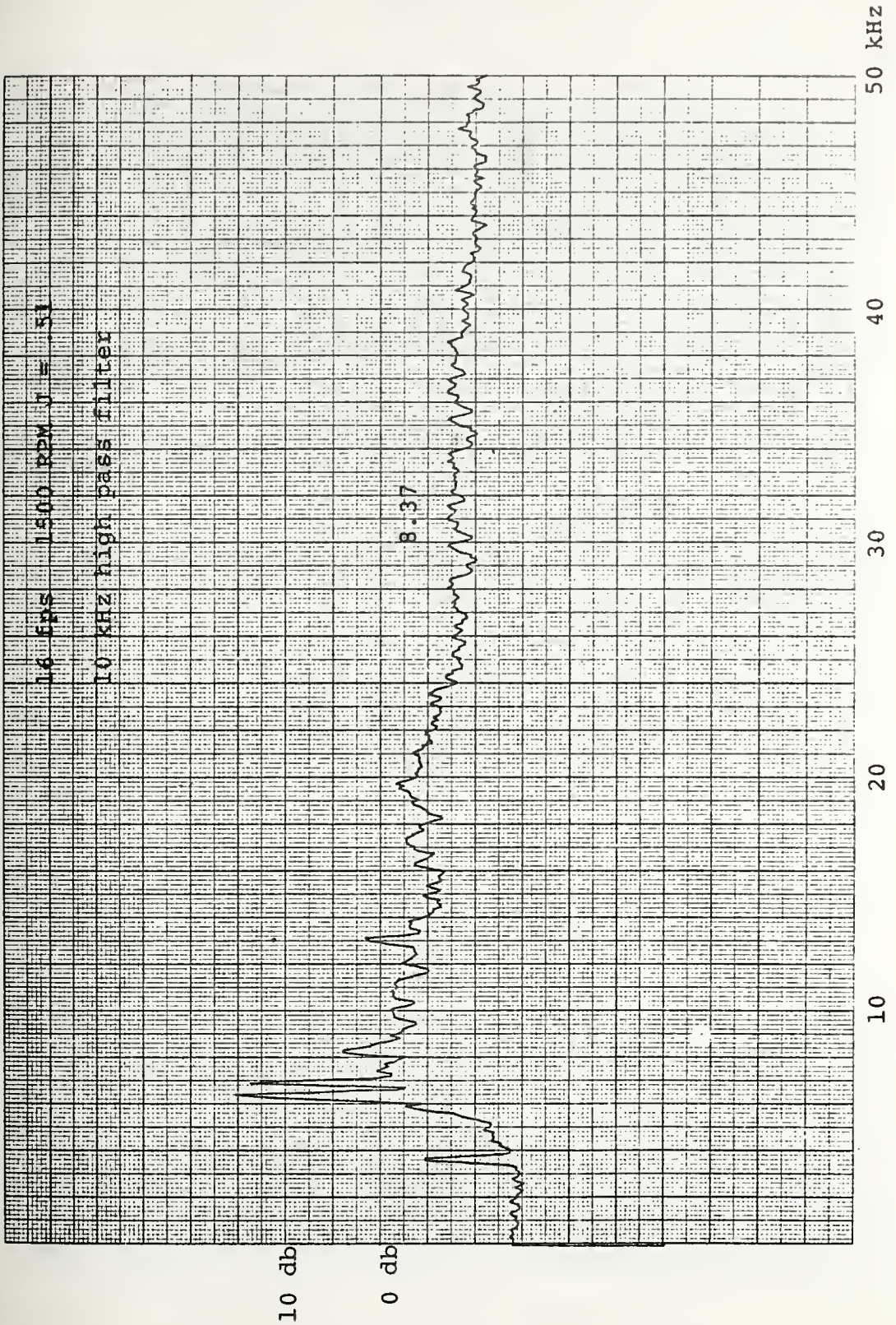


Figure 9

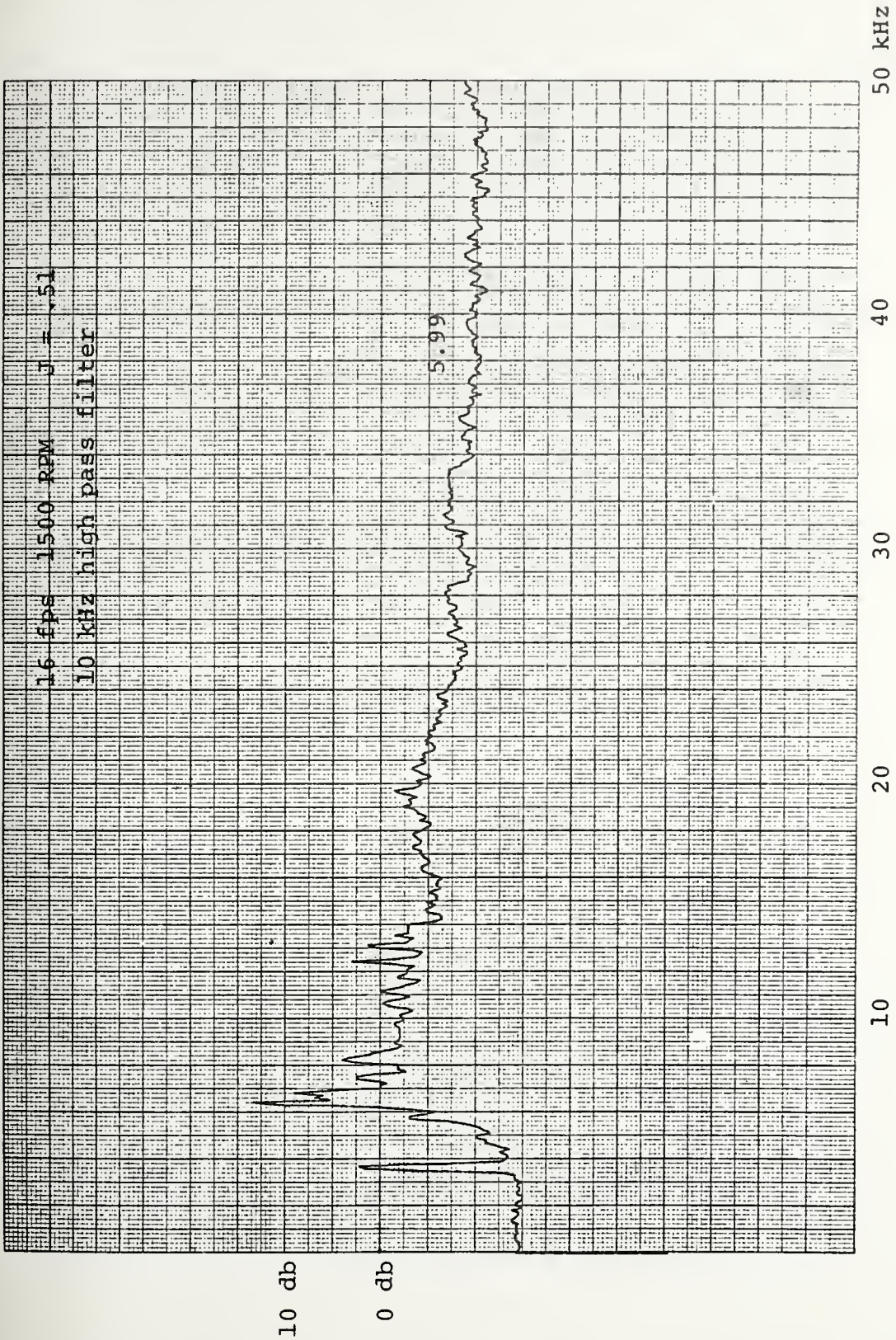


Figure 10

46 1510

K&E 10 X 10 TO THE CENTIMETER 18 X 25 CM.
KEUFFEL & ESSER CO. MADE IN U.S.A.

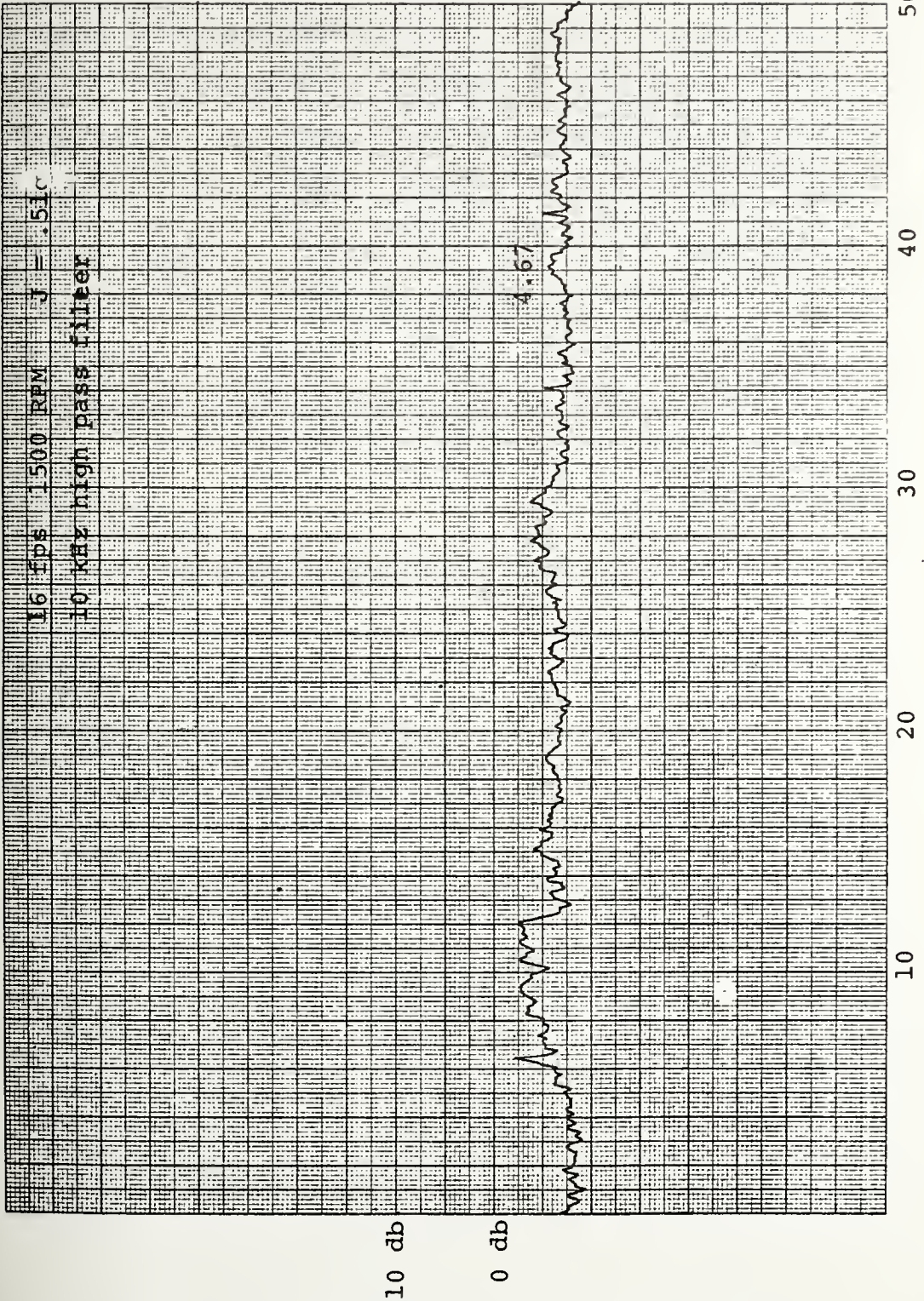


Figure 11

line at blade rate (number of blades times shaft rate) indicated all blades were cavitating (despite the possibility of the blade rate line merely being a harmonic of the shaft rate line). The inception criteria for this analysis was first taken to be the presence of lines at both shaft rate and blade rate which were at least 3 db above the general trend of the noise. A subsequent and less stringent criteria finally adopted was to require the presence of a line 3 db above the noise at blade rate frequency, with other lines present at shaft rate spacing to verify that cavitation was causing the line. Typical demodulated spectra are shown in figures 12 and 13.

For each test, the value of σ_i obtained was plotted against J to produce the cavitation inception curve. The two different inception criteria for the demodulated signal analysis were plotted on the same graph, but with contrasting symbols and curves.

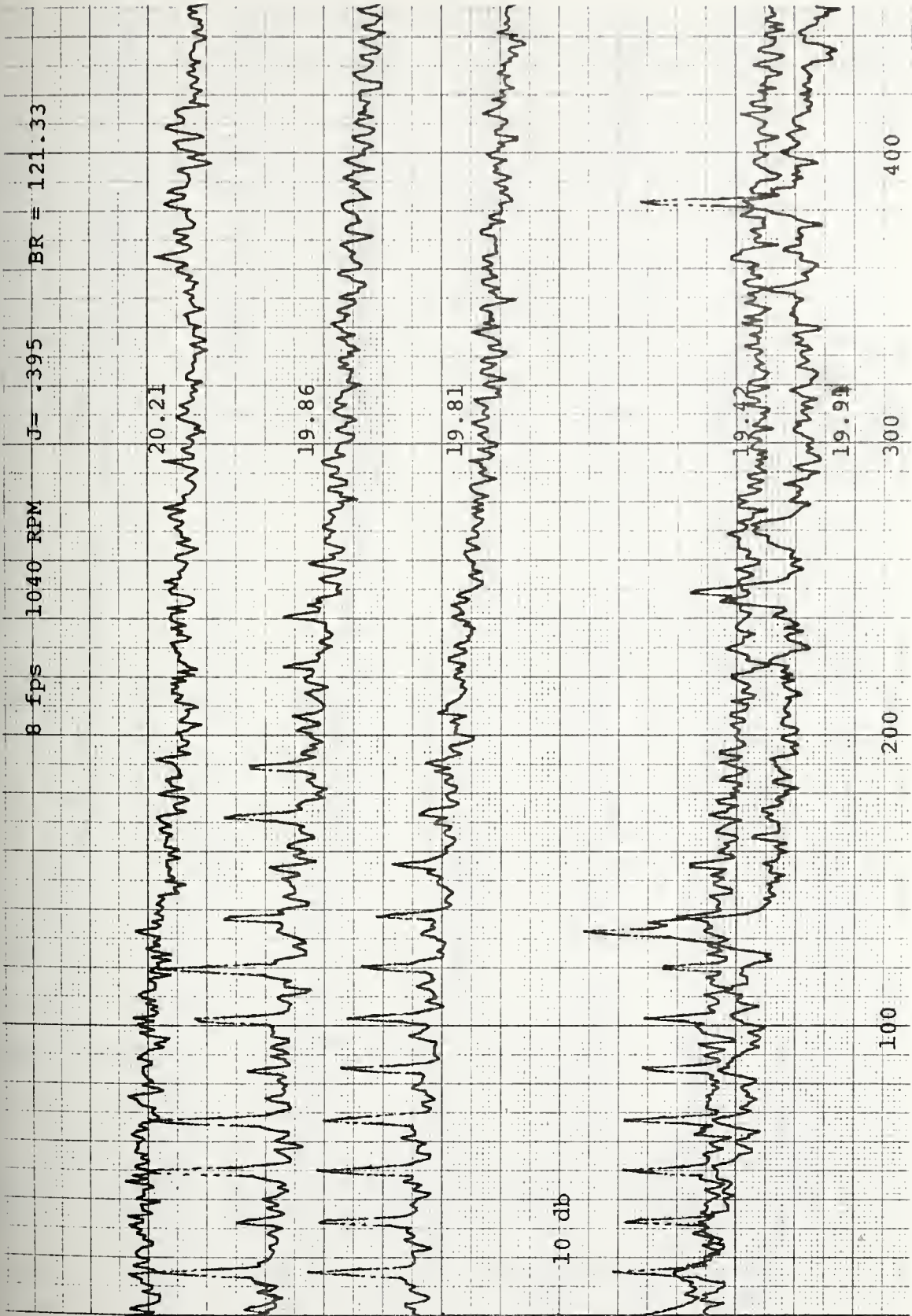


Figure 12

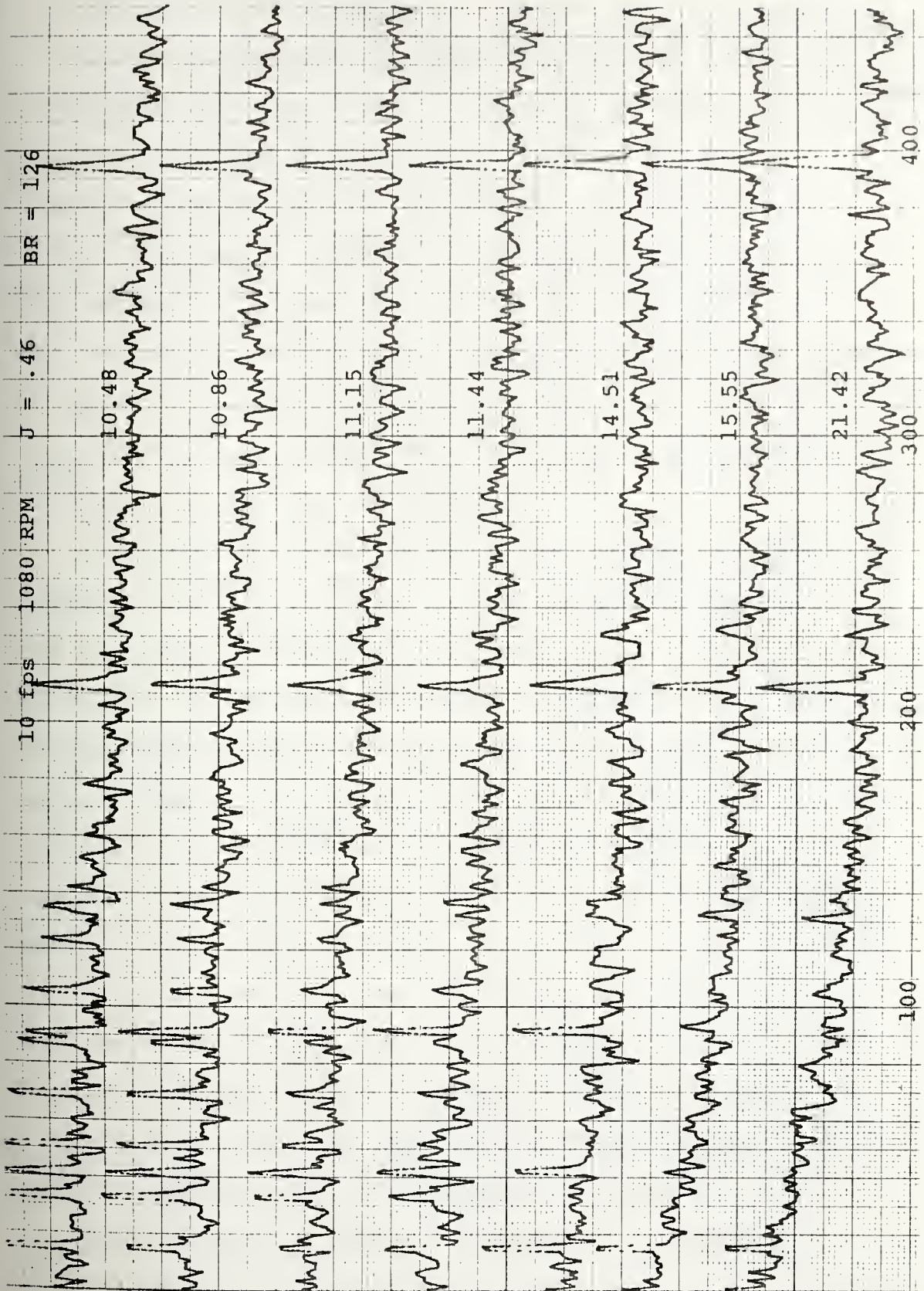


Figure 13

V. RESULTS AND DISCUSSION

Curves of σ_1 versus J for the visual and acoustic cavitation inception determinations are presented in figures 14 through 18. The comparison of acoustic and visual determinations for the one-third octave acoustic level measurements (figures 14 and 15) show a reasonably good agreement between the acoustically determined curve and the portion of the visually determined curve corresponding to the back bubble cavitation. However, tip vortex and leading edge face cavitation do not appear to be detected acoustically with the setup used.

Comparing the acoustic and visual results for the demodulated analysis of the acoustic signal figures 16, 17 and 18 shows a much better agreement for all types of cavitation, except for hub vortex cavitation. The results of the demodulated analysis of the 50-63 kHz band (figure 17) agrees almost exactly with the visually determined results for both of the inception criteria used with the acoustic analysis. The demodulated analysis of the acoustic signal above 20 kHz (figure 18) shows cavitation inception occurring at a higher value of σ for tip vortex cavitation than for the visual results, and at about equivalent values of σ for leading edge cavitation. The less stringent criteria for acoustically determined inception shows cavitation occurring at a higher value of σ than the more stringent criteria.

The two sets of results presented use different acoustic sensors. For the one-third octave level measurements,

Figure 14

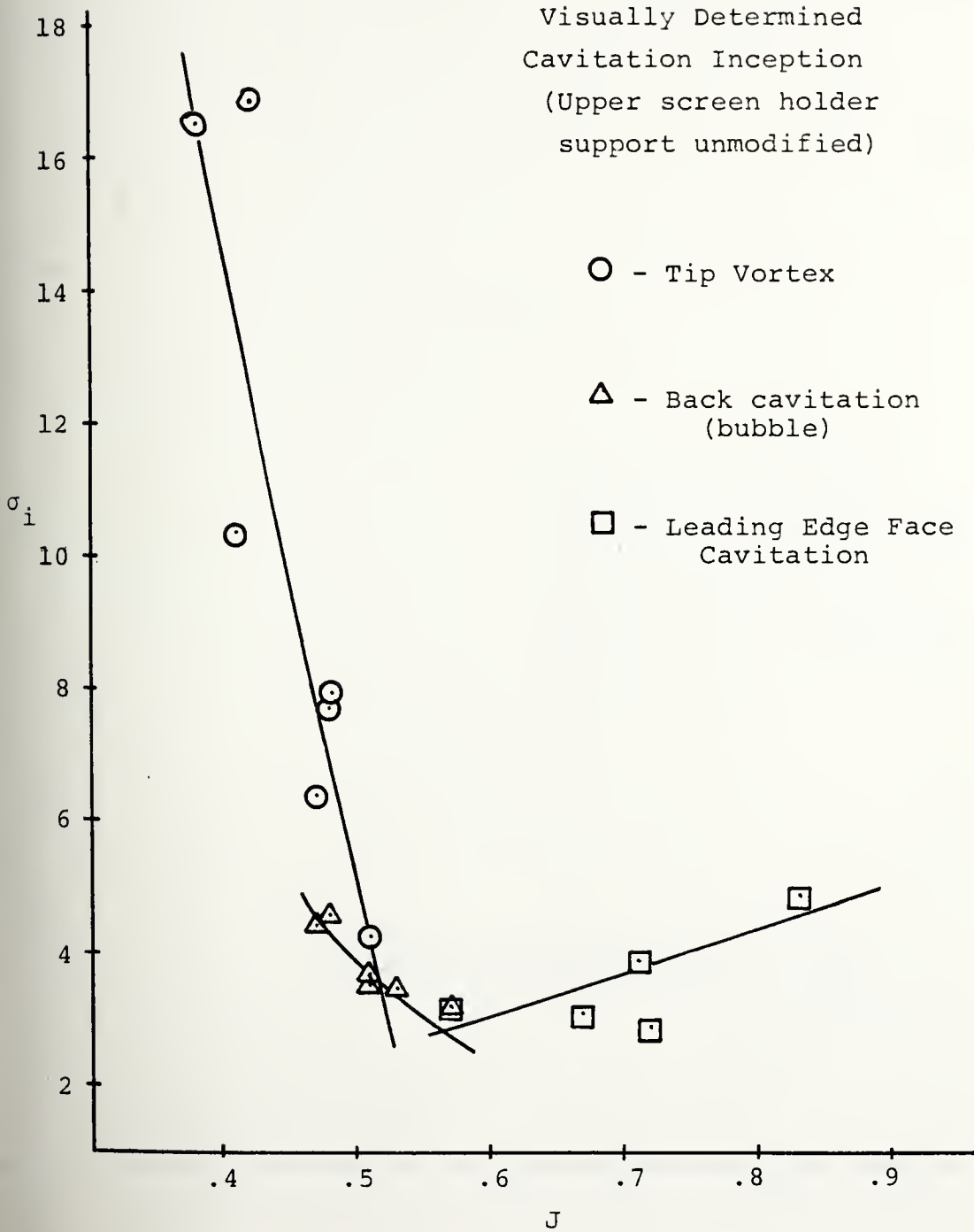
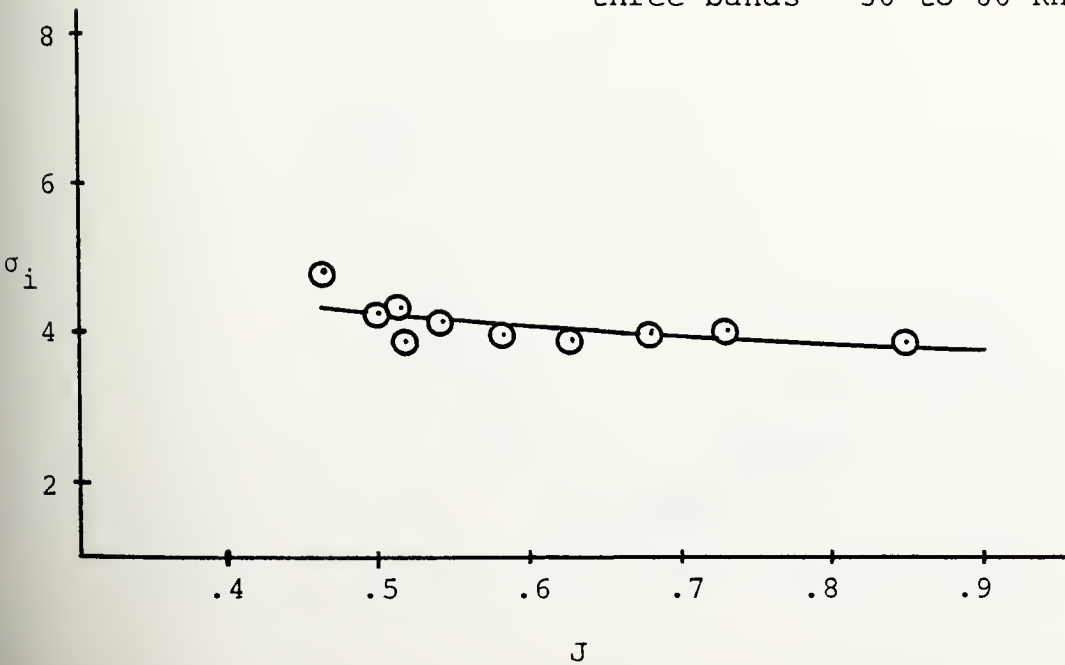


Figure 15

Acoustically Determined
Cavitation Inception
(Inception based upon one-
third octave band level.
Data point is average over
three bands - 30 to 60 KHz)



Visually Determined
Cavitation Inception

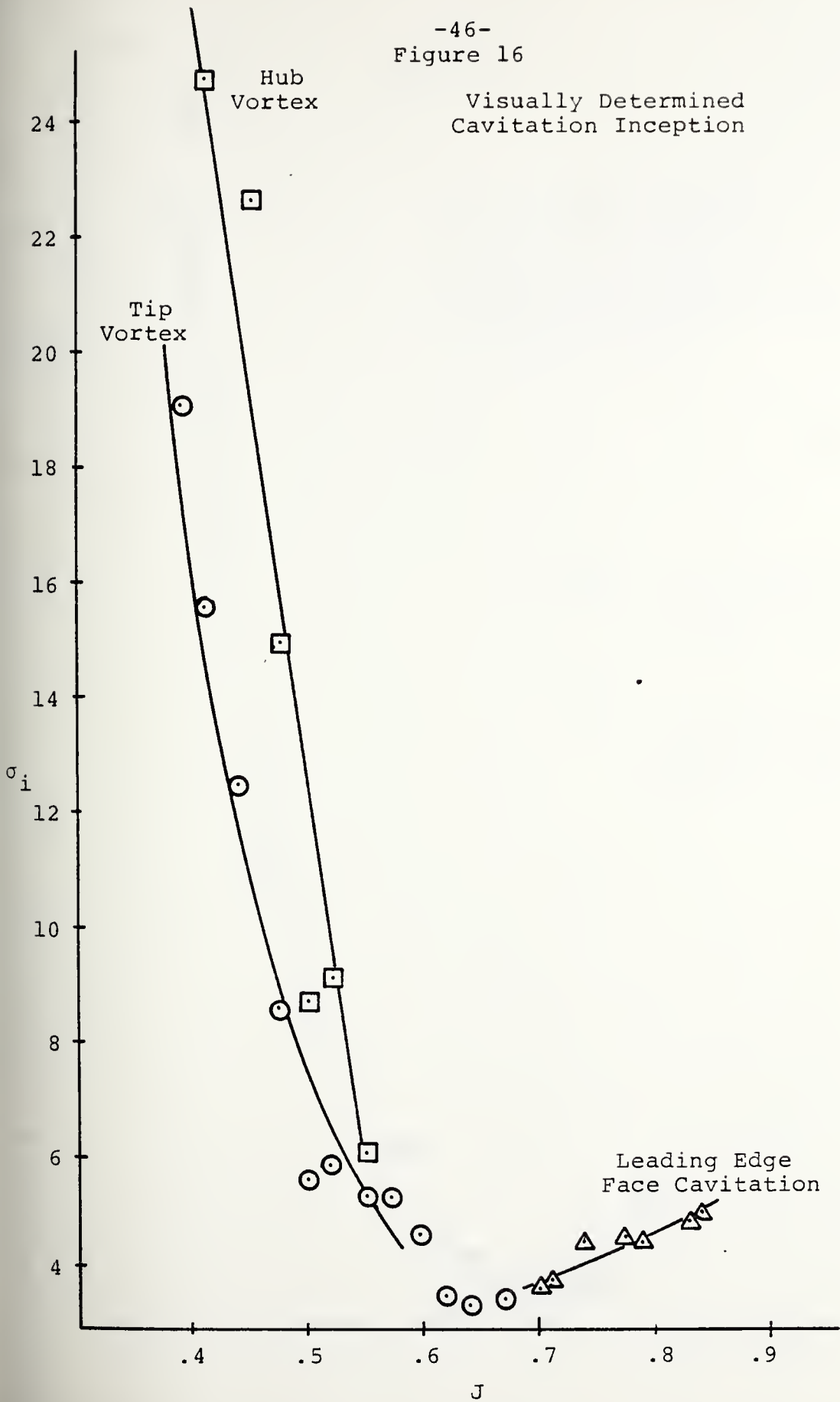


Figure 17

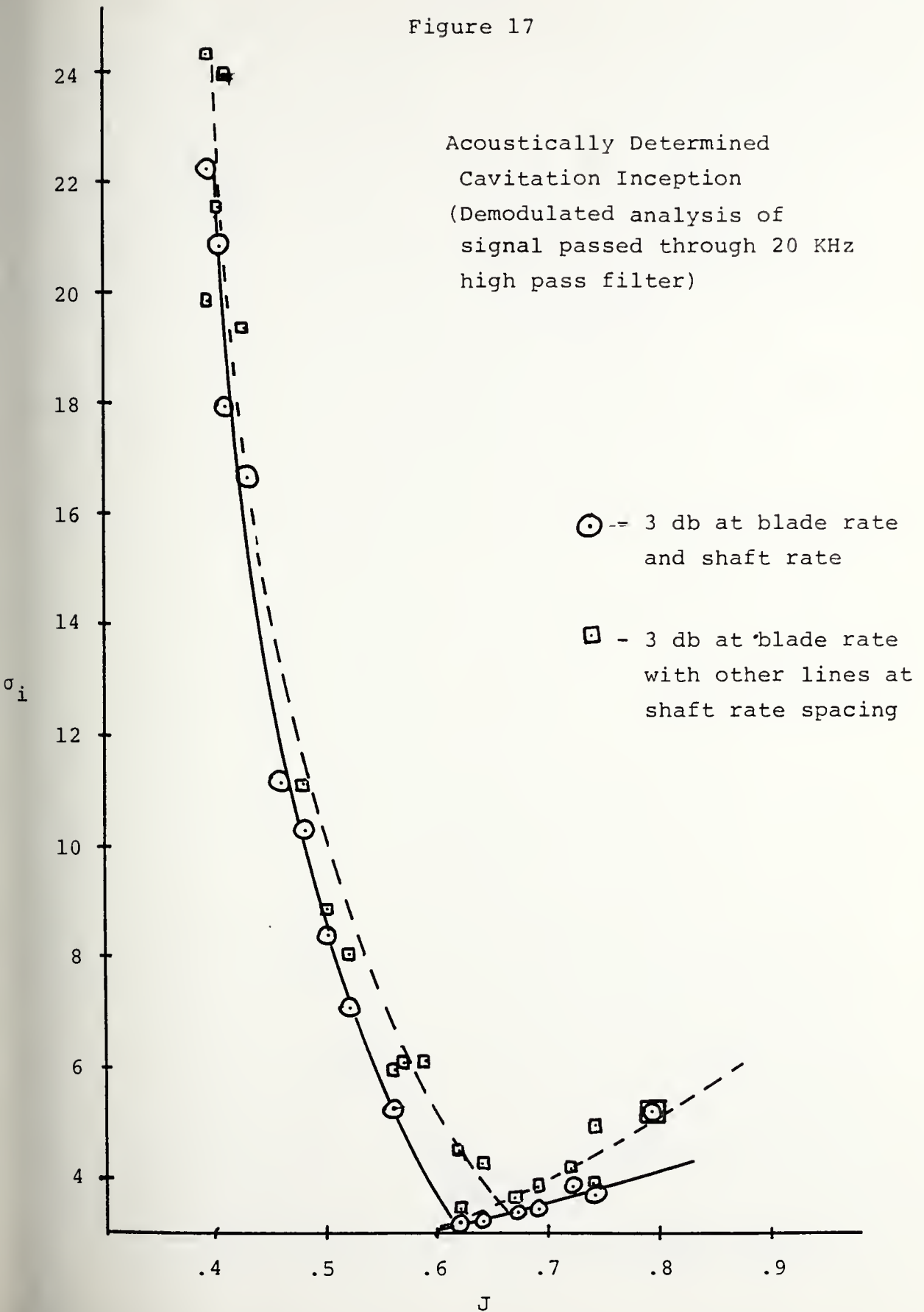
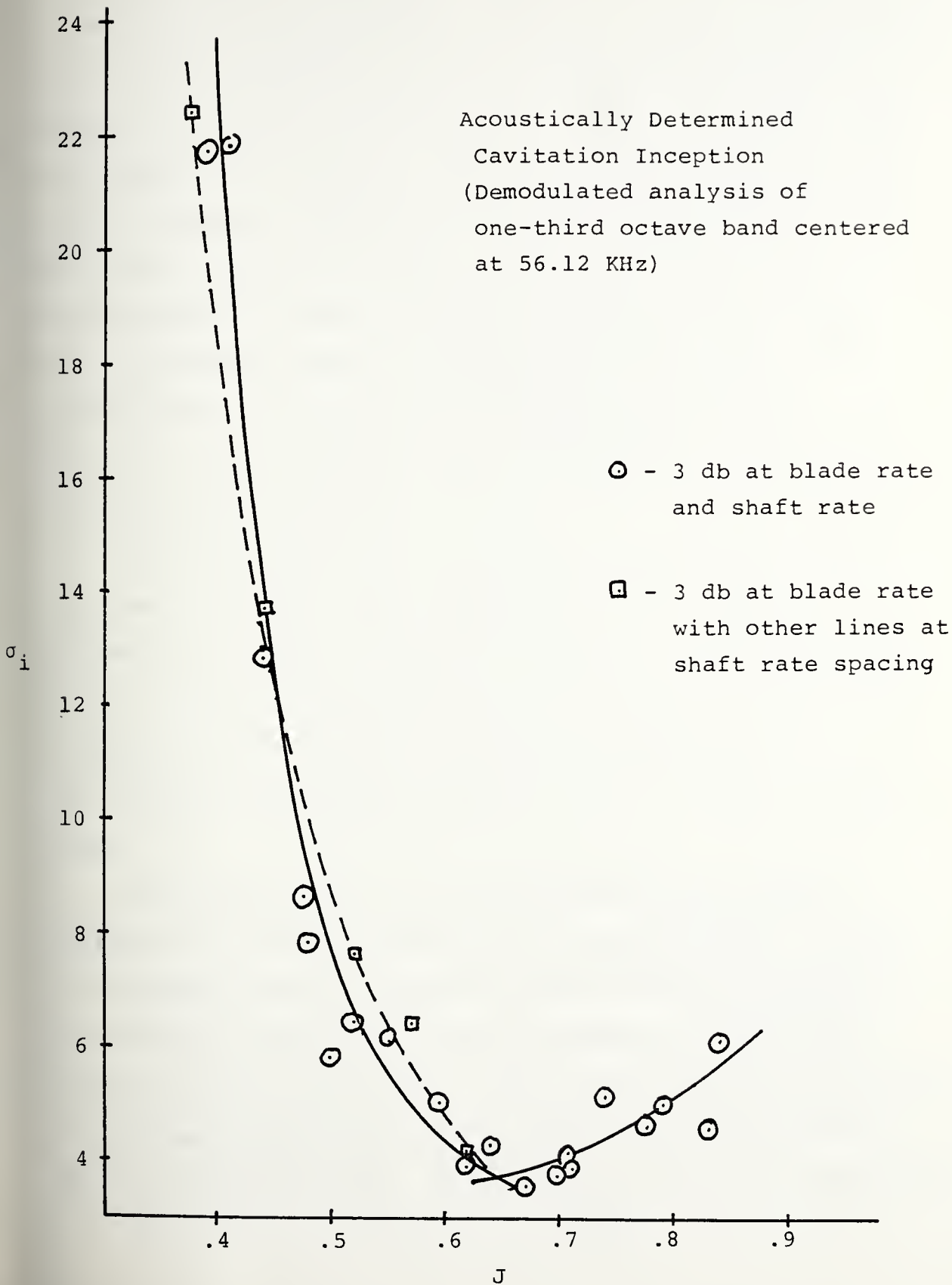


Figure 18



the accelerometer was used; but the demodulated analysis presented used the hydrophone, since it was felt that the higher usable frequency for the hydrophone was necessary. However, a test run at $J=0.62$ (run number 2 of 4 March) was performed to compare the acoustic information obtained from the two sensors. Examples of the demodulated spectra from the two sensors for a given σ are shown in figures 19 (hydrophone) and 20 (accelerometer). Except for the equipment gain adjustments needed to accommodate the different sensitivities of the sensors, the spectra are almost identical, indicating that either sensor was usable for an acoustic detection method.

It was expected that the curves of σ_i versus J would show good agreement between the acoustic and visually determined cavitation inception, and these results confirm this. It was also expected that the acoustically determined inception would anticipate (occur at a higher value of σ) the visually determined inception. This, in general, did not occur.

The higher value of σ at acoustically determined inception is based upon bubble size considerations. It was first assumed that the minimum bubble diameter which could be detected visually under the conditions of a propeller cavitation test was 0.001 in. This size was then taken to be the maximum diameter ($2R_1$) of a bubble in the calculation shown by Strasberg (1977) for the total lifetime of the cavity,

$$T = 2.7 R_1 \sqrt{\rho/P_0}$$

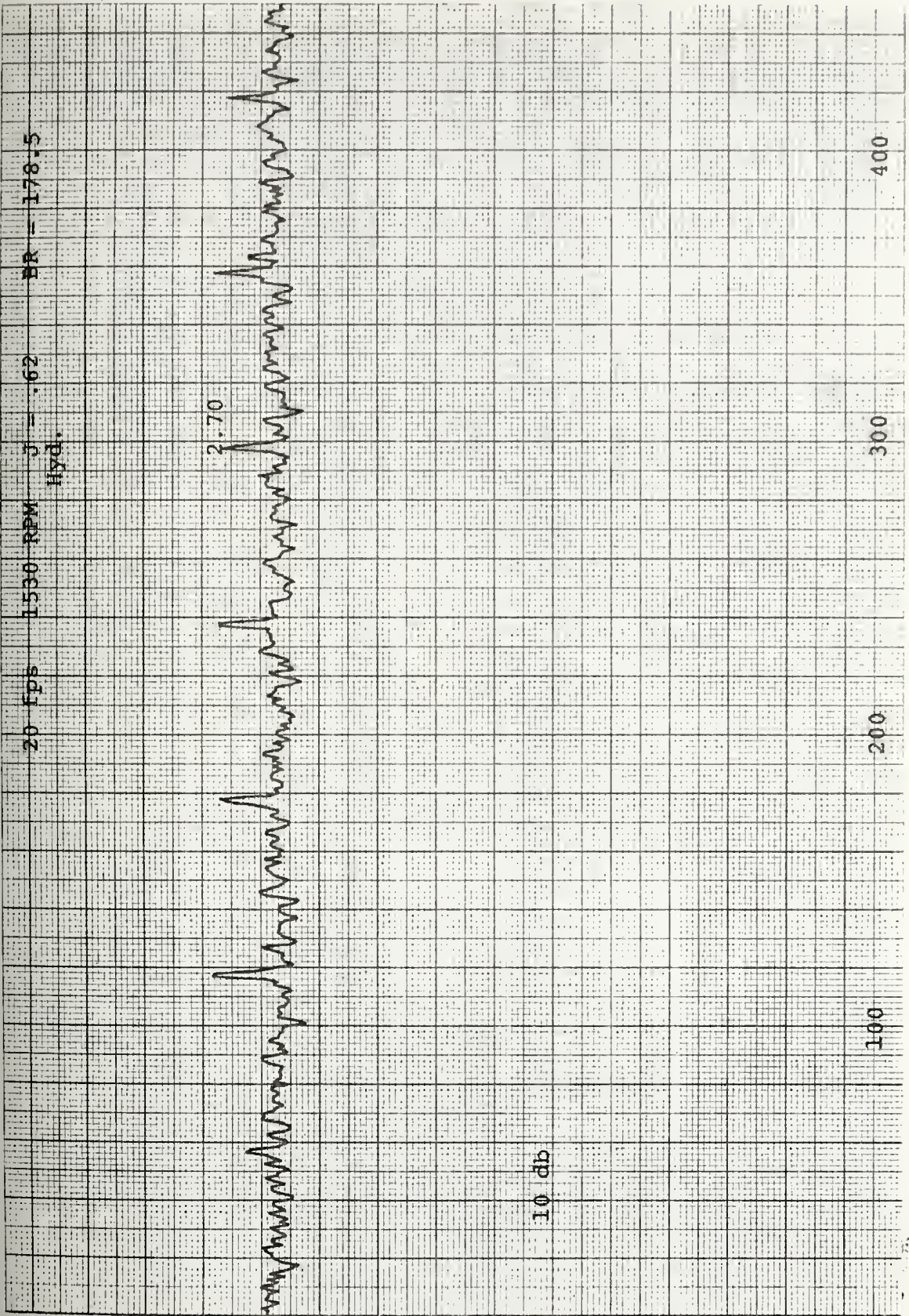


Figure 19

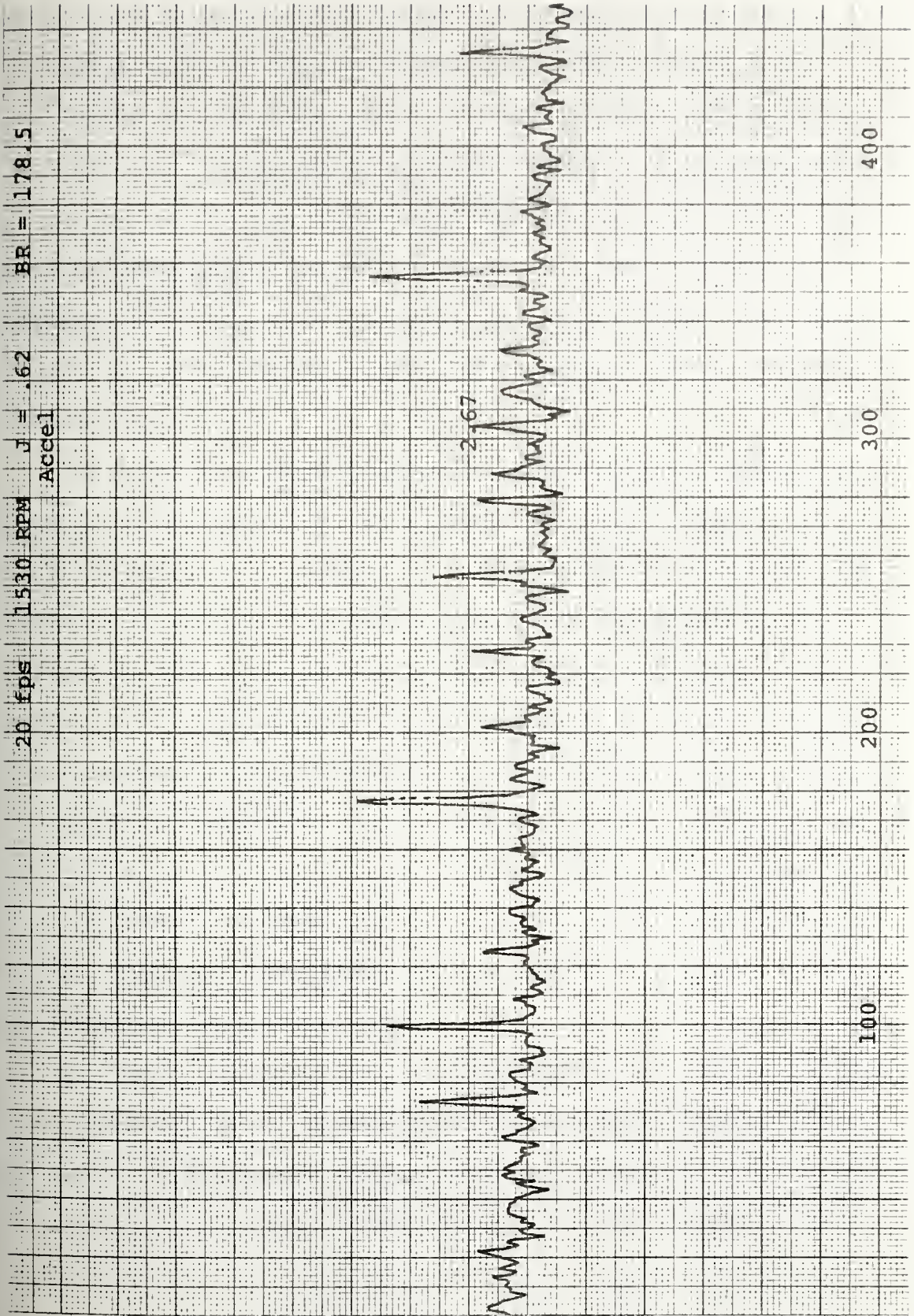


Figure 20

where ρ and P_0 were taken to be representative of the conditions in a cavitation test, $\rho = 1.93 \text{ lb-sec}^2/\text{ft}^4$, $P_0 = 400 \text{ mm Hg}$, or 1114 lb/ft^2 . Under these conditions, $T = 5.62 \times 10^{-4} \text{ sec}$, which corresponds to a frequency peak, f_p , in the cavitation noise spectrum of 17 kHz . With P_0 equal to atmospheric pressure, $f_p = 24.5 \text{ kHz}$. Since the frequency used for this analysis was much higher than these, it was felt that the detection of inception would occur at a higher value of σ .

Two possible explanations for the observed result not being in agreement with the prediction come to mind. The first is that the existence of scale effects (affecting the frequency scaling), due particularly to compressibility, surface tension and viscous effects, were not taken into account. If this caused the discrepancy, the use of high frequency acoustic information to anticipate visual inception determination would not be a workable scheme. However, if the expected acoustic signal was present, but was not detectable with the method or equipment used here, then anticipating the visual inception determination is possible, so long as the appropriate changes are made.

If the 0.001 in diameter bubble mentioned above is used with Strasberg's non-dimensionalization for acoustic power, the ratio of the power output with the spectral peak at 56 kHz to that with the just barely visible bubble are given by,

$$\frac{P_{\text{acoustic}}^2}{P_{\text{visual}}^2} = \frac{D_a}{D_v} = \frac{f_v}{f_a} = \frac{17}{56} = 0.304$$

or about 10 db. Thus, without considering the noise present or the increased absorption of the high frequency signal, 10 db of gain are required to have an equal acoustic signal with the two conditions. When these other considerations are included, it becomes obvious that increasing the gain of the signal or decreasing the level of noise, or both, is needed. The dramatic change between the inception information obtainable with a one-third octave analysis and that obtainable with the demodulated analysis tends to verify this.

By using an acoustic sensor which had some degree of directivity, either by using an array of hydrophones or by using some sort of reflector, an increase in the signal to noise ratio could be expected. Problems encountered with the instrumentation used could be corrected:

(1) There was no account taken of the changes in absorption that occurs as air bubbles grow when the pressure is reduced in the test section. The use of a calibrated reference signal in the frequency range of interest would enable correction of the acoustic signal levels for absorption.

(2) The combination of spectrum analyzer and X-Y plotter used required about three minutes to produce a paper copy of the demodulated spectrum, and the concurrent acoustic and visual cavitation inception determination extended this time span to the range of four to five minutes. Thus, for each value of static pressure for a given J , about four minutes were required, and the time required to produce each data point on the σ_1 versus J curve was about thirty minutes.

Because of time constraints on the availability of the test facilities and equipment, and the time required for each data point, two factors added to the inaccuracies in the results. First, each data point represented only one test at that value of J. Second, the steps in tunnel static pressure used were on the order of 25 mm Hg. This represents an error of 2 units of cavitation index at a tunnel flow speed of 6 feet per second or 0.3 units at 16 feet per second.

A more rapid analysis of the demodulated spectrum would make the method less time-consuming.

(3) During the time required for the spectrum analysis and averaging, tunnel flow speed and static pressure and propeller RPM would tend to drift on the order of one to five percent. The cumulative effects of these changes would also affect the accuracy of the analysis by causing variations (although slight) in the frequency of interest and by affecting the values of σ and J for the test run.

VI. CONCLUSIONS

Strasberg (1977) points out that "it is not possible to estimate the inception cavitation number of the prototype from model measurements without using empirically or theoretically determined scale factors." However, the results here show that it is possible to determine the cavitation inception performance of a model propeller by acoustic means at least as accurately as by visual means, as long as an adequate system for detecting the noise from all types of cavitation was available. And although the acoustically determined inception would require the same scale factors mentioned by Strasberg to predict full scale inception, the use of an acoustic inception determination technique for model tests does have advantages.

First, where full scale inception measurements are made acoustically, an acoustic measurement technique for the model would eliminate any scale effect that would occur between model and full scale measurements caused by visual observation on the model and acoustic determination on the full scale propeller. Although the results indicate that for the propeller tested here this scale effect would be small, the test of a different propeller, with a different length scale might show a greater difference between acoustic and visual results.

Second, displaying the spectrum of the demodulated cavitation noise signal gives a more definitive criteria for inception than visual methods, as expected.

Appendix A.

Details of the Wake Screen Design

The method developed by McCarthy (1963) and adapted into a FORTRAN program by Rose (1969) attempts to determine the value of the non-dimensional resistance coefficient for a grid,

$$K = \frac{\Delta p}{\frac{1}{2}\rho w_o^2} \quad (1)$$

where Δp is the local static pressure drop across the screen grid and w_o is the local velocity normal to the grid.

McCarthy points out that an empirical estimate for K for a given screen laid over a support screen is given by

$$K = 0.78 \frac{s}{(1-s)^2} + K_s \quad (2)$$

where: s , the solidity ratio for the screen =

$$MD(2-MD)$$

M is the number of wires per inch in the mesh

D is the diameter of the wire in inches

K_s is the resistance coefficient for the support screen

The program written by Rose requires that the test section area be subdivided into smaller areas, A_i , with a flow velocity, V_i , associated with each area, which is the average velocity for the subdivision. The overall velocity average is then calculated,

$$V_{avg} = \frac{\sum A_i V_i}{\sum A_i} \quad (3)$$

Then, for each area, the resistance coefficient, K_i , is calculated as follows:

(1) The integration constant, γ_0 , from McCarthy's solution is determined from the area having the maximum average velocity, V_{max} , which is assumed to have the resistance coefficient, K_s , for the support screen only:

$$\gamma_0 = \frac{1}{N} \left[\frac{(2+K_s - \chi_s)^2}{\chi_s + 1} \right]^{1/3} \left[\frac{V_{max}}{V_{avg}} - 1 \right] + \chi_s - \frac{1}{6(K_s + 1)} \quad (4)$$

$$\text{where } \chi_s = (1+K_s)^{1/2}$$

$$N = 1.02$$

(2) For each area, A_i , with its associated V_i , K_i is determined by solving the following equation for K_i :

$$\frac{V_i}{V_{avg}} = 1 + \left[\gamma_0 - \chi_i - \frac{1}{6(K_i + 1)} \right] N \left[\frac{\chi_i + 1}{(2+K_i + \chi_i)^2} \right]^{1/3} \quad (5)$$

$$\text{where } \chi_i = (1+K_i)^{1/2}$$

$$N = 1.02$$

(3) Once K_i is determined for each area, the last step is to account for the deflections of the streamlines by the changes in velocity caused by the wake screen. This is done by an iterative procedure which adjusts the areas, A_i , until the volume flow rate at the screen is equal to the volume flow rate at the propeller (this assumes that the screen is within

one tunnel diameter of the propeller, and it uses an empirical constant, α). The result is a correction to the actual screen area for each subdivision.

For this experiment, this program was adapted for use with a TI-59 programmable hand calculator. The test section was divided into four areas, each with its associated velocity, as shown in Table A-1. These areas and velocities were based upon the desired circumferential mean wake information provided for the velocities over the propeller disk, and an estimate for the average velocity outside that area. For each area, K_i and the area correction, ΔA_i , were determined from the program.

At this point Rose's method and the one used here become different. When a large number of screens with different meshes and wire diameters are available, having a screen available with the proper resistance coefficient enables the final wake screen to be assembled by piecing together the correct screens on the support screen. But here, the desired screens were not all available, so an alternative had to be developed.

The alternative was based on an interpretation of information given in Pope and Harper (1966) on turbulence generation by screens in wind tunnels. This text indicates that the cumulative effect of several layers of screens was additive. This seemed to be supported by the empirical formula for K in equation (2), where the effect of the support screen and the wake producing screen are added. It was

Table A-1

Wake Characteristics						
<u>Area Designation</u>	<u>Range of r/R</u>	<u>A_i</u>	<u>V_i</u>	<u>A_i cor</u>	<u>r/R corr</u>	<u>K_{req}</u>
1	∞ - 1.0	308.39	.97	317.86	∞ -.946	0.4612
2	1.0-0.7	46.72	.817	44.51	.946-.641	0.9462
3	.7-.5	21.99	.636	18.78	.641-.454	1.756
4	.5-.23	18.06	.510	14.01	.454-.23	2.531

felt that, even though Pope and Harper note that the effect of the screens was additive only if they did not touch, assuming that the effect was additive would be satisfactory for a first approximation.

Thus, the desired initial K_i values were obtained by using several layers of two different screens. The characteristics of these screens are listed in Table A-2, and the actual K_i for the screens used is listed in Table A-1. The was screen was then assembled, with the pieces of screen wired onto the support screen with pieces of 0.020 in stainless steel wire. A wake survey conducted with the Laser Doppler Anemometer was performed along the diagonal line shown in figure 3 previously.

The determination of velocities in the wake was done with the propeller removed from the shaft. The longitudinal flow speeds were determined in the plane 2.5 in downstream of the propeller blade leading edges. The results of this and all other wake surveys performed are contained in Appendix B.1. The results for this initial screen are plotted in figure A-1.

From the plot of non-dimensional velocity versus non-dimensional radius, r/R , it was possible to determine the average velocities actually obtained for each of the subdivided areas used, since the wake was to be axisymmetric. From the actual values of V_i , equations (4) and (5) were then used to determine the actual K_i obtained from the screen used for each area, shown in Table A-3. At this point it was

Table A-2

Screen Characteristics

<u>Mesh, M</u>	<u>Wire Diameter, D</u>	<u>Solidity ratio, s</u>	<u>K-K_s</u>
8×8	0.020 in	.2944	.4612
18×18	0.012 in	.3853	.7956

Table A-3

Comparison of Installed and Measured K Values

<u>Area</u>	<u>K_{req}</u>	<u>K_{inst}</u>	<u>ΔK_{inst}</u>	<u>K_{meas}</u>	<u>ΔK_{meas}</u>	<u>ΔK ratio</u>
1	0.4612	0.4612	-	0.4612	-	-
2	0.9462	0.9224	0.4612	1.1813	0.7201	1.560
3	1.756	1.7179	0.7954	2.4197	1.2384	1.557
4	2.531	2.5134	0.7954	4.106	1.6863	2.120

assumed that the calculated drag associated with the support screen was correct, and the remaining screen layers could be adjusted to develop the desired wake.

Still assuming that the effect of multiple layers of screen material was additive, the measured increase in K_i for each increment of screen material was determined (ΔK_i in Table A-3). In each case, the ratio of measured ΔK_i to installed ΔK_i was determined. The results of these calculations were interpreted as follows:

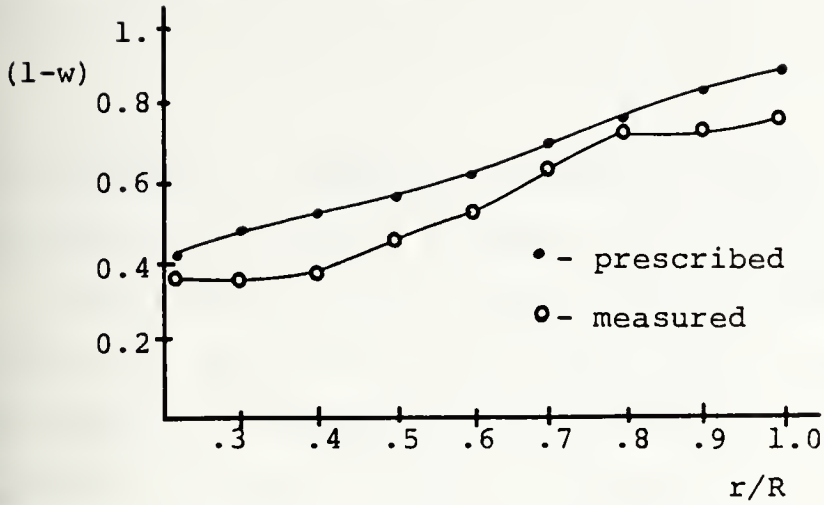
(1) In area 2, the same material as that found in 1 was added, and the increase in K was 1.56 times greater than that expected from the simple addition of resistance coefficients.

(2) Comparing measured results for areas 3 and 4, the increase from adding another layer of the same material was 1.36 ($\frac{1.6863}{1.2384} = 1.36$) times greater than the expected result.

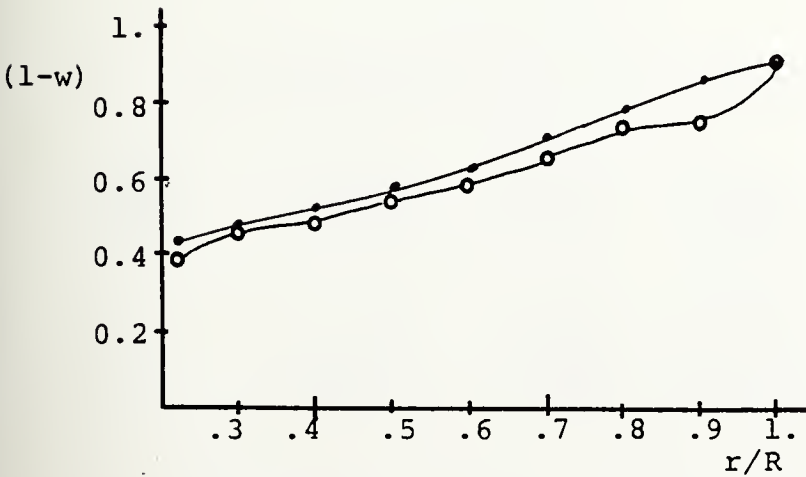
(3) The apparent effect of adding the screen of area 3 onto that of area 2 was 1.56 greater than expected.

(4) Thus, an average increase in the resistance coefficient from adding layers of screen material was felt to be on the order of 1.5 times the expected result.

In terms of the screen material available, this meant that the 8x8x.020" screen material would be used for all screen layers, with each added layer having 1.5 times the resistance coefficient of the single layer. Table A-4 shows the



Wake Survey - Initial Wake Screen
Figure A-1



Wake Survey - Final Wake Screen
Figure A-2

calculated $K_{\text{installed}}$ values for the four wake screen areas compared to the required K values, where

$$K_{\text{calc}} = K_s + 1.5K_{\text{screen}}$$

This screen was assembled as noted previously, and another wake survey was made at the same points as before.

The results of this survey are shown graphically in figure A-2. The low velocity seen at the outer radii correspond to the use of a screen giving higher than the required value of K in area 2. Lacking a screen with a small enough K to correct this discrepancy, this wake was considered to be acceptable.

Table A-4

Final Screen Resistance Coefficients

<u>Area</u>	<u>K_{req}</u>	<u>K added</u>	<u>K_{calc}</u>
1	0.4612		0.4612
2	0.9462	0.4612	1.148
3	1.756	0.4612	1.836
4	2.531	0.4612	2.523

APPENDIX B

Raw Data

The following pages of this section contain the propeller operating conditions data sheets, the graphs of sound level versus cavitation index for one-third octave level measurements, and the X-Y plotter outputs for the demodulated spectra and for the analysis of the complete spectrum. Since, in some cases, the recorded data may not be completely clear as to what is being presented, some clarifying explanations are presented here.

Wake survey data - For tables B-1 and B-2, the velocity used to obtain (1-w) is the $V_{\infty\text{avg}}$ calculated from the 6,7, and 8 inch radial positions. For table B-3, the velocity used is the velocity from the manometer height, 12.0 fps.

One-third octave band level - The conversion factors for T to thrust and Q to torque for this series of tests and for the data of sections B.5, B.6 and B.7 are on the data sheet for run number 1. In these and all subsequent data sheets the first number in the "GAIN CHANGE" column refers to the code number for the amplifier shown in the upper section, the second number gives the setting to which the selector was changed. In the "REMARKS" column for this section only are three numbers which refer to the displayed

level on the measuring amplifier meter for the 31.5-40 kHz band, the 40-50 kHz band, and the 50-63 kHz band, respectively. For all sections of the appendix this column also contains the visual inception determinations as follows: any visual inception determination will have a * , together with a TV for tip vortex cavitation, HV for hub vortex cavitation, LEPF for leading edge pressure face cavitation, LESF for leading edge suction face cavitation, BB or BACK for back bubble or back cavitation. The points plotted on the plots of db versus σ are the arbitrary level from the measuring amp meter. The top plot is the 31.5-40 kHz level, the middle is the 40-50 kHz level, and the bottom is the 50-63 kHz level.

Demodulated Analysis - The conversion factors for thrust and torque for these two sections are on the first data sheet for the 20 kHz high pass signal. On these and all plots from the X-Y plotter, 10 db is represented by 20 of the smallest divisions (2 cm total). For the plots in these two sections, the first plot made was the one at the bottom of the page. For each subsequent plot, the zero setting for the X-Y plotter was placed 2 cm higher (10 db). Unless noted on the associated data sheet, no gain adjustments were made. On these and all subsequent

plots the number typed in beside a particular curve is the value of the cavitation index associated with that plot.

Table B-1

Wake Survey Data -
Initial Wake Screen

R	θ	Scale		Volts	(1-w)
		Hor.	Vert.		
8	135	11.74	91.60	.831, .831, .831	-
7	135	13.08	89.80	.837, .837, .837	-
6	135	14.43	88.01	.827, .827, .827	-
5.4	135	15.24	86.93	.690, .693, .692	.827
4.86	135	15.97	85.96	.637, .638, .637	.762
4.32	135	16.69	84.99	.622, .623, .623	.745
3.78	135	17.42	84.02	.546, .546, .547	.653
3.24	135	18.15	83.05	.443, .440, .443	.528
2.70	135	18.87	82.08	.361, .366, .365	.436
2.16	135	19.60	81.11	.280, .284, .283	.338
1.62	135	20.33	80.14	.269, .268, .270	.321
1.24	135	20.84	79.46	.298, .294, .296	.354
1.24	315	24.18	75.00	.328, .331, .330	.394
1.62	315	24.69	74.32	.339, .341, .343	.408
2.16	315	25.42	73.35	.365, .362, .360	.433
2.70	315	26.15	72.38	.408, .407, .407	.487
3.24	315	26.87	71.41	.443, .443, .443	.530
3.78	315	27.60	70.44	.540, .539, .540	.645
4.32	315	28.33	69.47	.623, .622, .622	.744
4.86	315	29.05	68.50	.633, .634, .632	.757
5.4	315	29.78	67.53	.759, .771, .770	.917
6	315	30.59	66.45	.844, .844, .844	-
7	315	31.94	64.66	.839, .841, .838	-
0	0	22.51	77.28	-	-

1 Volt = 20.805 ft/sec

$V_{\infty avg} = .836 \text{ V} = 17.4 \text{ ft/sec}$

Table B-1 (Continued)

Comparison With Prescribed Wake
Initial Wake Screen

r/R	(1-w) _{avg}	(1-w) _{req}	Error
1.	.872	.903	-.03
0.9	.759	.846	-.10
0.8	.745	.784	-.05
0.7	.649	.710	-.09
0.6	.529	.636	-.17
0.5	.461	.573	-.19
0.4	.385	.528	-.27
0.3	.365	.488	-.25
0.23	.374	.431	-.13

Table B-2

Wake Survey Data -
Final Wake Screen
(Unmodified upper support)

R	θ	Scale		Volts	(1-w)
		Hor.	Vert.		
8	135	11.74	91.60	.836,.837,.837	-
7	135	13.08	89.80	.838,.835,.838	-
6	135	14.43	88.01	.836,.836,.837	-
5.40	135	15.24	86.93	.741,.739,.739	.883
4.86	135	15.97	85.96	.617,.617,.618	.737
4.32	135	16.69	84.99	.603,.602,.601	.718
3.78	135	17.42	84.02	.529,.526,.523	.625
3.24	135	18.15	83.05	.477,.476,.477	.567
2.70	135	18.87	82.08	.441,.441,.443	.525
2.16	135	19.60	81.11	.406,.407,.406	.485
1.62	135	20.33	80.14	.391,.390,.395	.468
1.24	135	20.84	79.46	.272,.288,.287	.332
1.24	315	24.18	75.00	.378,.379,.379	.459
1.62	315	24.69	74.32	.404,.404,.400	.483
2.16	315	25.42	73.35	.418,.416,.415	.499
2.70	315	26.15	72.38	.480,.478,.479	.574
3.24	315	26.87	71.41	.514,.516,.517	.618
3.78	315	27.60	70.44	.575,.579,.578	.693
4.32	315	28.33	69.47	.621,.623,.623	.745
4.86	315	29.05	68.50	.630,.629,.631	.754
5.40	315	29.78	67.53	.762,.769,.769	.919
0	0	22.51	77.28		

$$V_{\text{avg}} = .836 \text{ V} = 17.4 \text{ ft/sec}$$

Table B-2 (Continued)

Comparison With Prescribed Wake
Final Wake Screen
(Unmodified upper support)

r/R	(1-w) _{avg}	(1-w) _{req}	Error
1.0	.901	.903	-.003
0.9	.746	.846	-.118
0.8	.732	.784	-.066
0.7	.659	.710	-.072
0.6	.593	.636	-.068
0.5	.550	.573	-.040
0.4	.491	.528	-.070
0.3	.475	.488	-.027
0.23	.395	.431	-.083

Table B-3

Wake Survey Data -

Final Wake Screen

(Modified upper support)

y	z	Scale		Volts	Speed	(l-w)
		Hor.	Vert.			
6	1	37.91	75.84	.646	13.44	1.12
	0		78.38	.687	14.29	1.19
	-1		80.92	.656	13.65	1.14
5	-3	36.00	86.00	.633	13.17	1.10
	-2		83.46	.546	11.36	.95
	-1		80.92	.513	10.67	.89
	0		78.38	.597	12.42	1.04
	1		75.84	.578	12.03	1.0
	2		73.30	.601	12.50	1.04
	3		70.76	.648	13.48	1.12
4	4	34.10	68.22	.655	13.63	1.14
	3		70.76	.505	10.51	.88
	2		73.30	.470	9.78	.81
	1		75.84	.462	9.61	.80
	0		78.38	.543	11.30	.94
	-1		80.92	.501	10.42	.87
	-2		83.46	.478	9.94	.83
	-3		86.00	.506	10.53	.88
	-4		88.54	.556	11.57	.96
	3	-4	32.19	88.54	.516	10.74
-3			86.00	.507	10.55	.88
-2			83.46	.438	9.11	.76
-1			80.92	.407	8.47	.71
0			78.38	.483	10.05	.84
1			75.84	.411	8.55	.71
2			73.30	.410	8.53	.71
3			70.76	.460	9.57	.80
4			68.22	.549	11.42	.95

Table B-3 (Continued)

y	z	Scale		Volts	Speed	(1-w)
		Hor.	Vert.			
2	5	30.29	65.68	.656	13.65	1.14
	4		68.22	.476	9.90	.83
	3		70.76	.455	9.47	.79
	2		73.30	.363	7.55	.63
	1		75.84	.287	5.97	.50
	0		78.38	.355	7.39	.62
	-1		80.92	.334	6.95	.58
	-2		83.46	.369	7.68	.64
	-3		86.00	.469	9.76	.81
	-4		88.54	.434	9.03	.75
	-5		91.08	.430	8.95	.75
1	-6	28.38	93.62	.459	9.55	.80
	-5		91.08	.340	7.07	.59
	-4		88.54	.370	7.70	.64
	-3		86.00	.370	7.70	.64
	-2		83.46	.269	5.60	.47
	-1		80.92	.259	5.39	.45
	1		75.84	.266	5.53	.46
	2		73.30	.357	7.43	.62
	3		70.76	.450	9.36	.78
	4		68.22	.480	9.99	.83
	5		65.68	.645	13.42	1.12
6		63.14	.657	13.67	1.14	
0	6	26.48	63.14	.690	14.36	1.20
	5		65.68	.673	14.00	1.17
	4		68.22	.556	11.57	.96
	3		70.76	.480	9.99	.83
	2		73.30	.394	8.20	.68
	-2		83.46	.257	5.35	.45
	-3		86.00	.289	6.01	.50
	-4		88.54	.297	6.18	.51
	-5		91.08	.290	6.03	.50
	-6		93.62	.400	8.32	.69

Table B-3 (Continued)

y	z	Scale		Volts	Speed	(1-w)
		Hor.	Vert.			
-1	-6	24.58	93.62	.491	10.22	.85
	-5		91.08	.360	7.49	.62
	-4		88.54	.354	7.36	.61
	-3		86.00	.355	7.39	.62
	-2		83.46	.329	6.84	.57
	-1		80.92	.273	5.68	.47
	1		75.84	.308	6.41	.53
	2		73.30	.359	7.47	.62
	3		70.76	.401	8.34	.70
	4		68.22	.484	10.07	.84
	5		65.68	.638	13.27	1.11
	6		63.14	.659	13.71	1.14
	-2	5	22.67	65.68	.646	13.44
4			68.22	.486	10.11	.84
3			70.76	.444	9.24	.77
2			73.30	.317	6.60	.55
1			75.84	.329	6.84	.57
0			78.38	.346	7.20	.60
-1			80.92	.377	7.84	.65
-2			83.46	.366	7.61	.63
-3			86.00	.438	9.11	.76
-4			88.54	.438	9.11	.76
-3	-5		91.08	.483	10.05	.84
	-4	20.77	88.54	.500	10.40	.87
	-3		86.00	.476	9.90	.83
	-2		83.46	.430	8.95	.75
	-1		80.92	.405	8.43	.70
	0		78.38	.504	10.49	.87
	1		75.84	.447	9.30	.77
	2		73.30	.455	9.47	.79
	3		70.76	.457	9.51	.79
	4		68.22	.517	10.76	.90

Table B-3 (Continued)

y	z	Scale		Volts	Speed	(l-w)
		Hor.	Vert.			
-4	4	18.86	68.22	.629	13.09	1.09
	3		70.76	.495	10.30	.86
	2		73.30	.459	9.55	.80
	1		75.84	.492	10.24	.85
	0		78.38	.481	10.01	.83
	-1		80.92	.438	9.11	.76
	-2		83.46	.501	10.42	.87
	-3		86.00	.507	10.55	.88
	-4		88.54	.602	12.52	1.04
	-5	-3	16.96	86.00	.648	13.48
-2			83.46	.572	11.90	.99
-1			80.92	.523	10.88	.91
0			78.38	.552	11.48	.96
1			75.84	.632	13.15	1.10
2			73.30	.618	12.86	1.07
3			70.76	.648	13.48	1.12
-6			15.05	75.84	.648	13.48
-6	0		78.38	.686	14.27	1.19
	-1		80.92	.651	13.54	1.13
	-6.5	-6.5	14.10	94.89	.651	13.54
-6	-6	15.05	93.62	.653	13.59	1.13
-5.5	-5.5	16.01	92.35	.666	13.86	1.15
-5	-5	16.96	91.08	.657	13.67	1.14

$U_{\text{nominal}} = 12 \text{ fps}$ 1 Volt = 20.805 fps

Coordinates are in inches. (l-w) is based on 12 fps

DATA SHEET

RUN NO 3/9
DATE 2/25

U_{nom} 10 RPM 1300 J_{nom} .378 Shaft rate _____
(Taps: 6/5 blue) Blade rate _____

Ithaco amp ① +80 db; Filter: Hi pass _____ Trans Anal _____
Lo pass _____ ② _____ db

Measuring Equipment: Input atten ③ 0.3U db Meas amp X (# of _____)
Output gain ④ X1 db Spect anal. _____ spectra _____

Temperature: (Start) water 78 air 75 Reynolds number: _____
(End) 78 75 8.19 x 10⁵

MAN	STAT	RPM	T	Q	GAIN CHANGE		K _T	J	σ	REMARKS
370	783	1300	762	221			.255	.38	22.49	19 15 12
371	665	1300	744	220.5	1	+70				13.2 9 6.5
371	606	1297	734	219.5						13 9 6.5
370	578	1299	734	220						13 9.2 7
371	559	1299	730	220						13.2 9 6.8
370	535	1300	732	221						13.4 9.1 7
371	509	1301	730	221						13.5 9 6.2
371	483	1302	728	221.5						13 8.6 6
371	460	1302	724	221.5						13.5 8 5.4
371	436	1300	718	221						12.6 8.2 6
370	409	1300	714	220.5						11.9 7.6 5.8

TU
X

DATA SHEET

RUN NO 419

DATE 2/25

U_{nom} 16 RPM 1050 J_{nom} .746 Shaft rate _____
 (Taps: 6/5 blue) Blade rate _____

Ithaco amp^① +60 db; Filter: Hi pass _____ Trans Anal _____
 Lo pass _____ ② _____ db

Measuring Equipment: Input atten^③ .3V db Meas amp X (# of _____)
 Output gain^④ x1 db Spect anal. _____ spectra _____

Temperature: (Start) water 78 air 75 Reynolds number: _____
 (End) 78 75 6.86 x 10⁵

MAN	STAT	RPM	T	Q	GAIN CHANGE	K _T	J	σ	REMARKS	
917	747	1050	174	72		0.09	0.72	8.30	12.4 8.1 6	
909	699	1050	170	72.5				7.84	12.6 8.1 6.1	
908	650	1050	160	71.5				7.29	13.1 8.8 6.2	
912	611	1050	156	72				6.82	13 8.8 6.2	
911	577	1050	154	71.5				6.45	13.5 9 6.6	
911	546	1050	150	72.5				6.10	13.4 9 6.8	
912	521	1050	144	71.5				5.81	13.7 9.2 7	
912	488	1050	140	72				5.44	13.5 9.1 7.0	
912	488	1050	1	—						
912	455	1050	138	72.5				5.07	13.8 9.2 7.1	
911	415	1050	132	72.0				4.62	14.2 10 7.2	
912	389	1050	128	72.0				4.33	15 10.7 7.9	
912	364	1050	124	71.5				4.05	17 13 10.5	
913	321	1050	114	70.5	1 +50			3.56	14 11.6 10	
913	300	1050	106	70.0				3.32	15.4 12 8.4	
906	260	1050	100	69.5	1 +60				8 2 10	
					observed by Leubbers					

T
X
cut

DATA SHEET

RUN NO 819

DATE 2/25

U_{nom} 16

RPM 1510

J_{nom} 0.519

Shaft rate _____

(Taps: 6/5 blue)

Blade rate _____

Ithaco amp ① +60 db; Filter: Hi pass _____

Trans Anal _____

Lo pass _____

② _____ db

Measuring Equipment: Input atten ③ 0.3V db Meas amp X (# of
Output gain ④ x1 db Spect anal. _____ spectra _____)

Temperature: (Start) water 78 air 75 Reynolds number:

(End) 78 75 9.62×10^5

MAN	STAT	RPM	T	Q	GAIN CHANGE		K_T	J	σ	REMARKS
912	749	1510	784	240			0.195	0.51	8.38	149 10.9 8.7
911	658	1509	770	240						148 10.9 8.6
912	614	1510	766	240						14.7 10.9 8.5
911	567	1510	754	241						14.7 10.6 8.7
911	519	1510	750	241					5.80	14.7 10.8 8.4
913	486	1510	744	241						14.7 10.5 8.4
913	451	1510	738	241						14.5 10.4 8.0
912	422	1510	736	241.5					4.70	14.4 10.1 7.9
911	378	1510	730	241.5					4.21	15.4 11.0 8.2
913	345	1510	718	240					3.83	19 14.6 11.8
912	320	1510	712	239	1	+50			3.55	12 7 3.6
912	287	1510	698	242.5					3.18	10.5 5 1
910	267	1510	662	240	1	+60				1 20 20
Obscured by bubbles										

BACK *

DATA SHEET

RUN NO 3

DATE 2/26

U_{nom} 20 RPM 1800 J_{nom} .543 Shaft rate —
 (Taps: 6/5 blue) Blade rate —

Ithaco amp 1 +50 db; Filter: Hi pass — Trans Anal —
 Lo pass — 2 db

Measuring Equipment: Input atten 3 0.30 db Meas amp α (# of
 Output gain 4 x1 db Spect anal. — spectra —)

Temperature: (Start) water 83 air 75 Reynolds number:
 (End) 85 75 1.16x10⁶

MAN	STAT	RPM	T	Q	GAIN CHANGE		K _T	J	σ	REMARKS
1403	715	1800	1040	325.0			.183	.53	5.09	7.4 3.0 0.5
1402	691	1800	1036	328.5						7.6 3.1 0.5
1402	643	1800	1038	325.5					4.58	7.9 3.0 0.5
1402	607	1800	1034	326.0					4.32	7.5 3.1 0.2
1401	568	1800	1016	326.0					4.04	12.6 7.1 3.8
1404	543	1800	1010	325.0					3.85	18.8 15.2 14.6
1404	527	1800	1004	324.5	1	+40			3.73	9.6 7.0 5.9
1403	506	1800	1006	325.0					3.59	10.5 8.0 6.8
1405	489	1800	1000	324.0					3.46	11.4 8.5 7.7
1406	469	1800	970	330.5					3.31	11.7 9.0 7.9
1404	445	1800	978	323.0					3.14	12.1 8.9 7.0
1406	426	1800	966	322.5					3.00	12.1 7.9 5.0

BB
*
TV
*

DATA SHEET

RUN NO 1

DATE 2/27

U_{nom} 10
(Taps: 6/5 blue)

RPM 1200 J_{nom} 0.41

Shaft rate —

Blade rate —

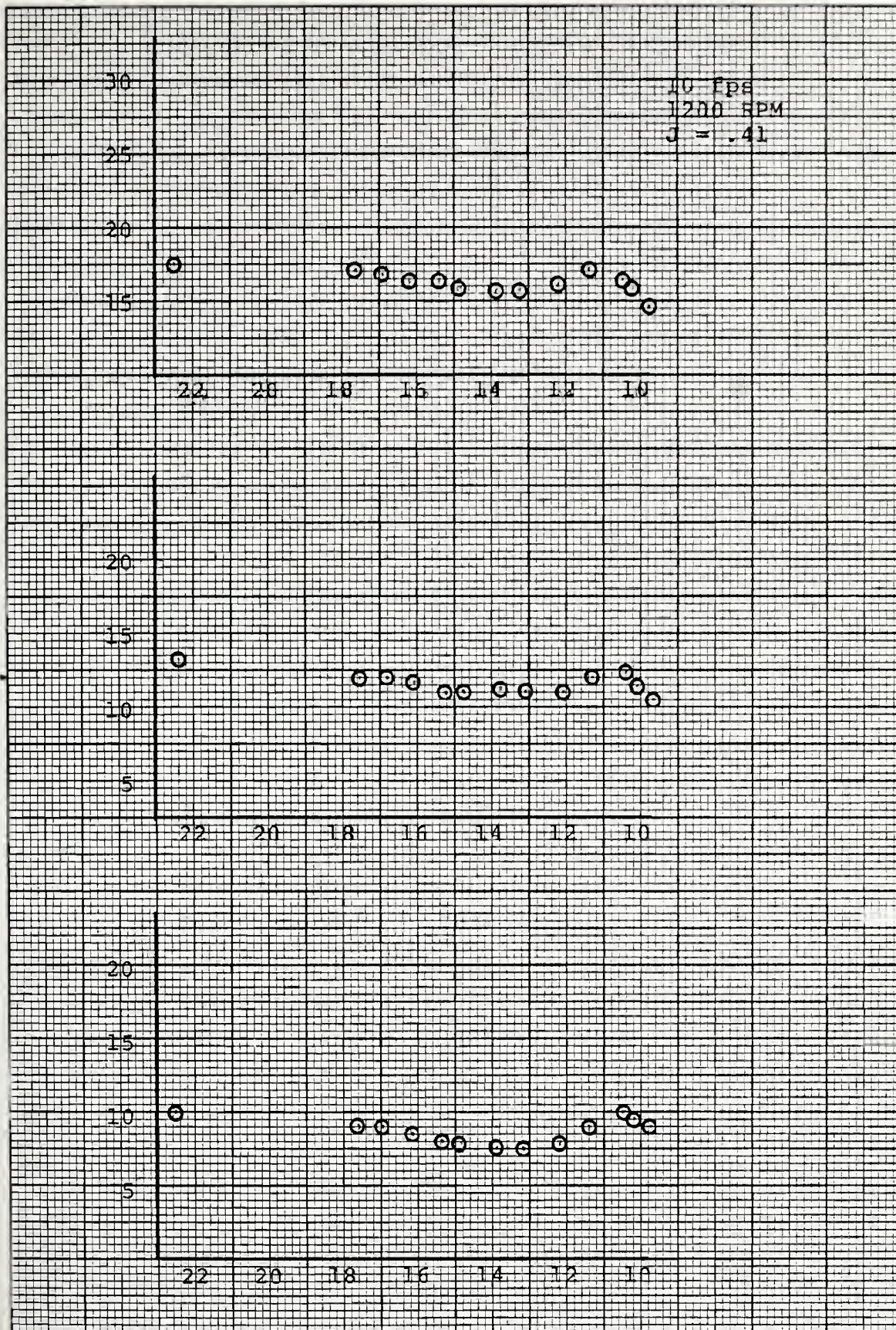
Ithaco amp ① +70 db; Filter: Hi pass — Trans Anal
Lo pass — ② db

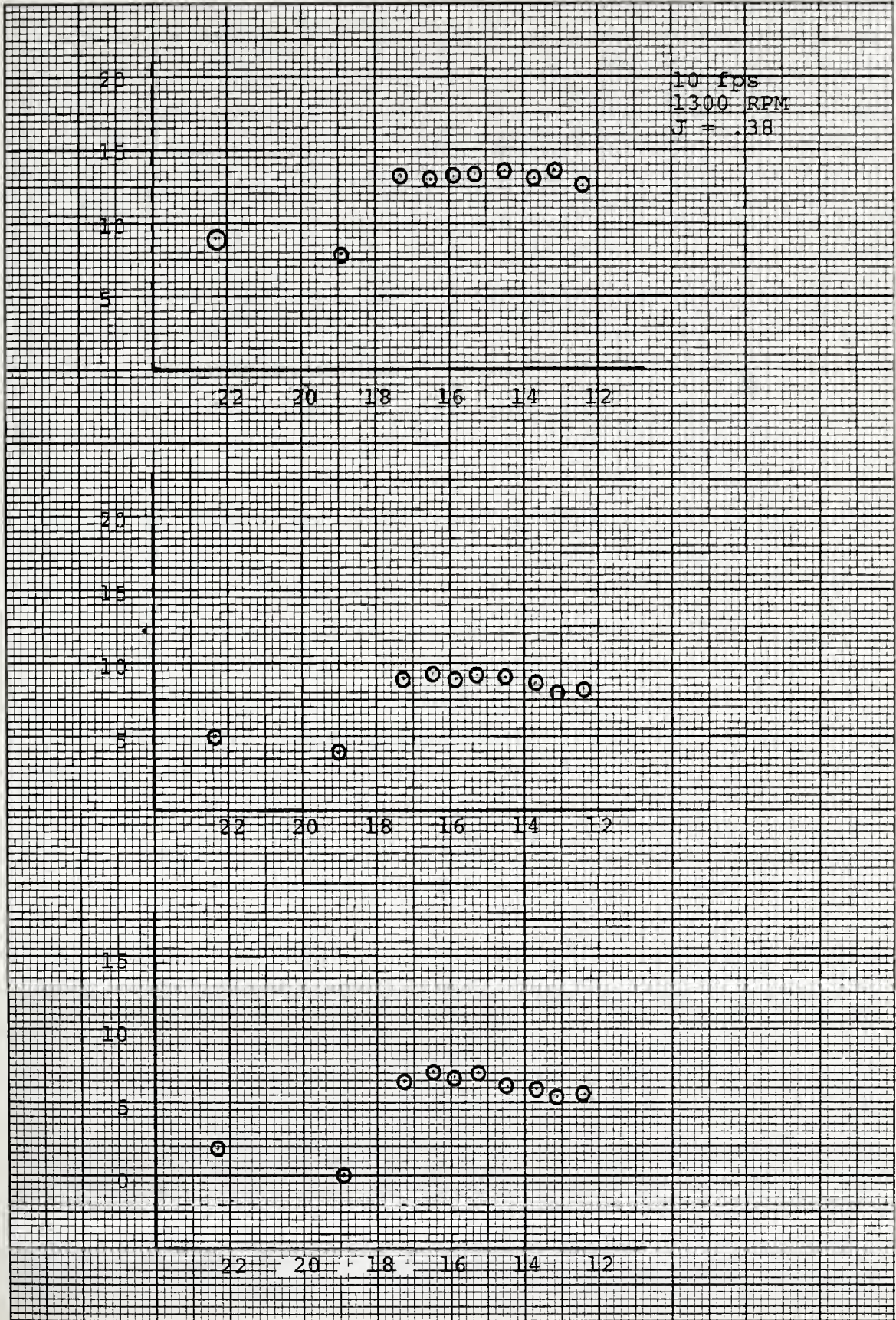
Measuring Equipment: Input atter ③ 0.3V db Meas amp X (# of
Output gain ④ X1 db Spect anal. — spectra —)

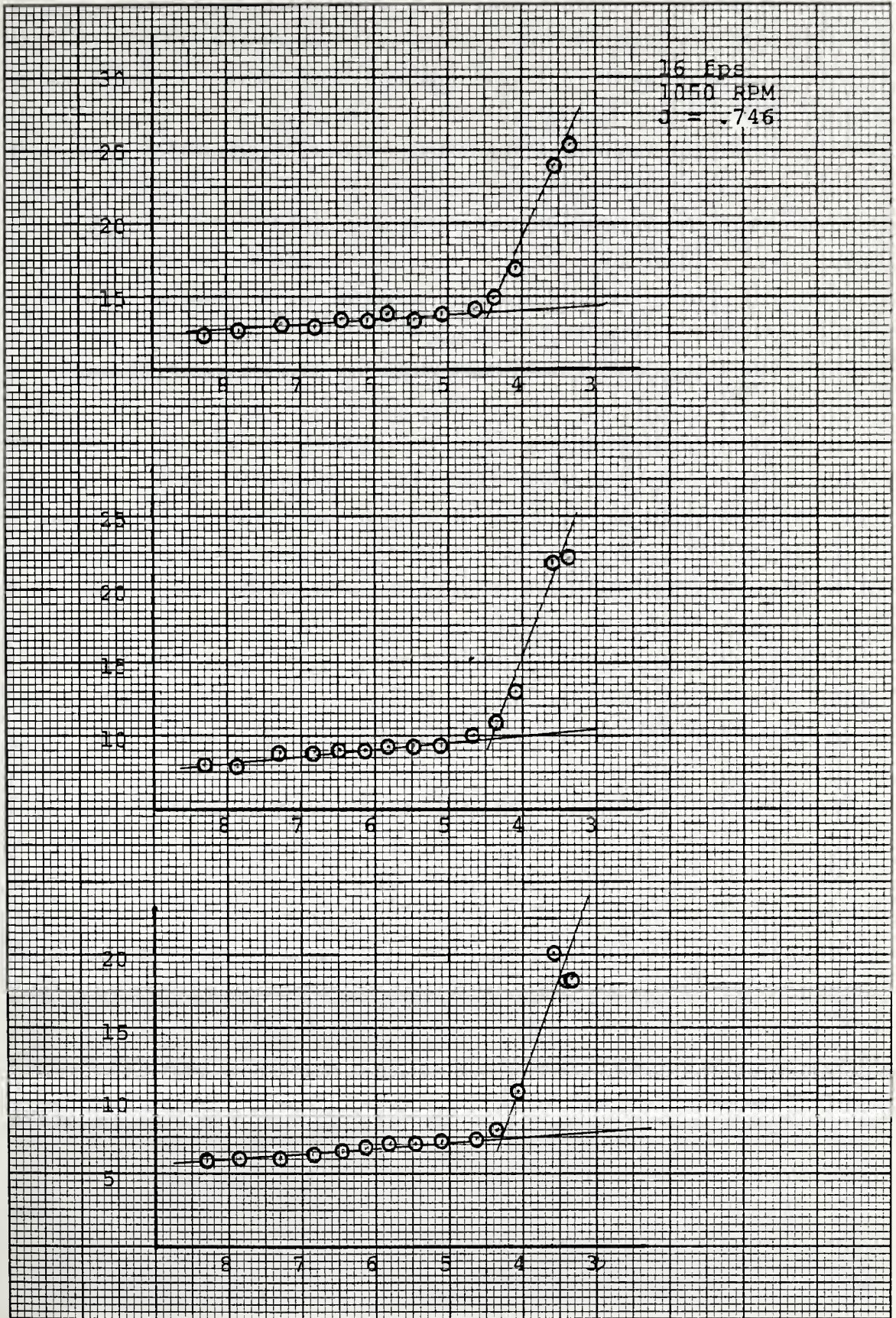
Temperature: (Start) water 87 air 77 Reynolds number:
(End) 87 77 8.32×10^5

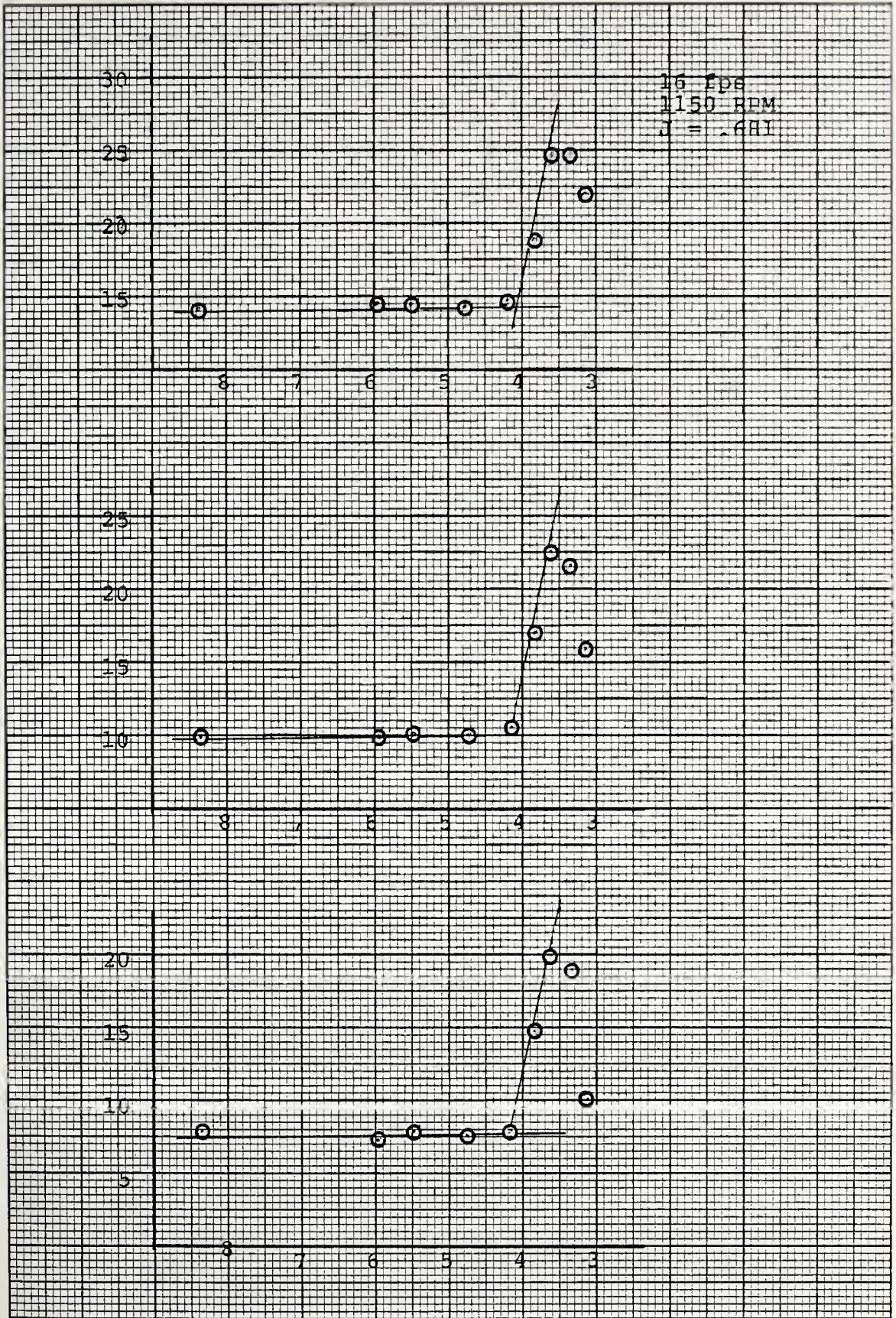
MAN	STAT	RPM	T	Q	GAIN CHANGE		K_T	J	σ	REMARKS
17	BAL 757.1		2	9.5						TARE
373	770	1200	610	181			0.238	0.42	22.08	7.1 3.6 0.2
374	726	1200	602	180						8.0 3.1 0.1
373	657	1200	596	180.5						8.0 3.5 0
374	615	1200	590	180.5					17.53	8.3 3.7 0.1
374	592	1200	586	180						8.1 3.0 0
374	566	1200	582	180						7.9 3.1 0
373	543	1200	580	180					15.49	7.9 3.1 <0
373	520	1200	578	180						7.6 2.8 <0
373	501	1200	576	180	1	+80			14.27	18.4 13.3 10.2
373	477	1200	572	180					13.58	15.2 12.5 9.2
371	458	1200	570	180						16.1 12.2 9.5
372	433	1200	568	180						15.8 12.2 9.6
372	405	1200	562	179.5					11.52	14.1 11.5 10.5
374	376	1200	558	179.5						10 6 7.5
372	345	1200	552	178.5						<0 <0 6
373	321	1200	548	178.5						<0 <0 2

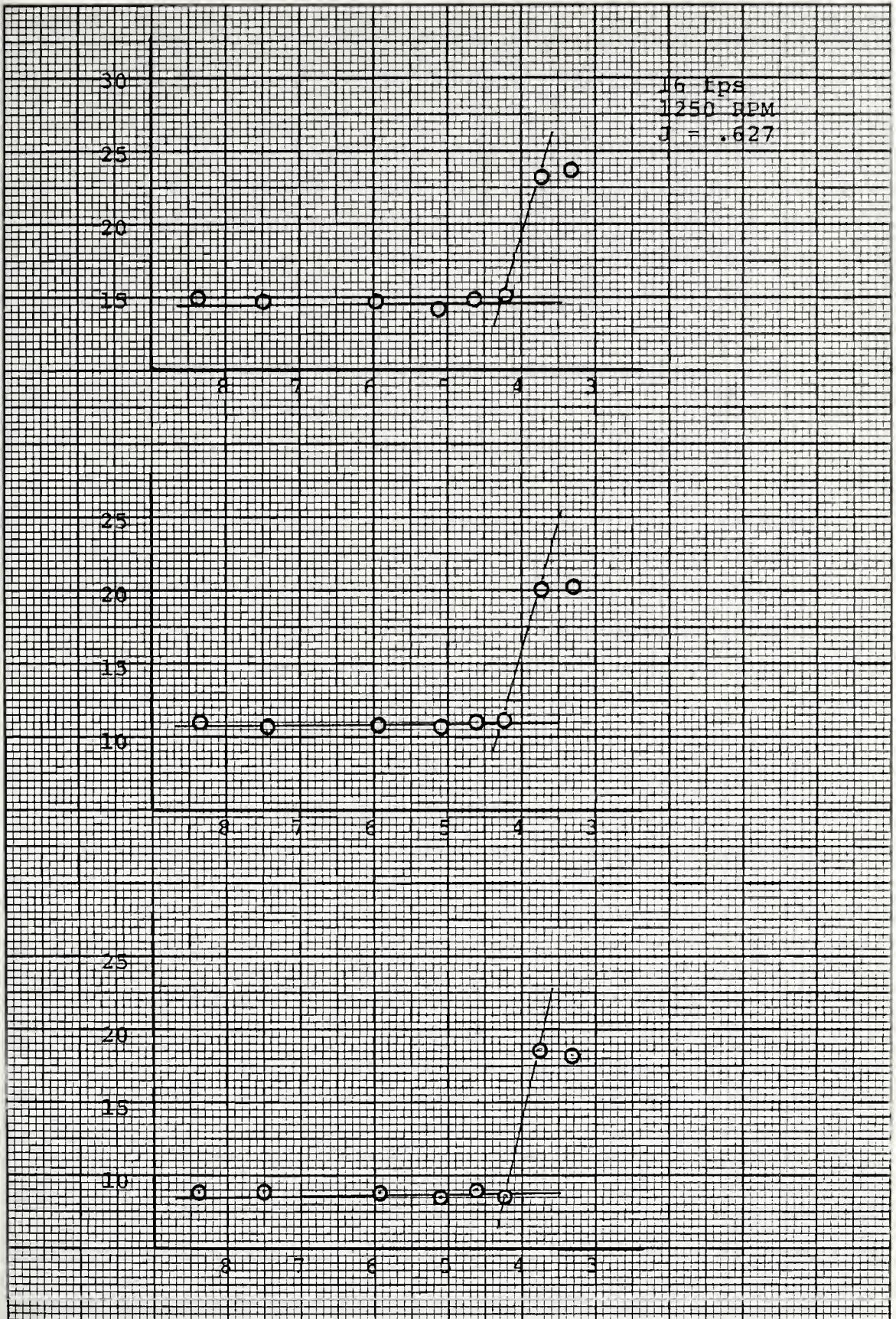
JL

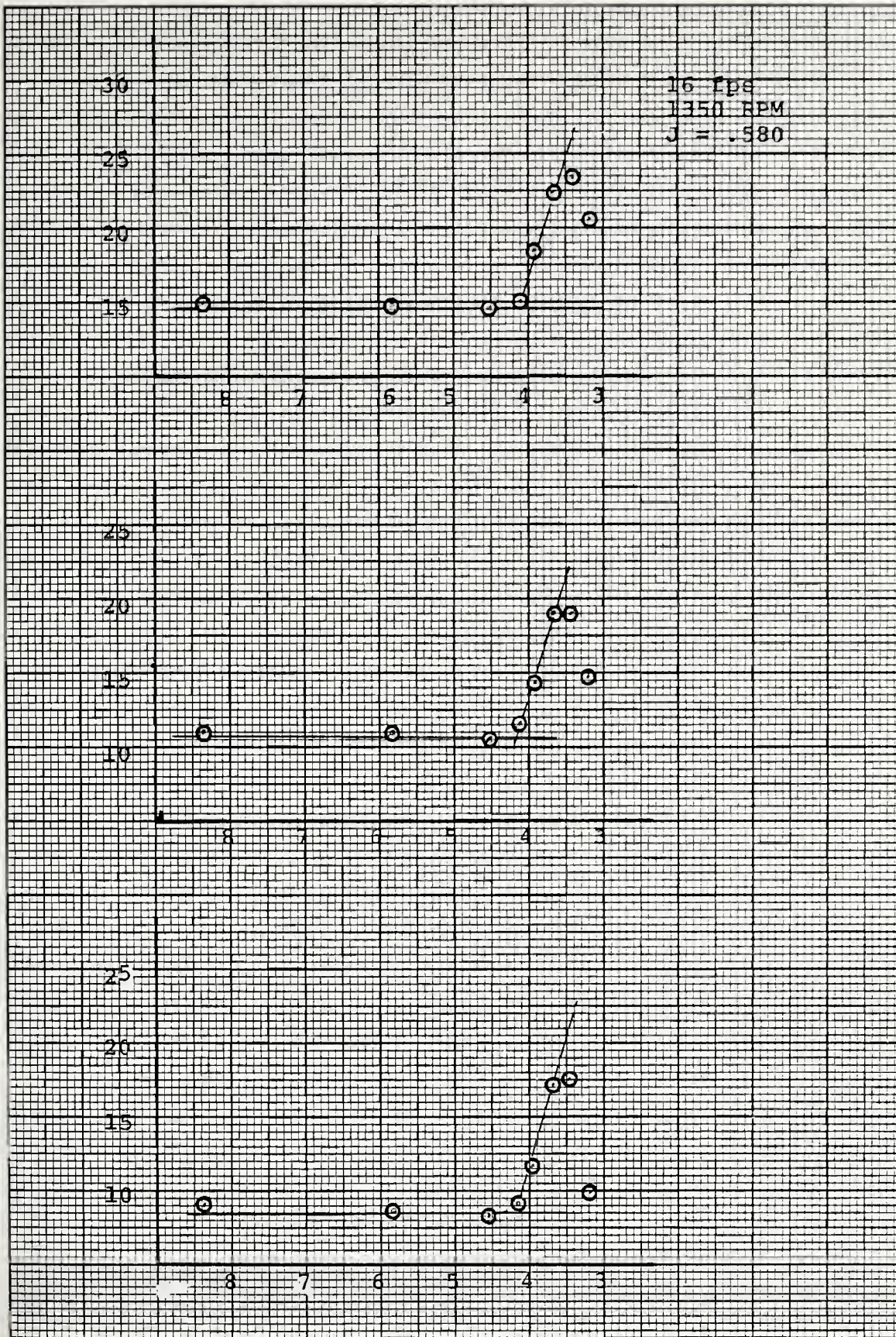


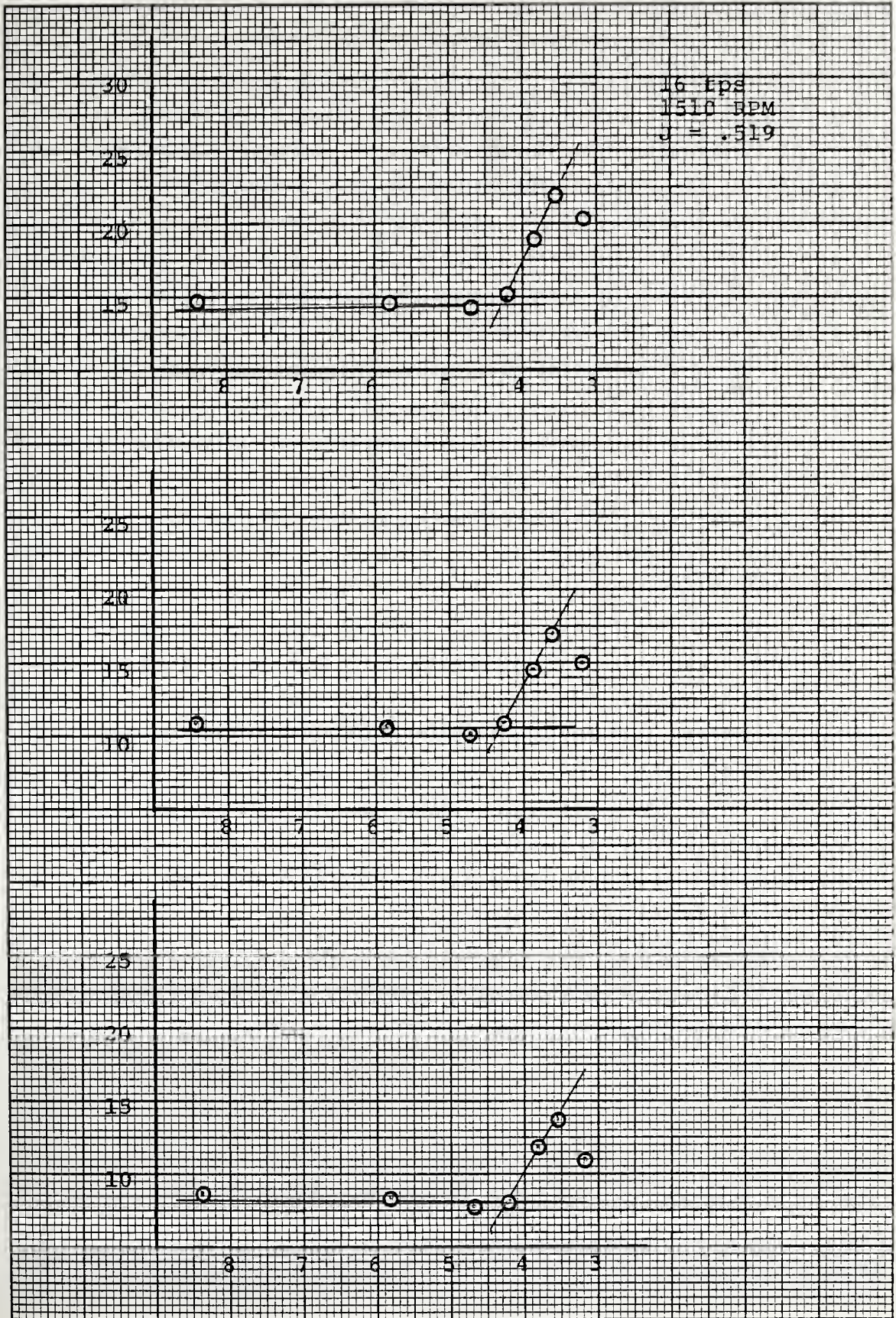


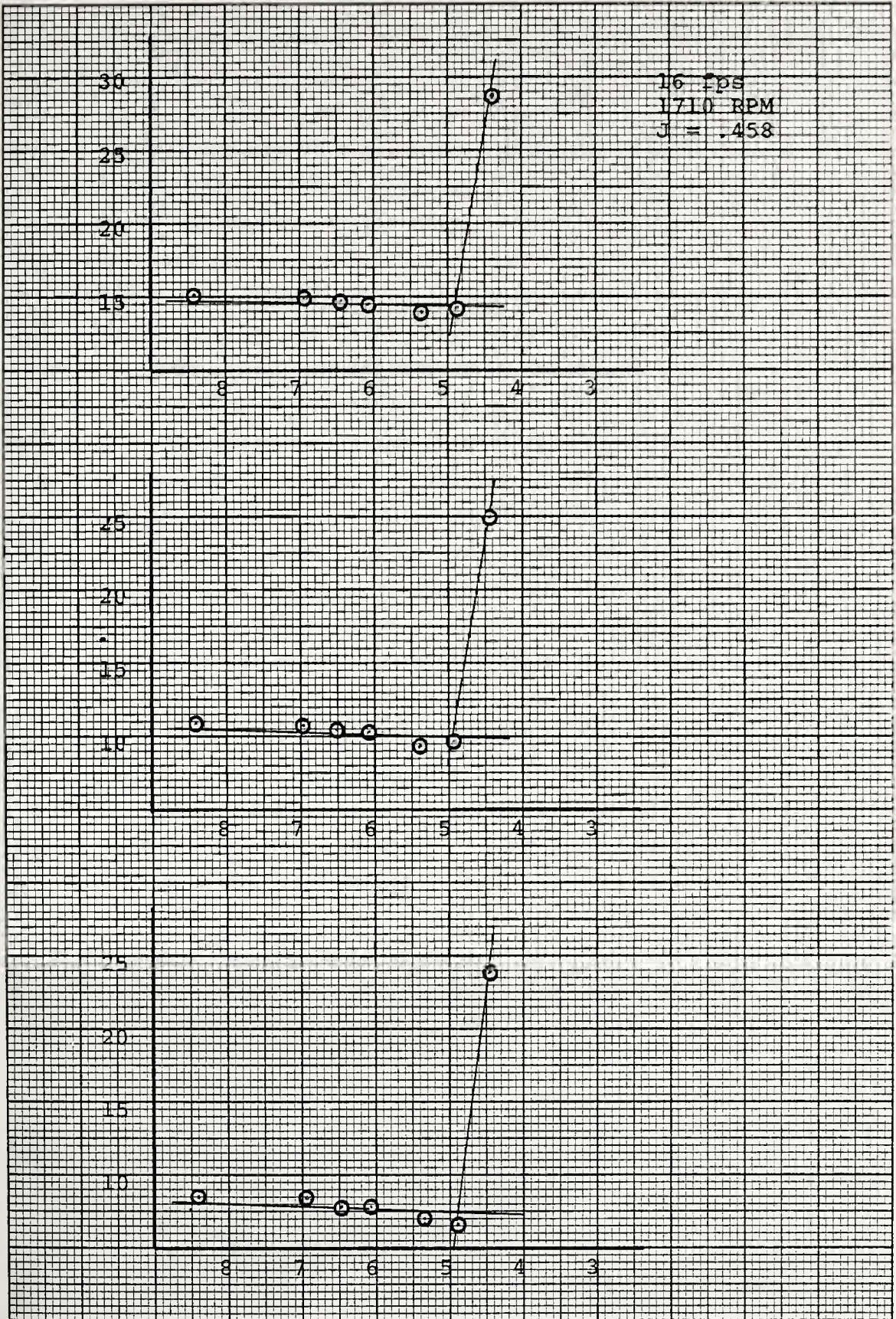


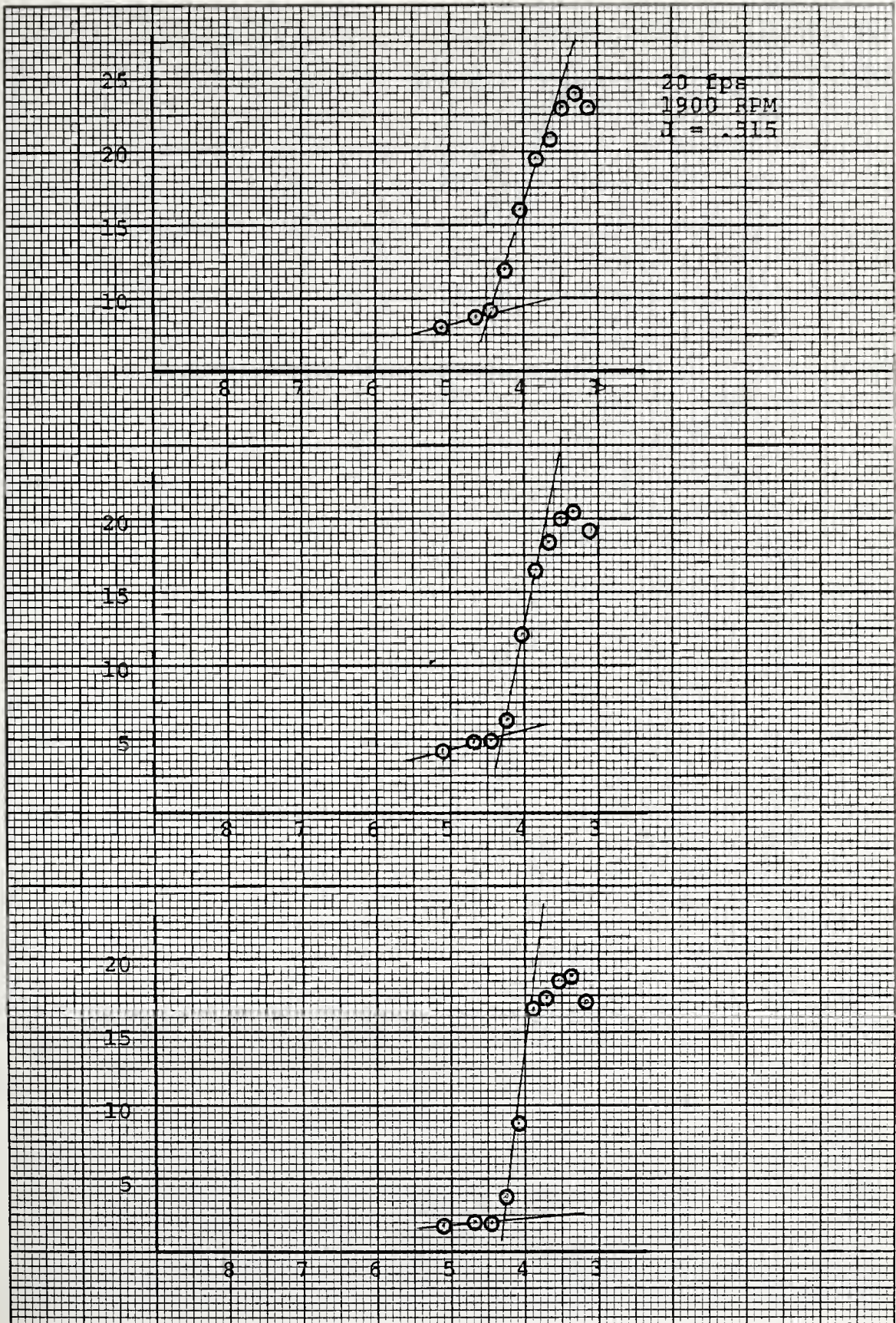


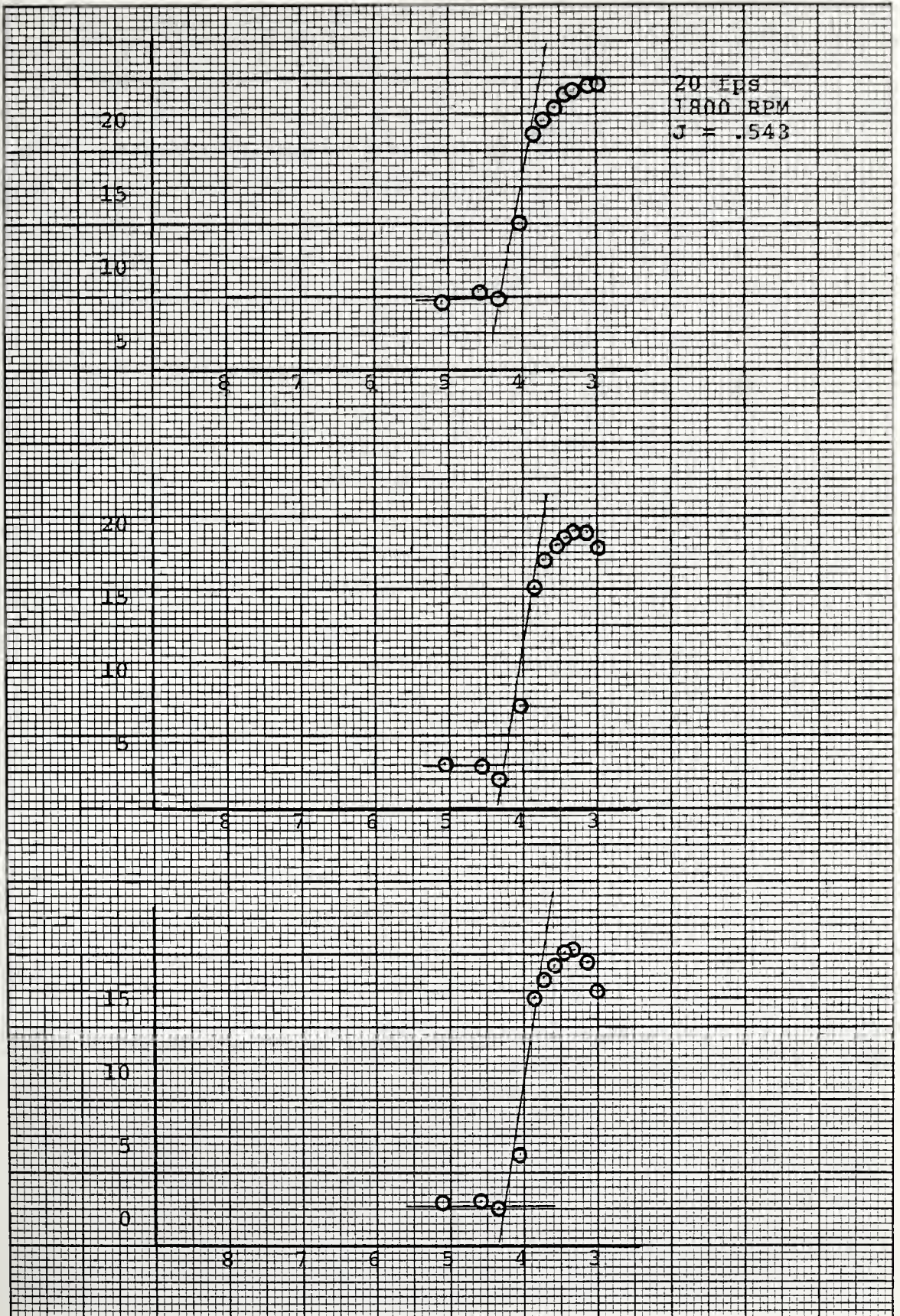


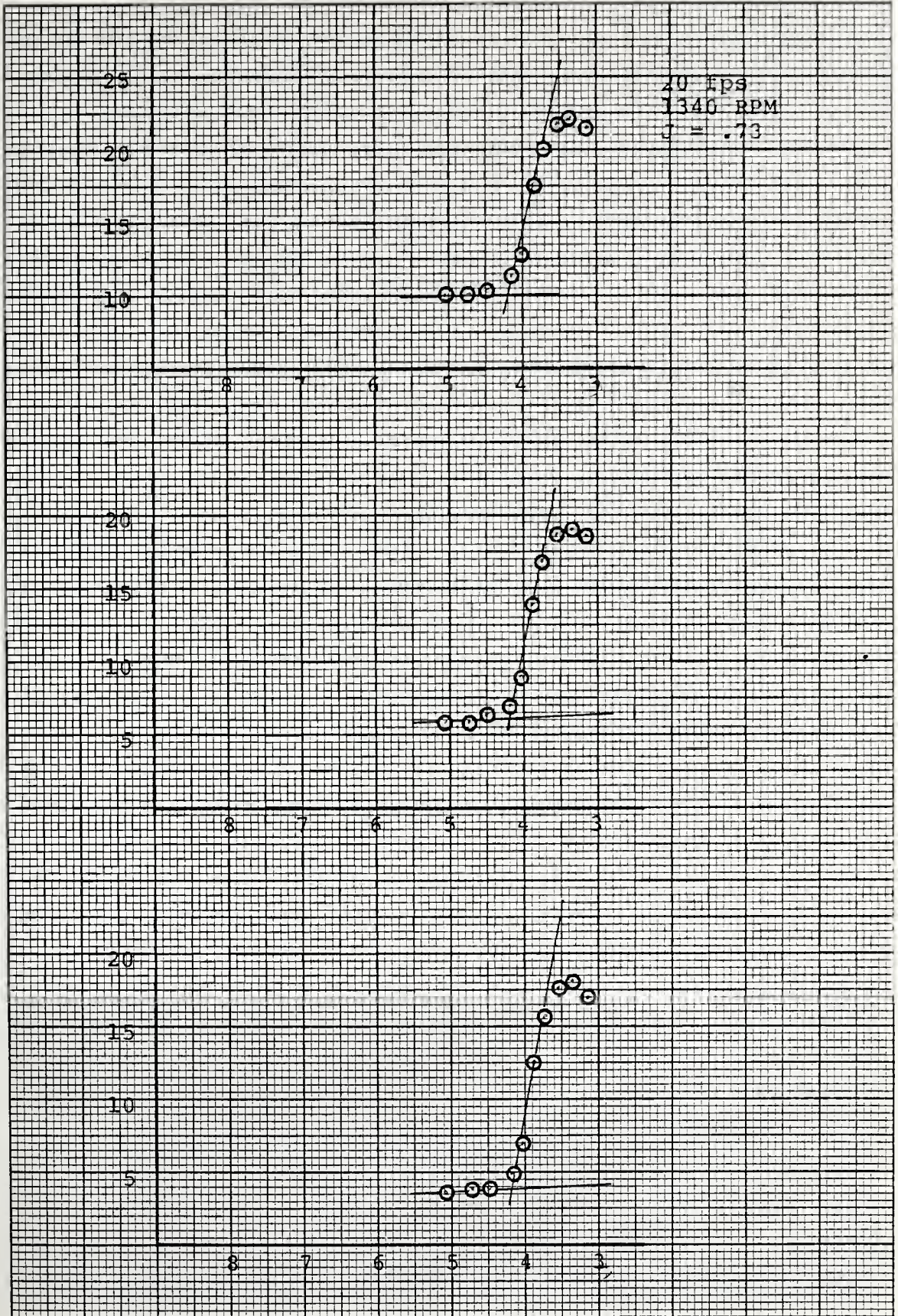


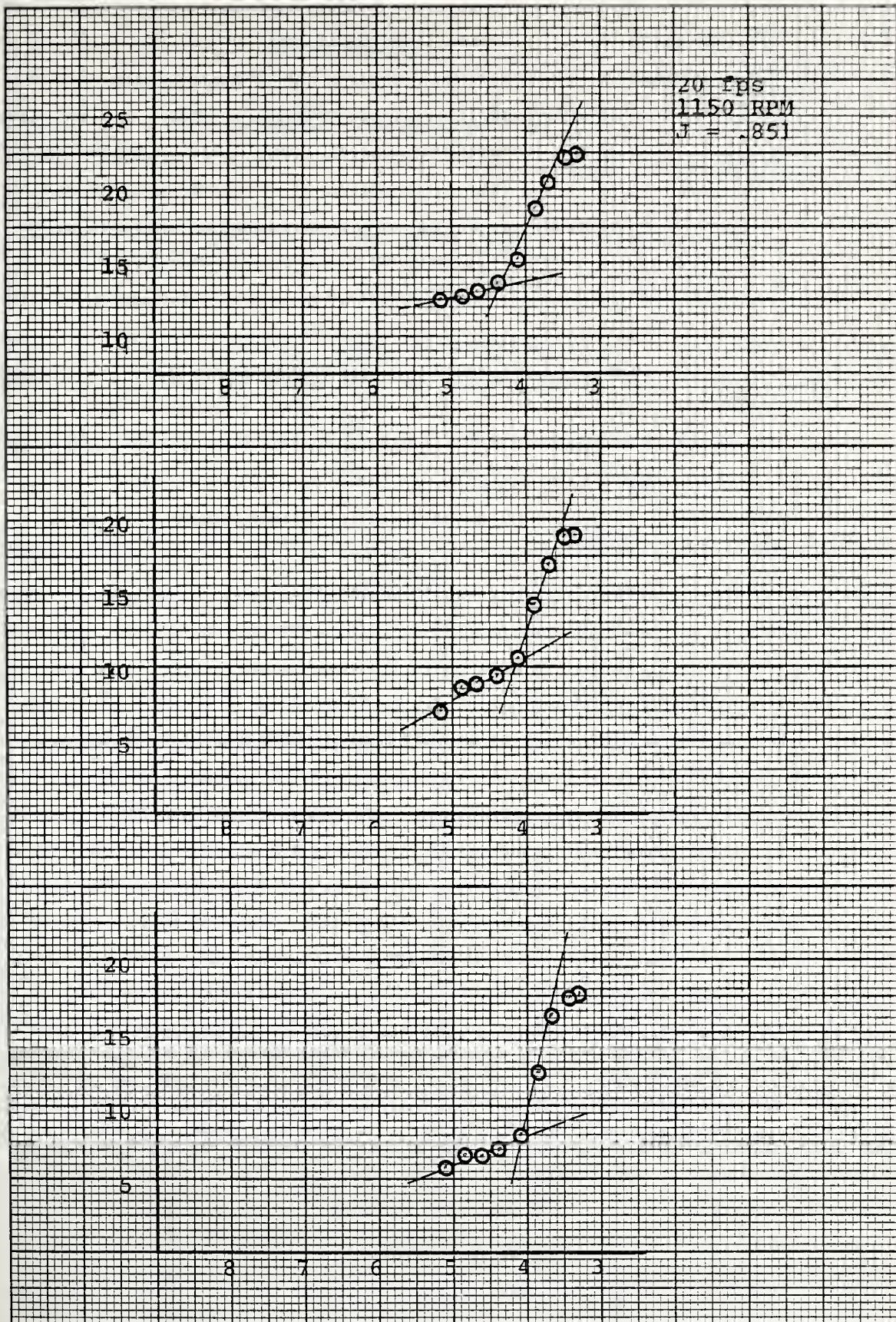




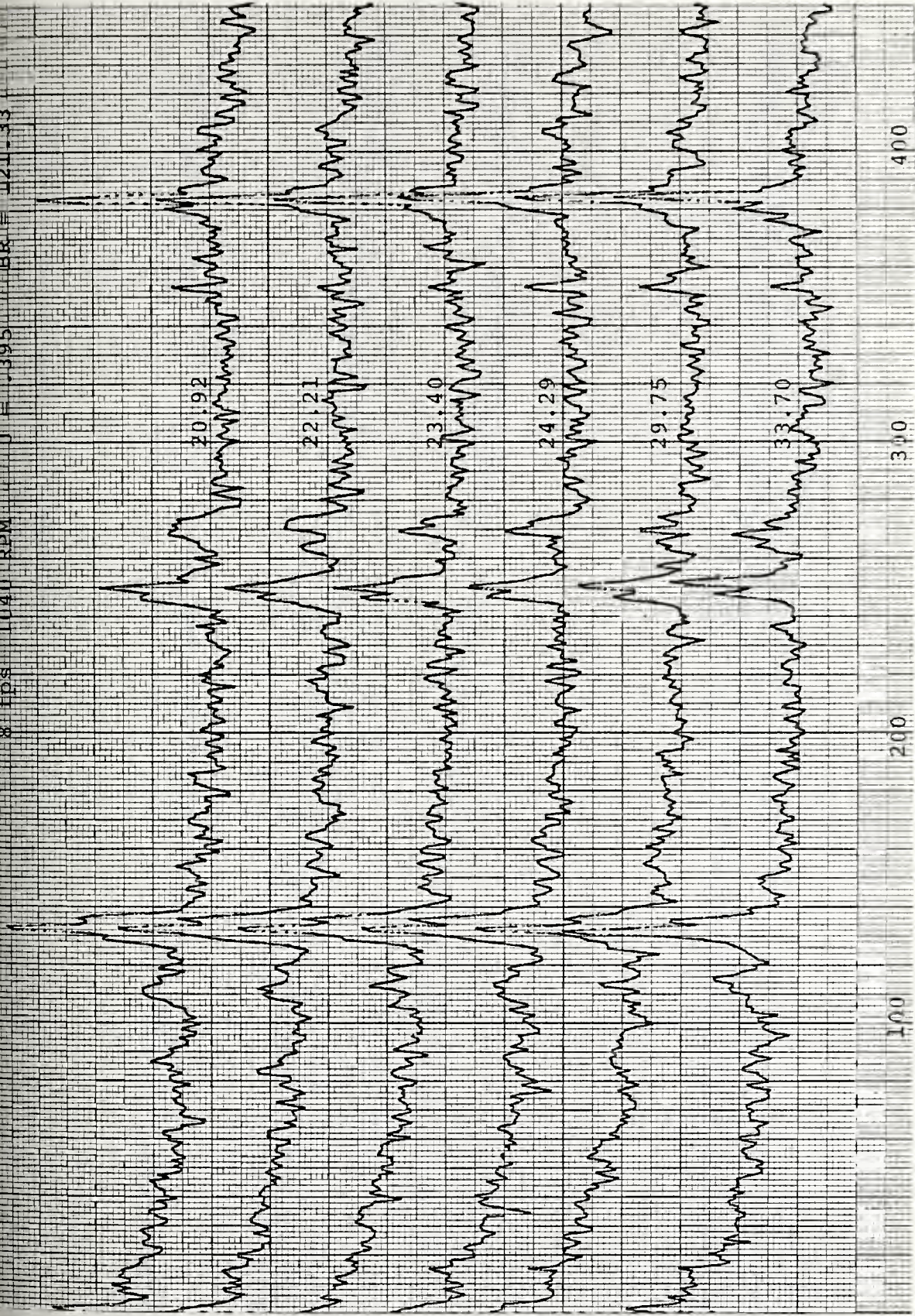




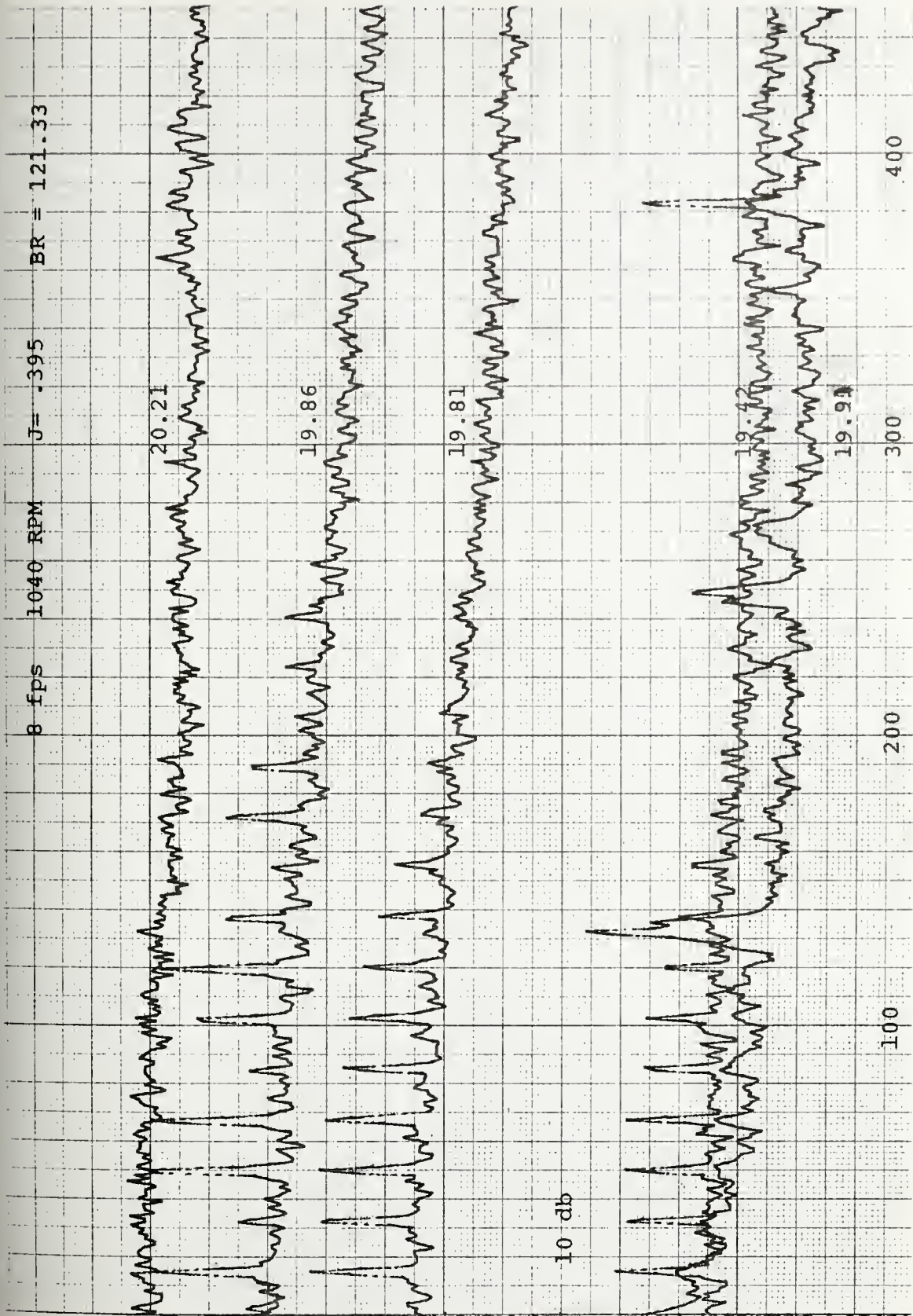




8 fps 1040 RPM J = .395 BR = 121.33

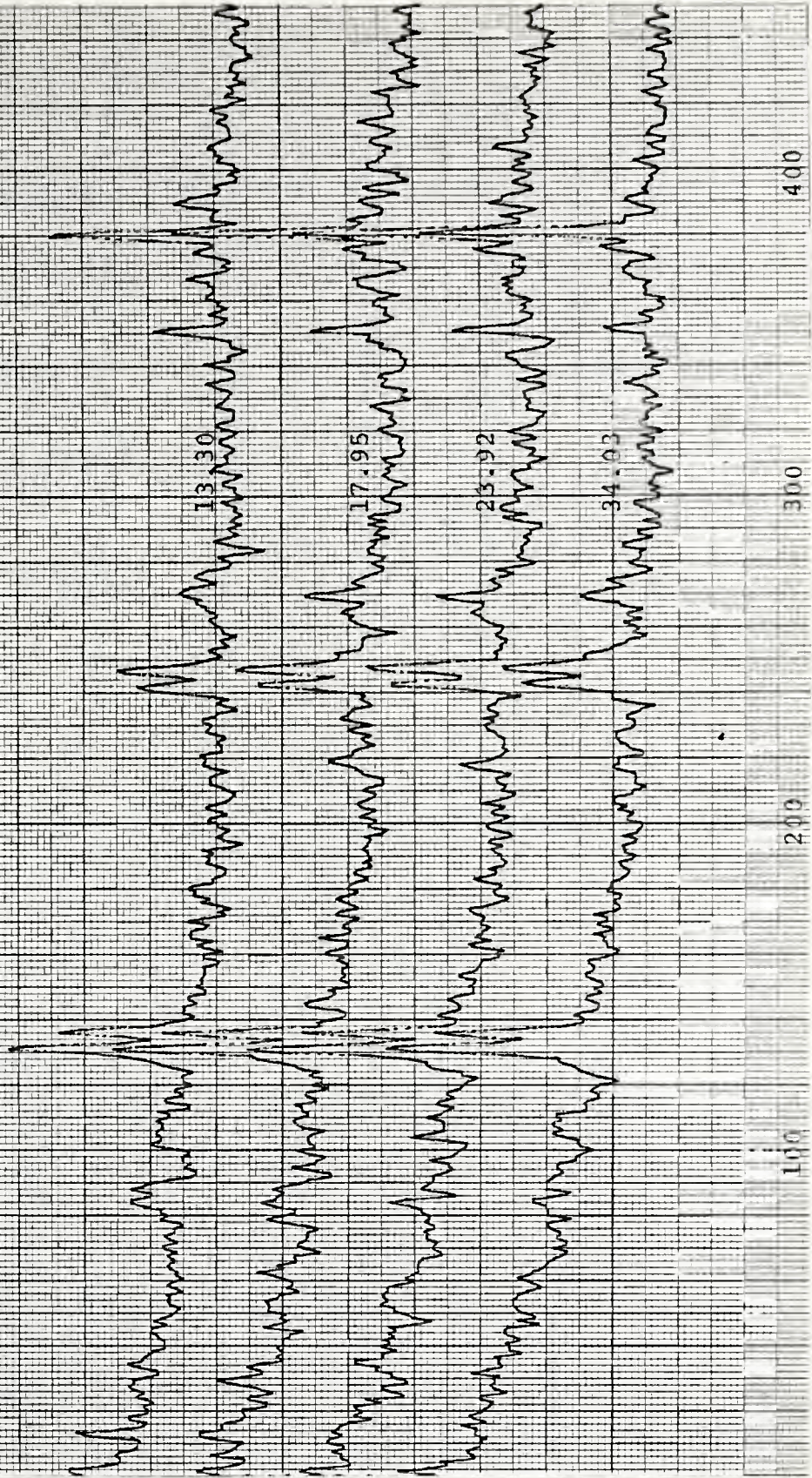


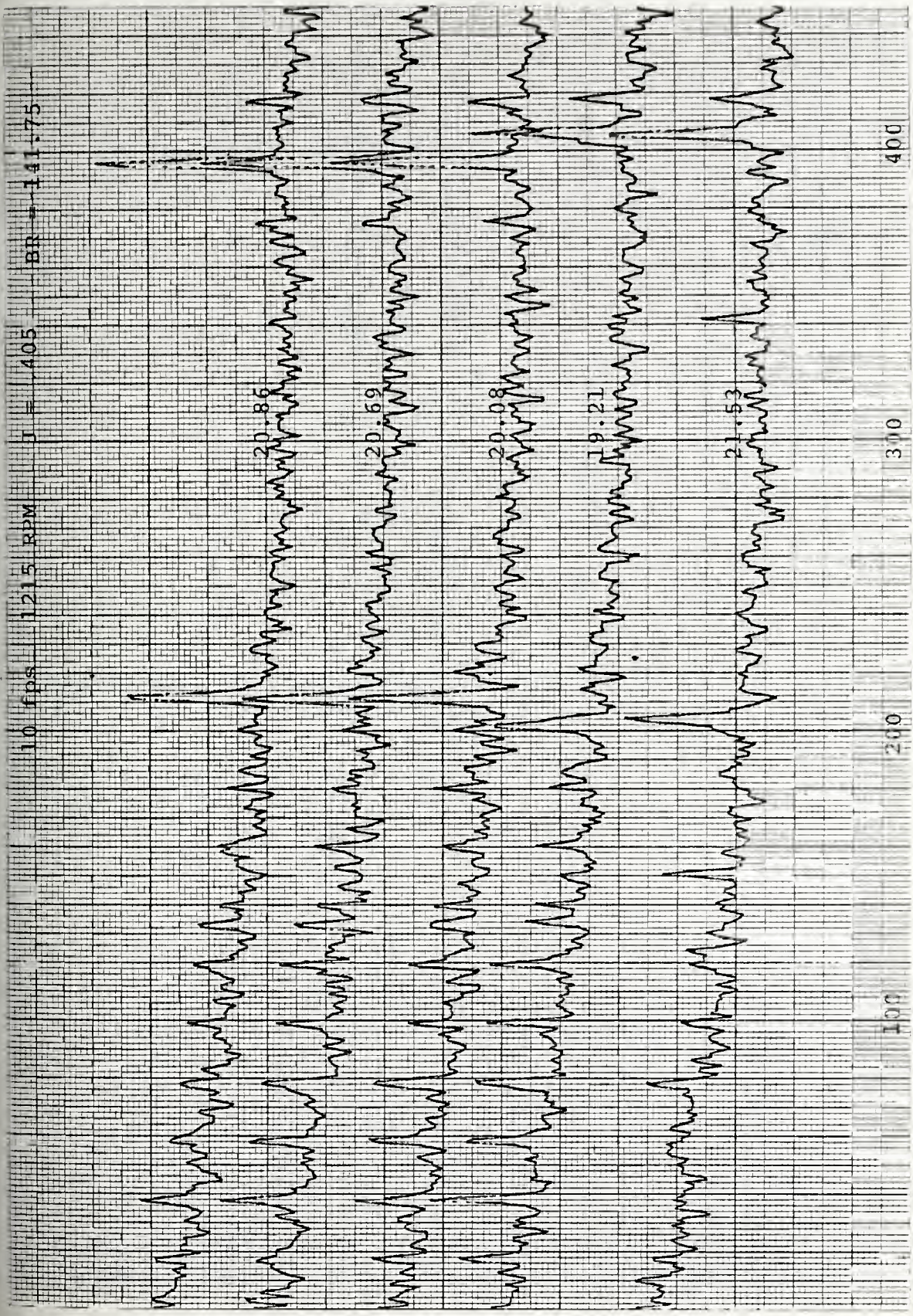
100 200 300 400



8 FPS 975 RPM J = .41

BR = 113.75



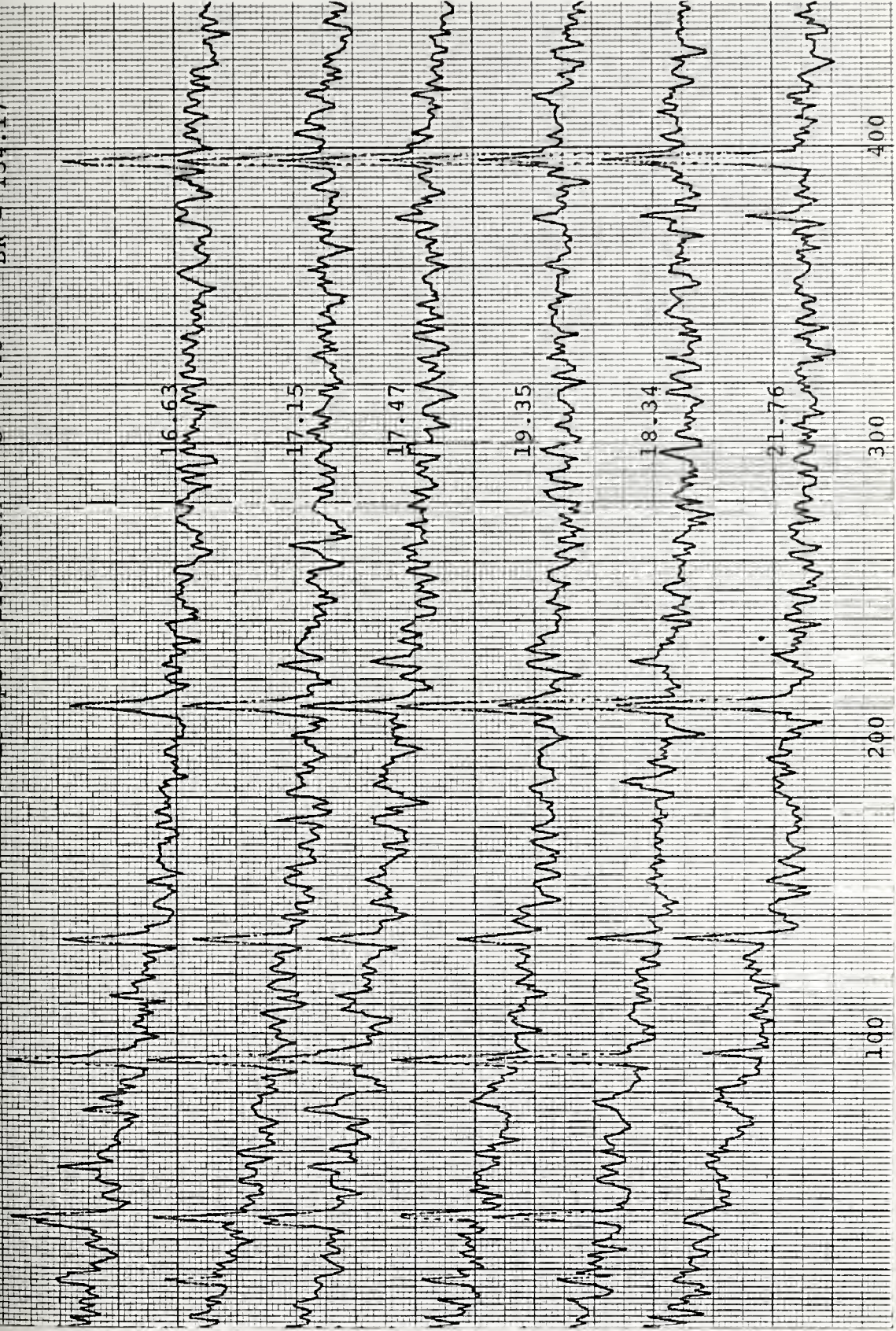


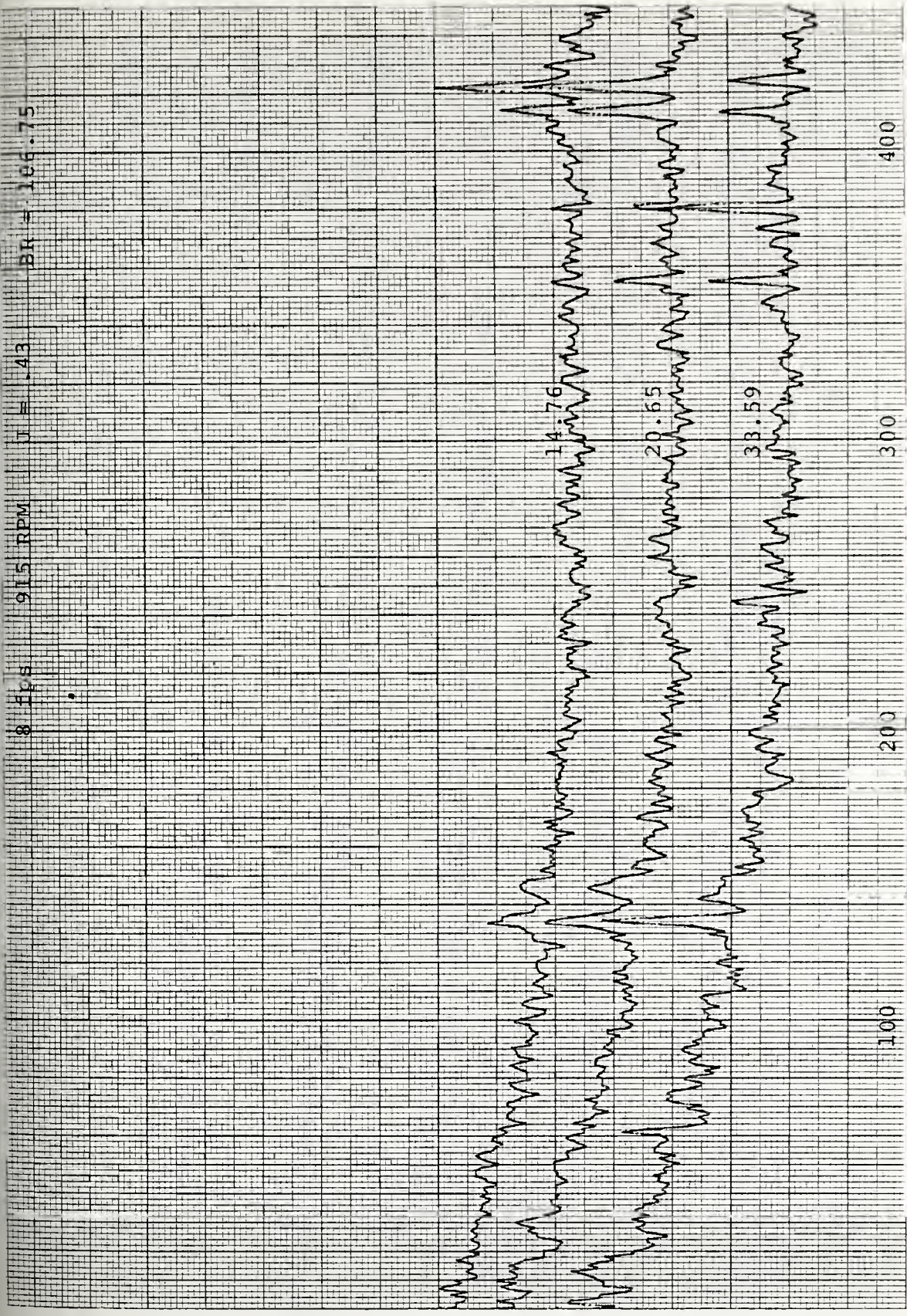
BR = 134.17

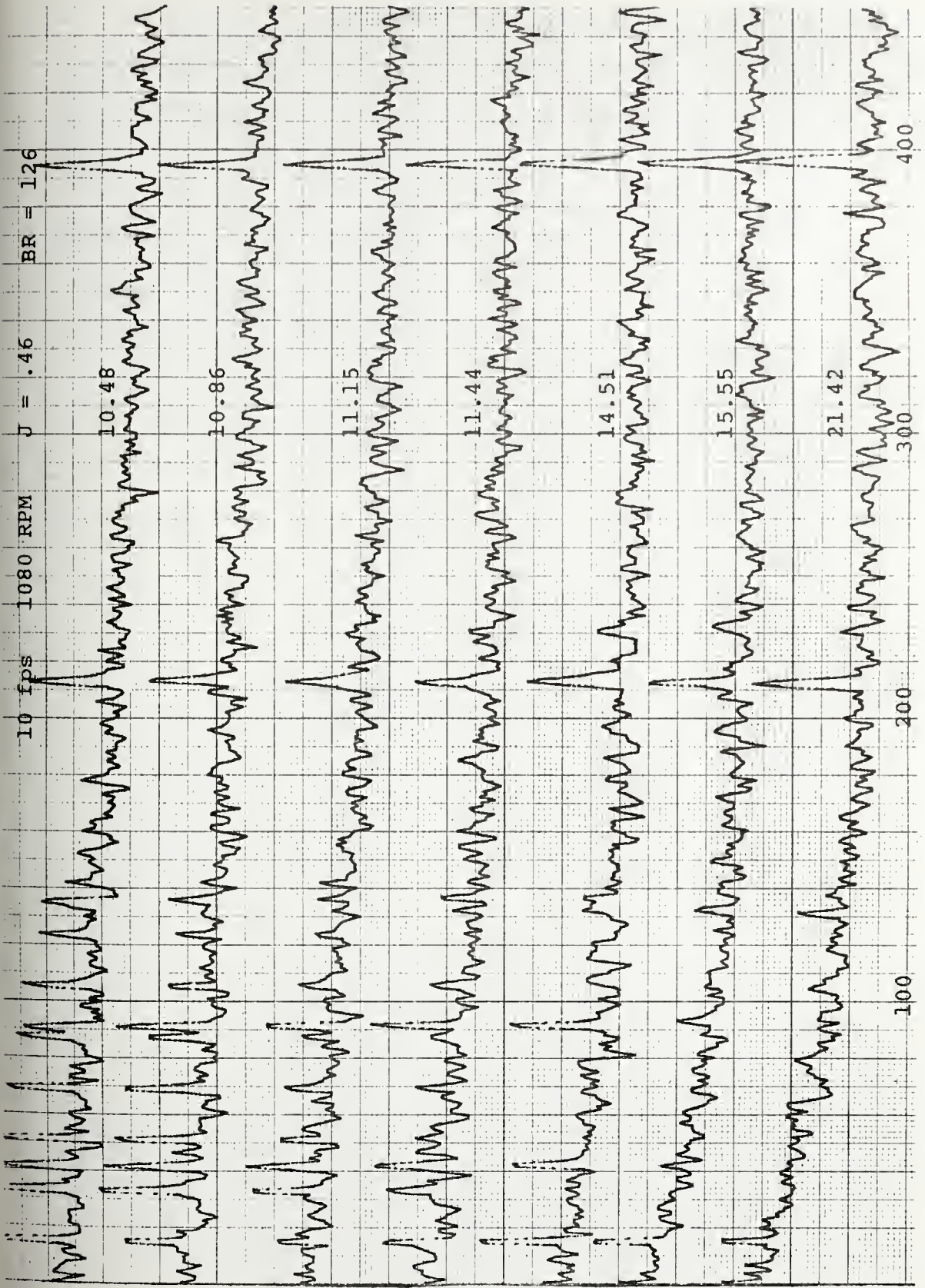
J = .43

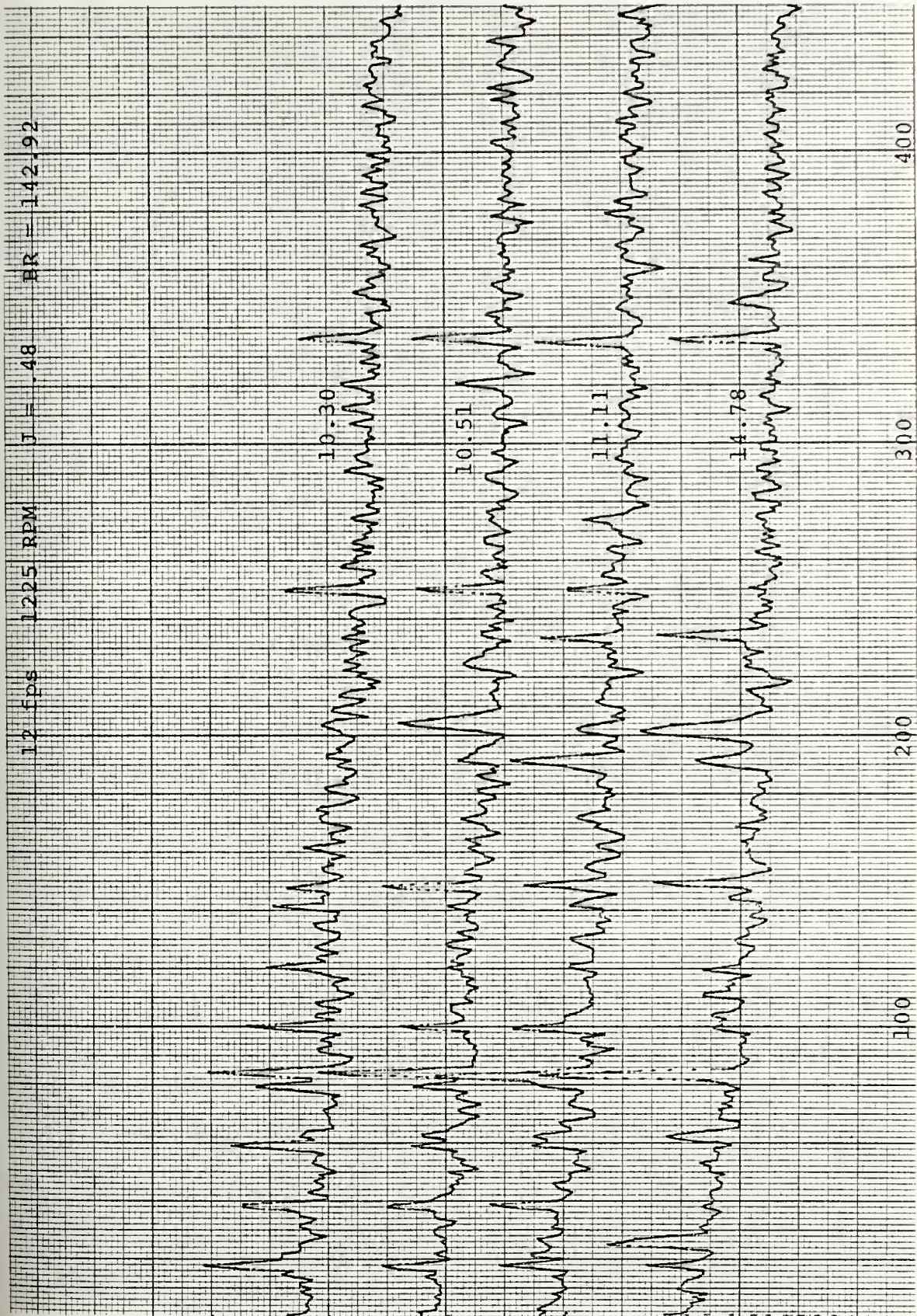
1150 RPM

10 fps







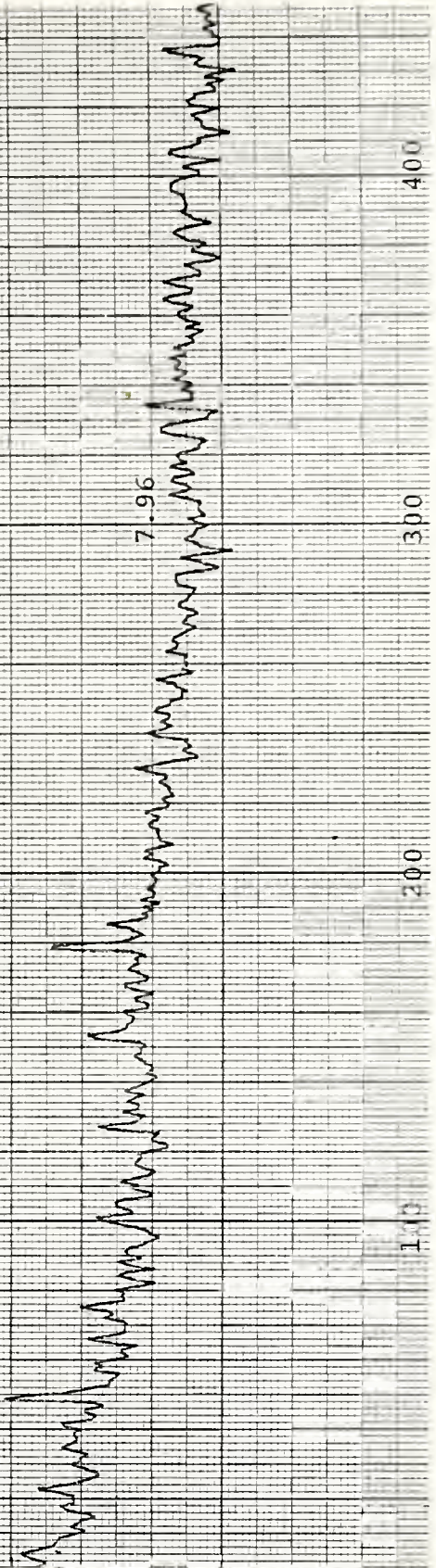


BR = 180.83

J = 5

1550 RPM

16 fps



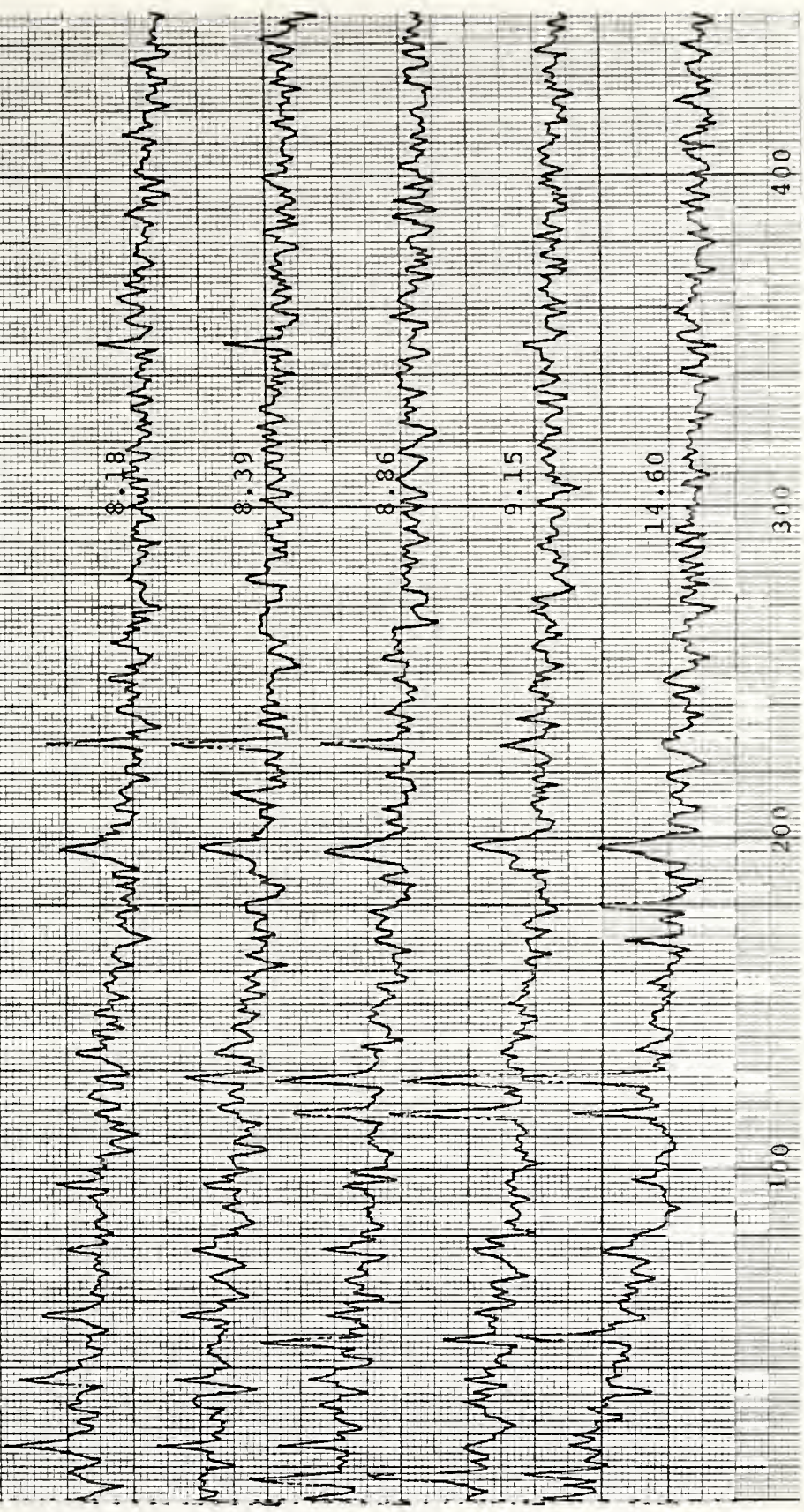
BR = 137.08

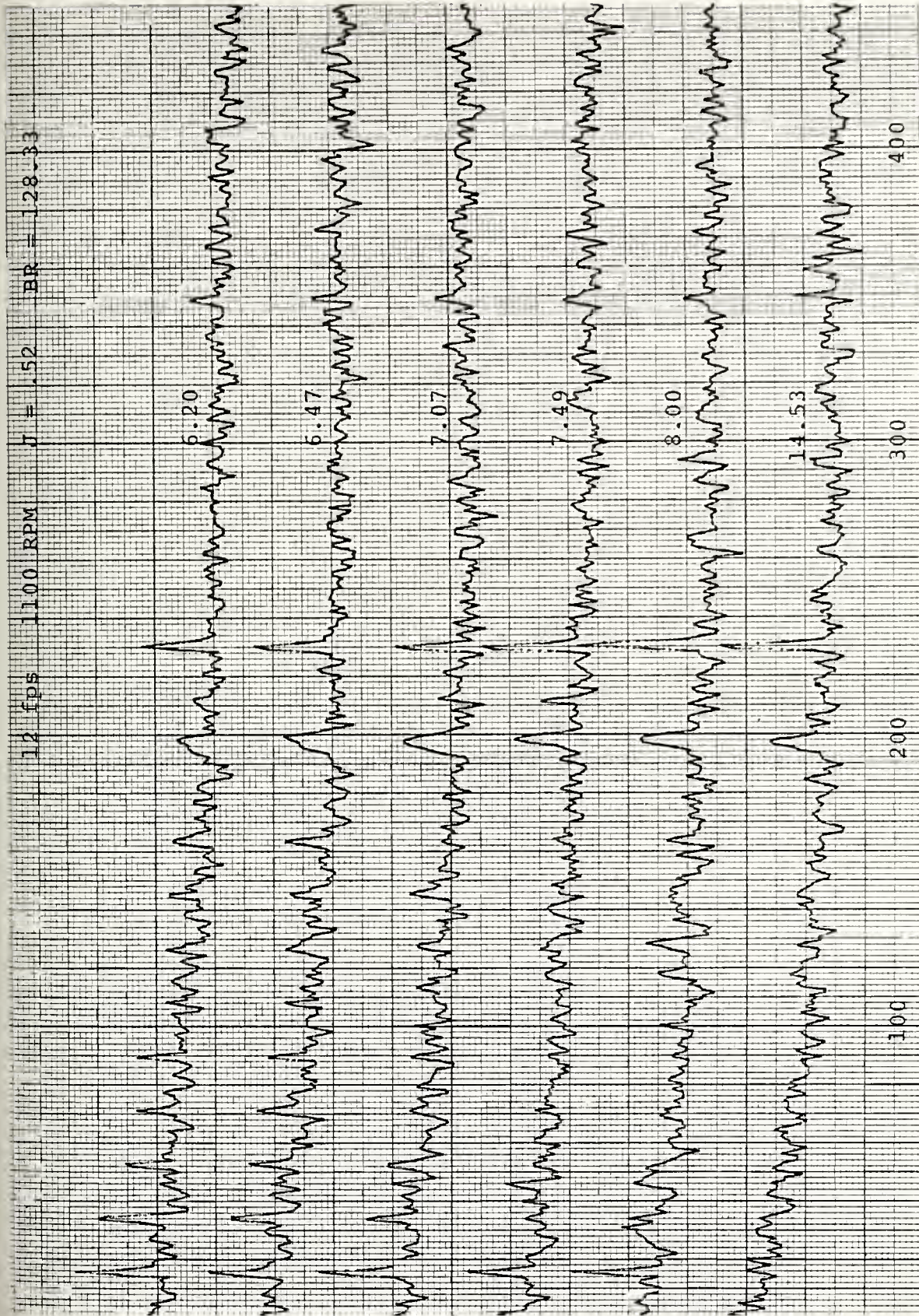
I = 1.5

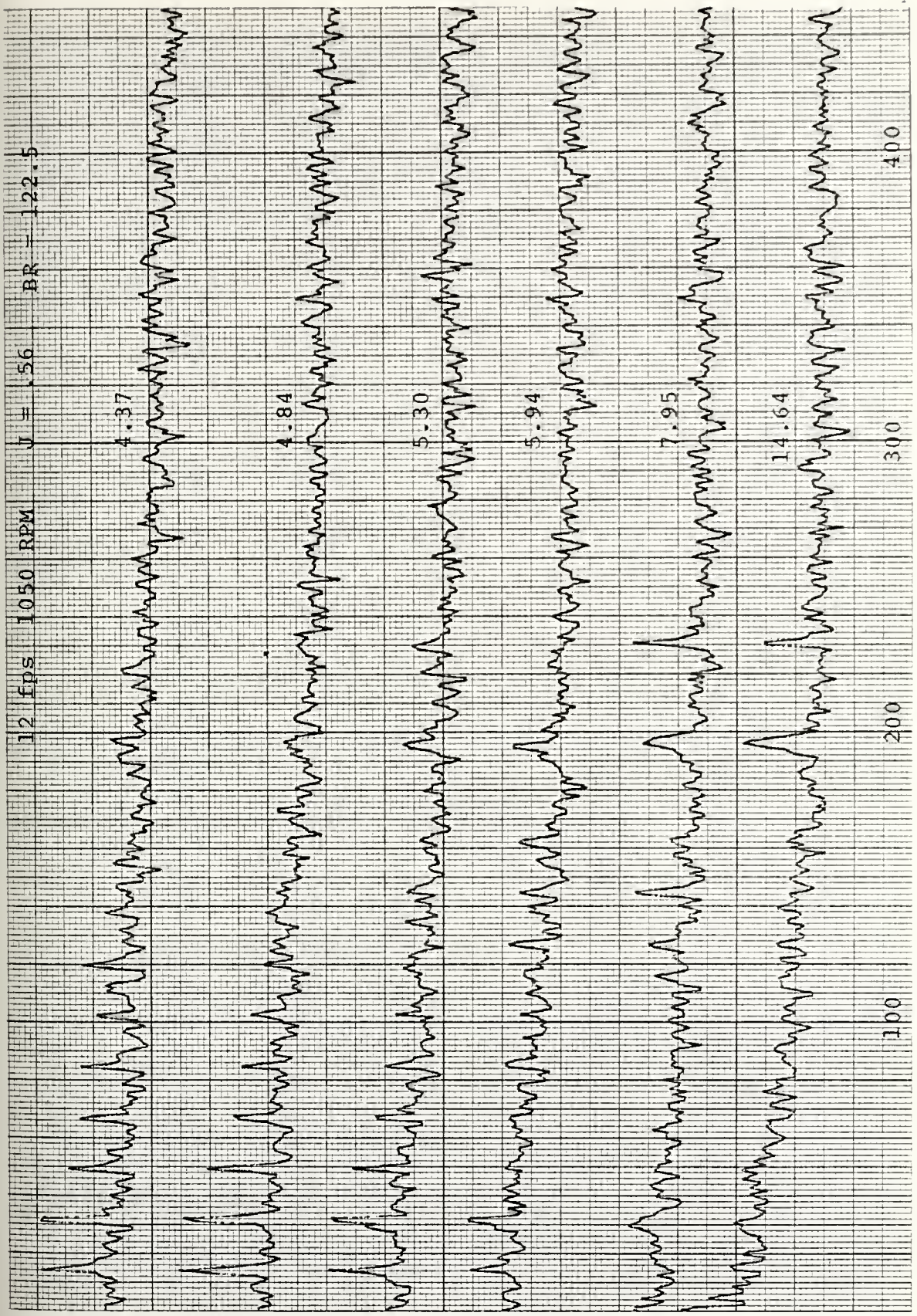
RPM

1175

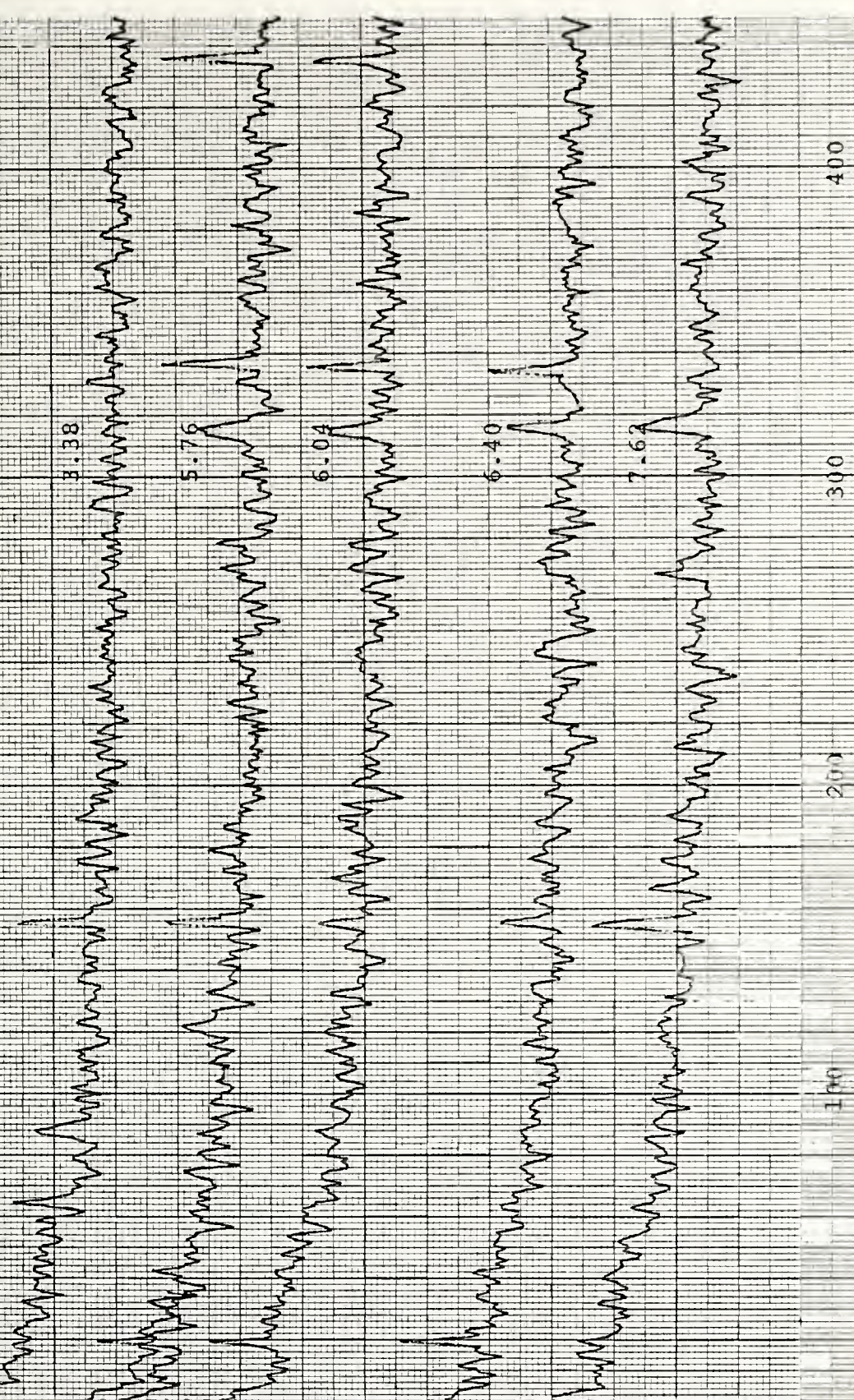
12 fps







16 fps 1350 RPM J = .57 BR = 157.5



100 200 300 400

16 FPS 1300 RPM J = .59 BR = 151.67

4.74

5.08

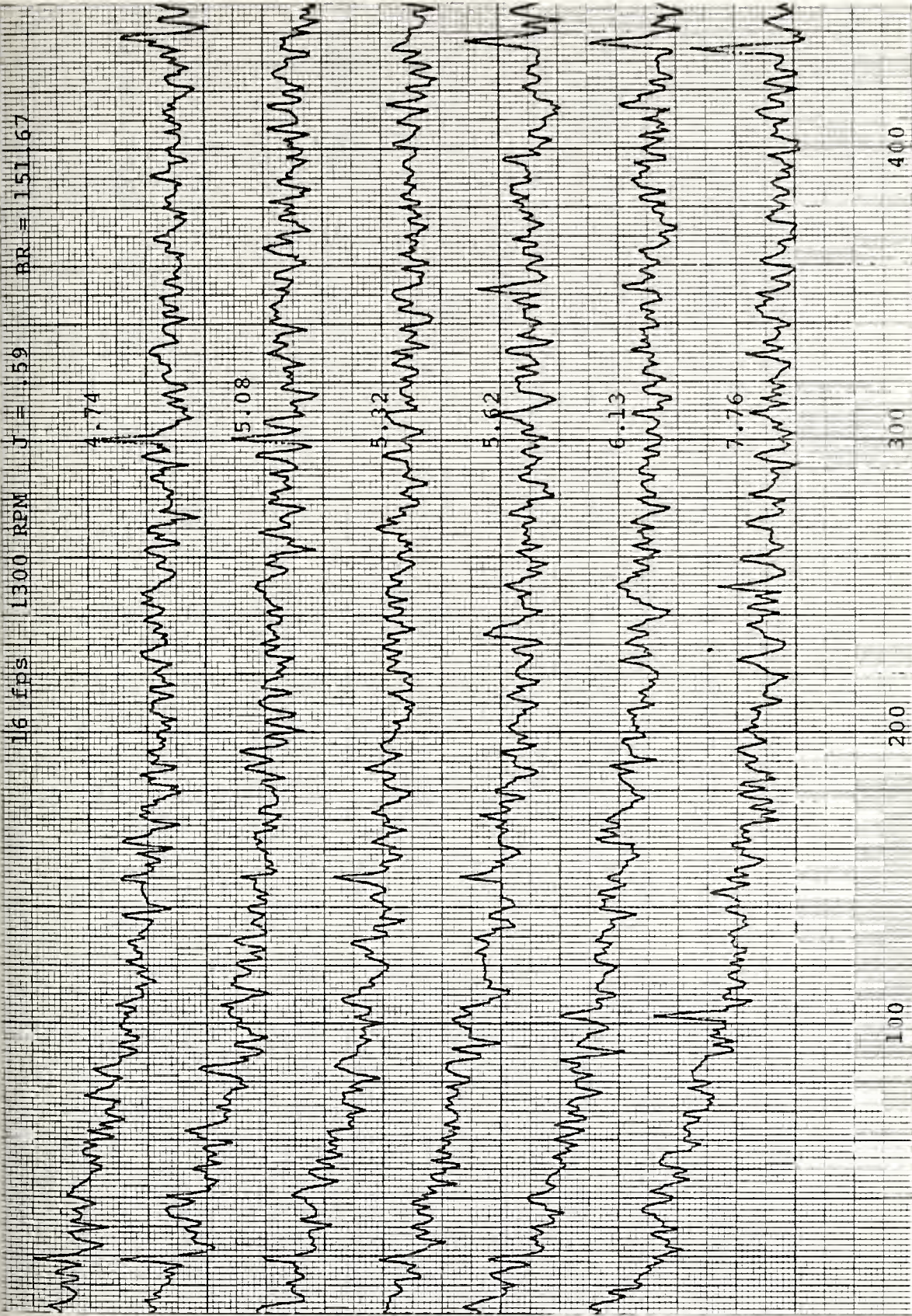
5.32

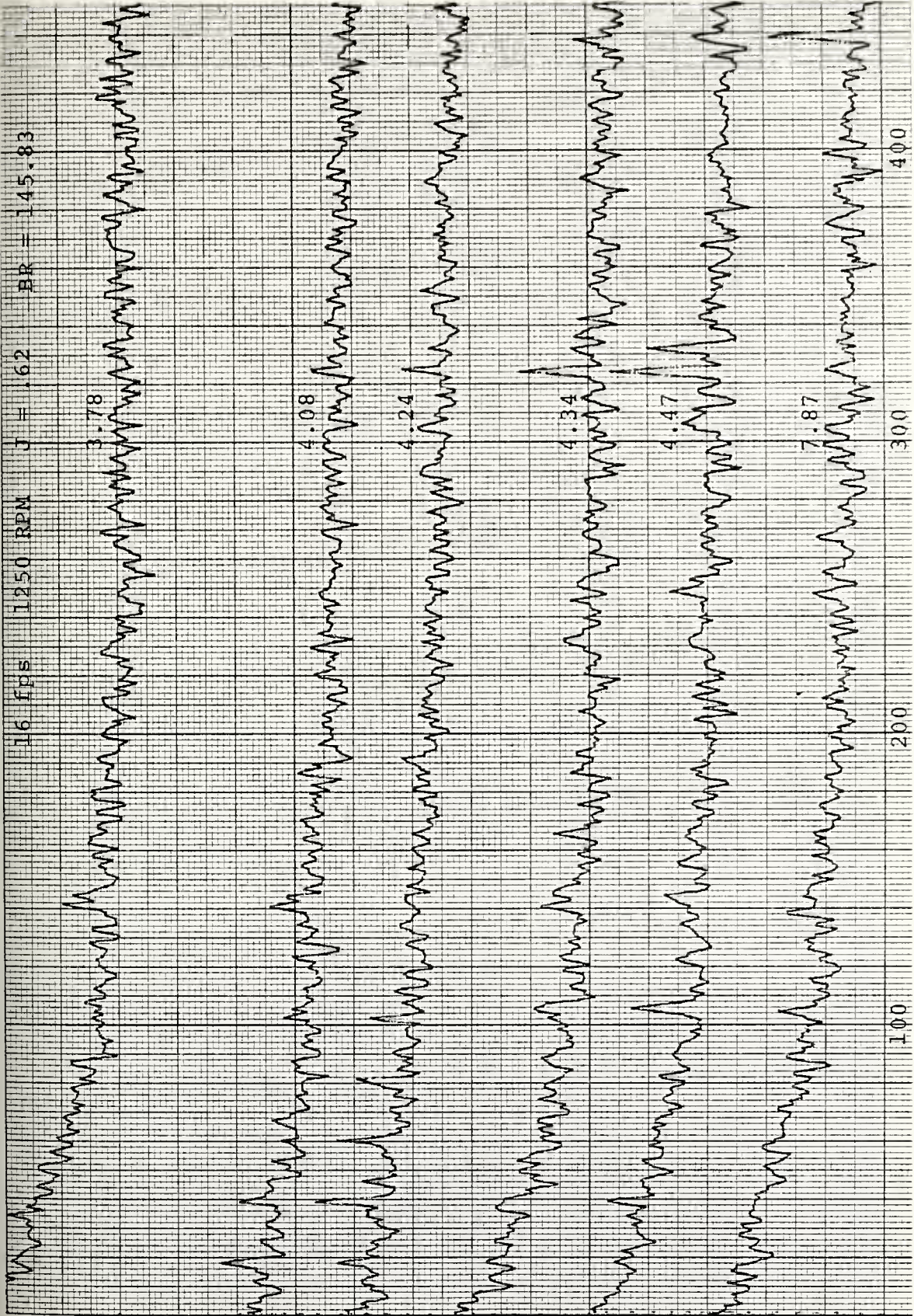
5.52

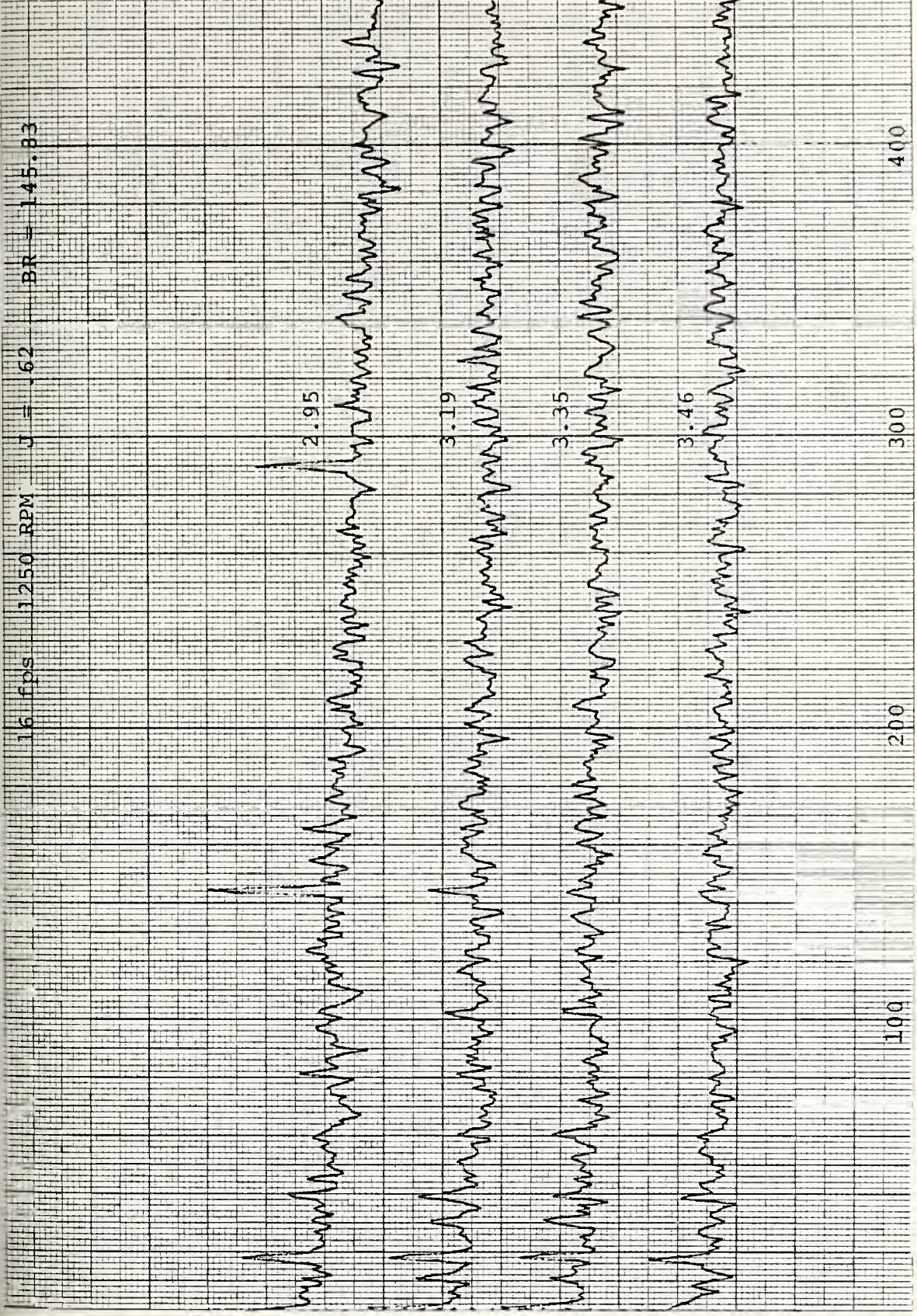
6.13

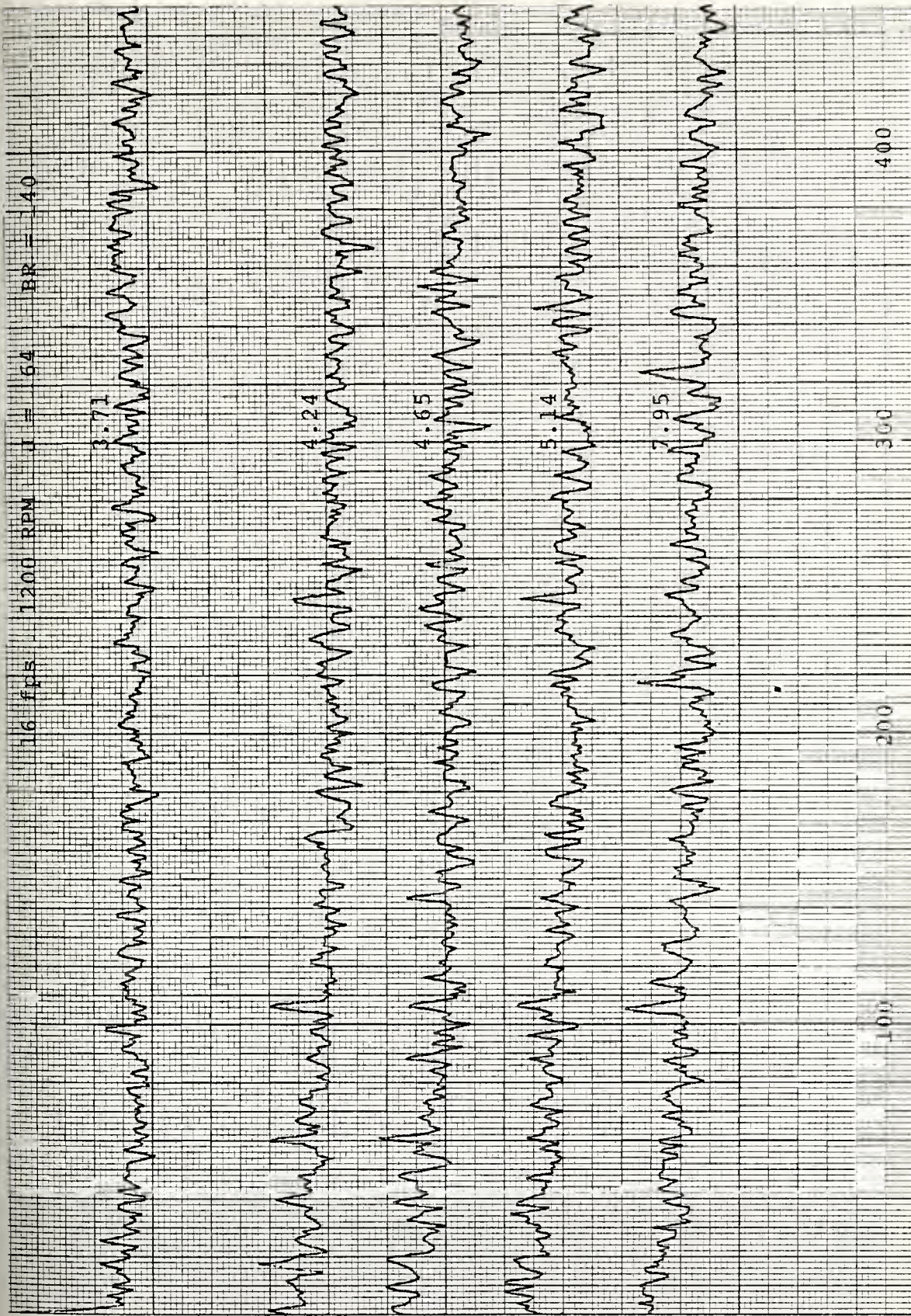
7.76

100 200 300 400

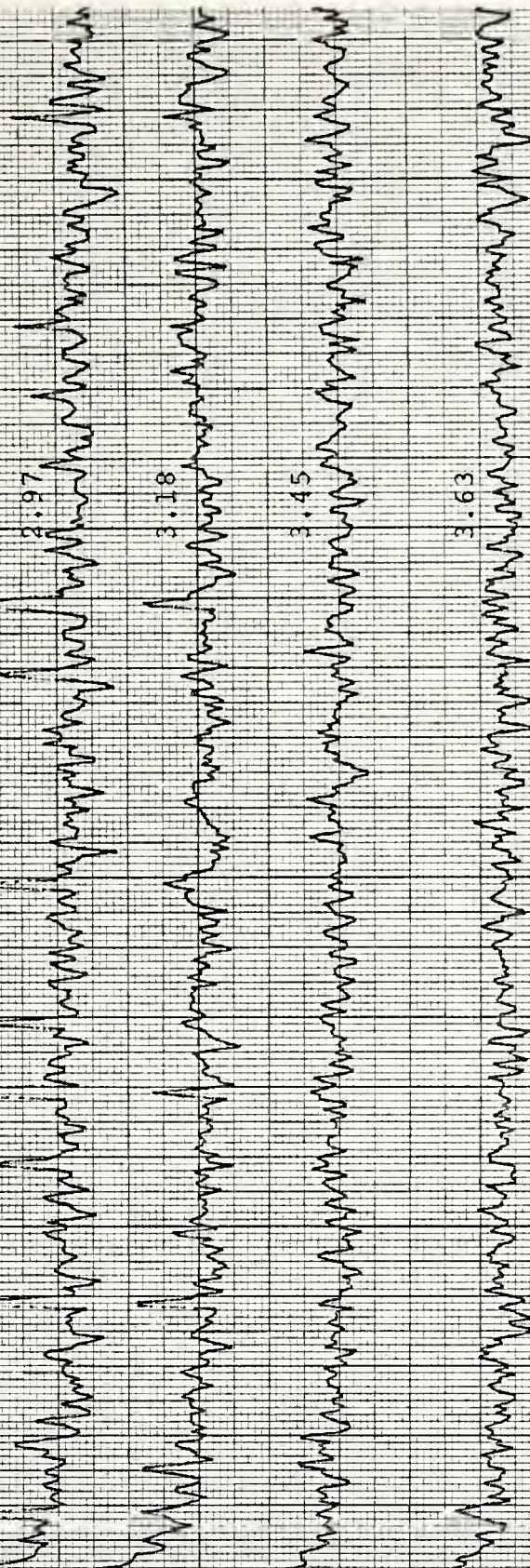








16 EPS 1200 RPM $f = .64$ BR = 140



100 200 300 400

BR = 134.17

G = .67

1150 RPM

16 fps

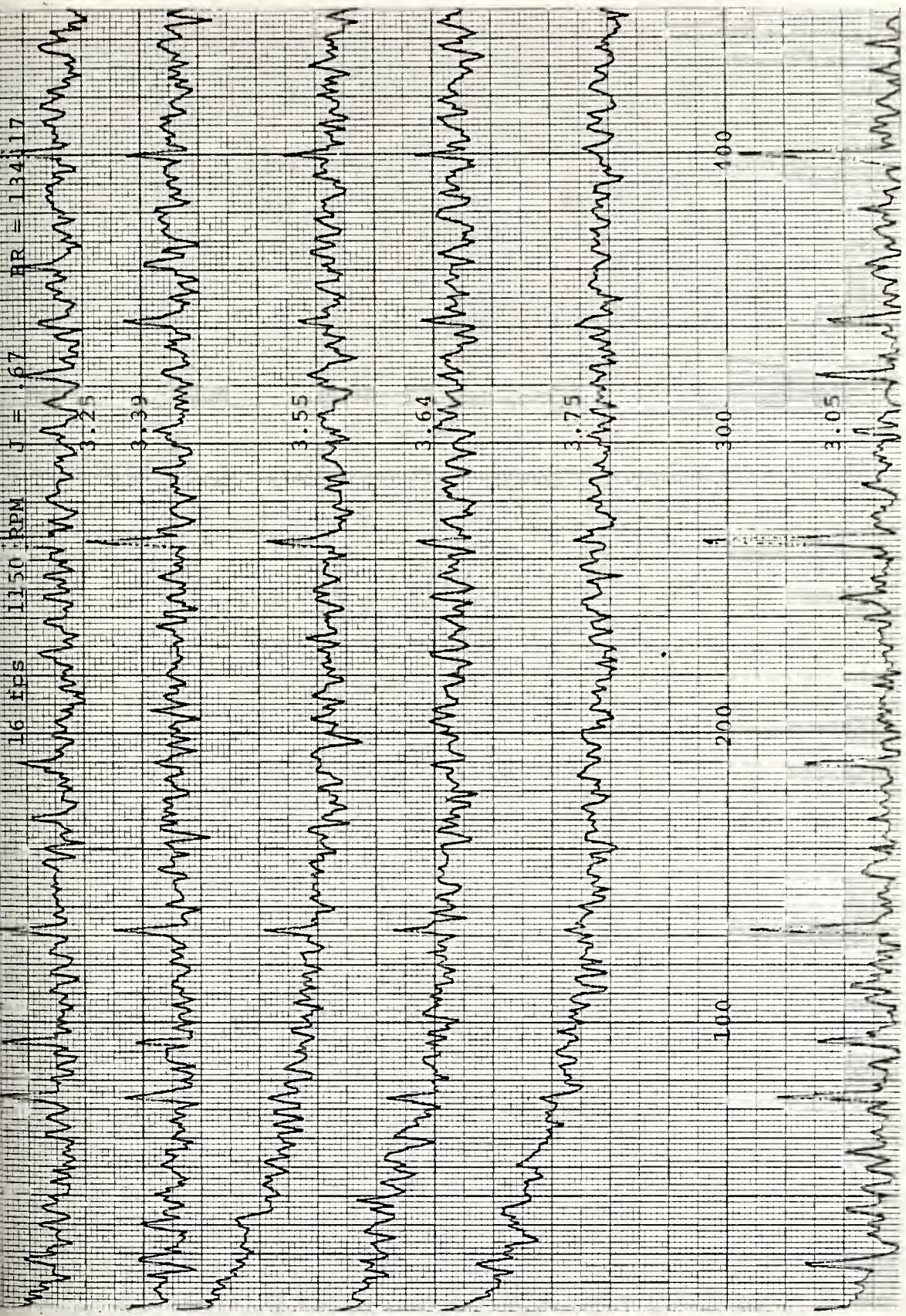


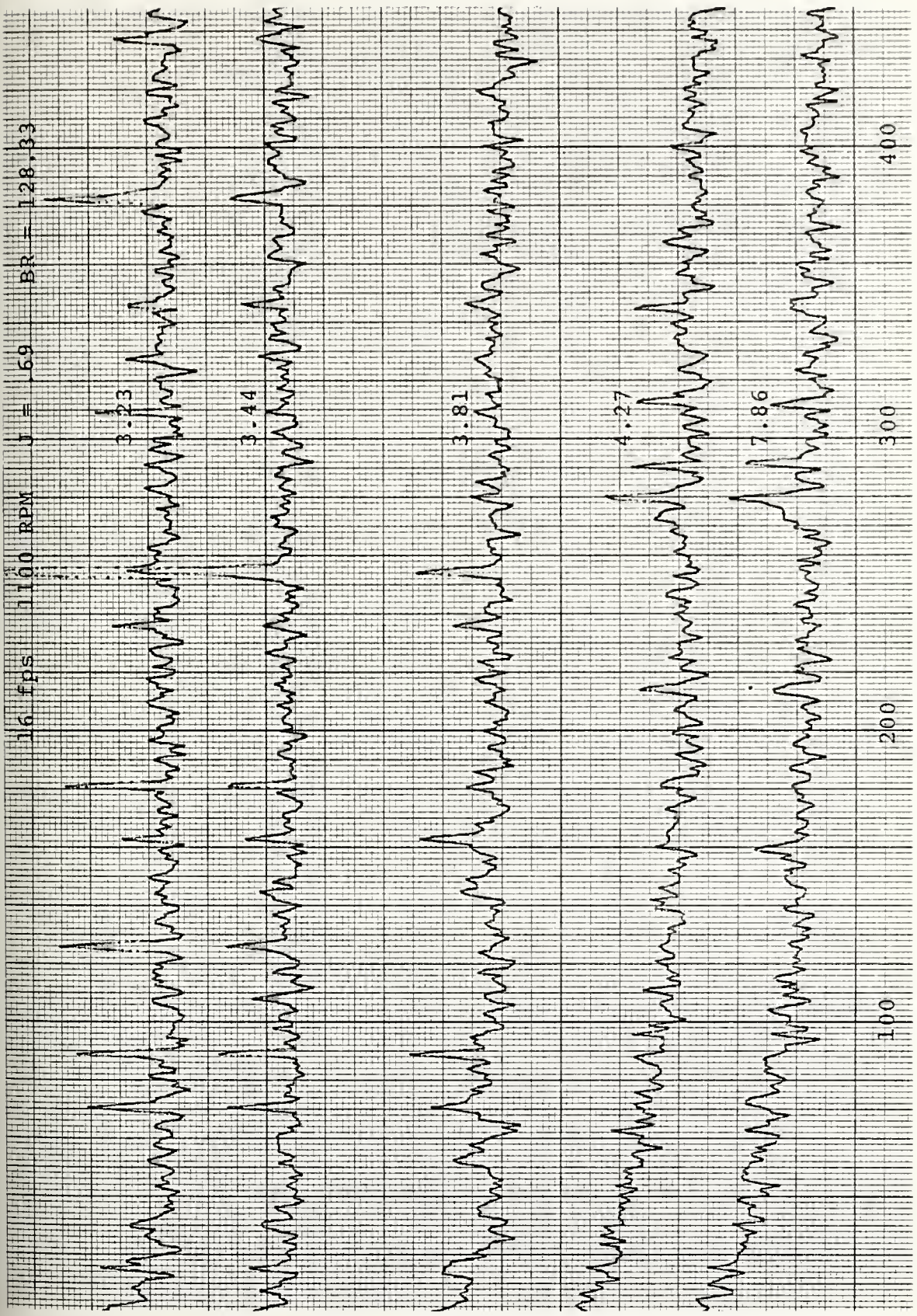
400

300

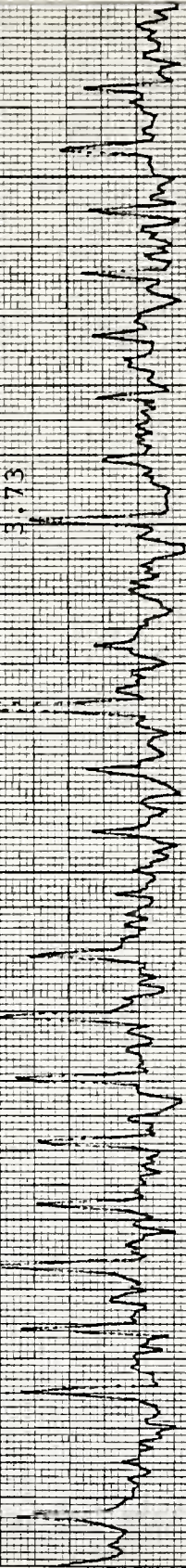
200

100

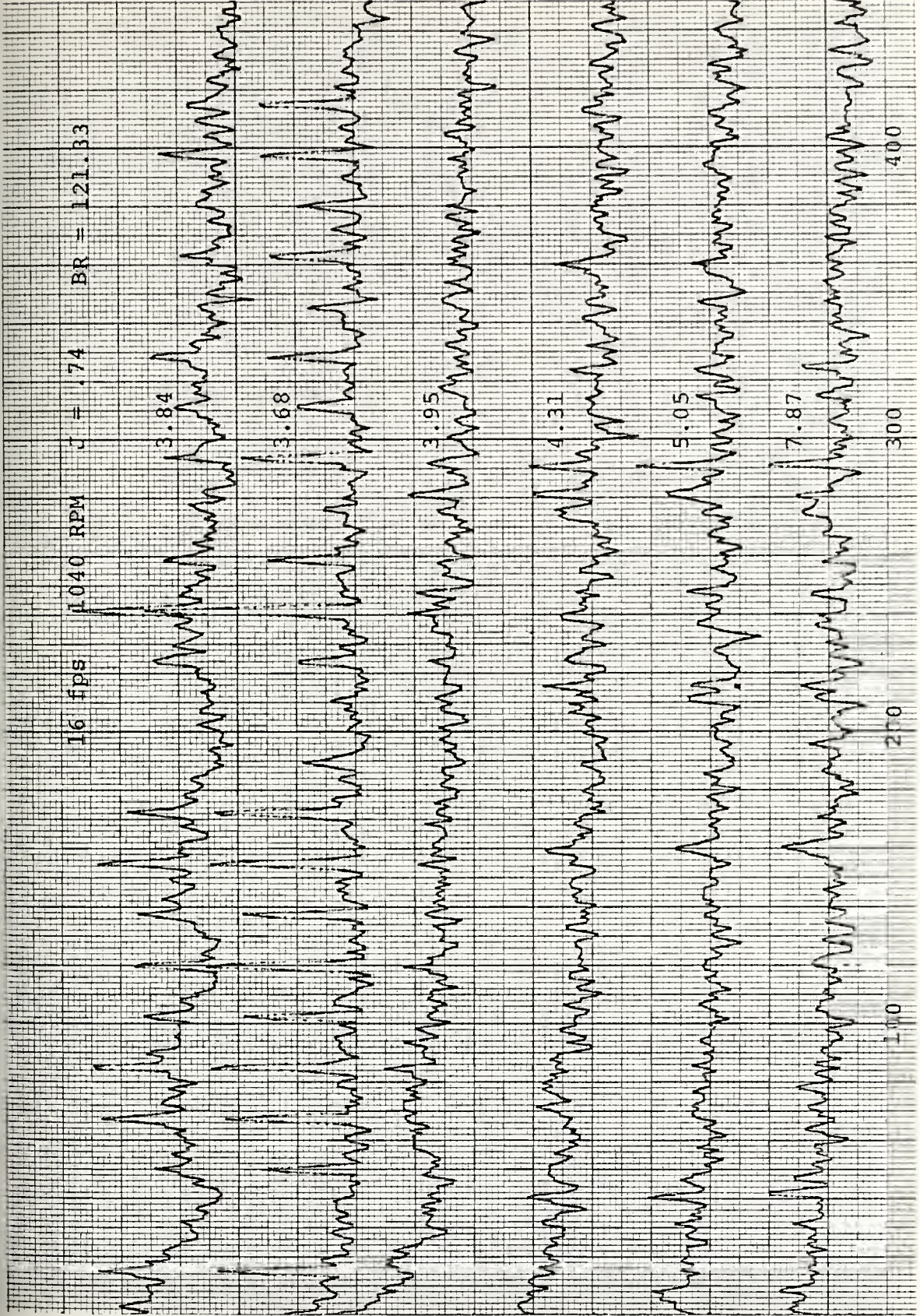


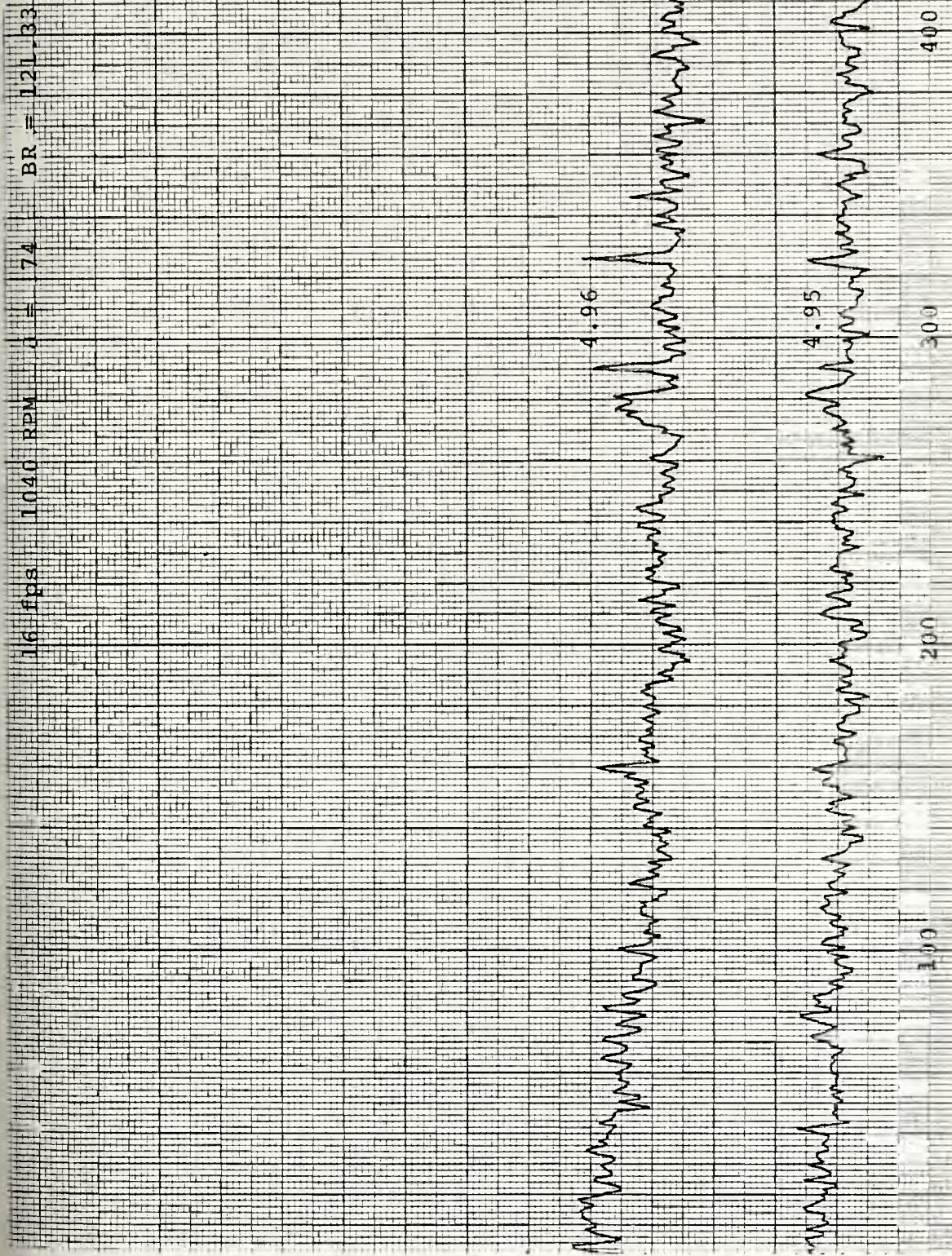


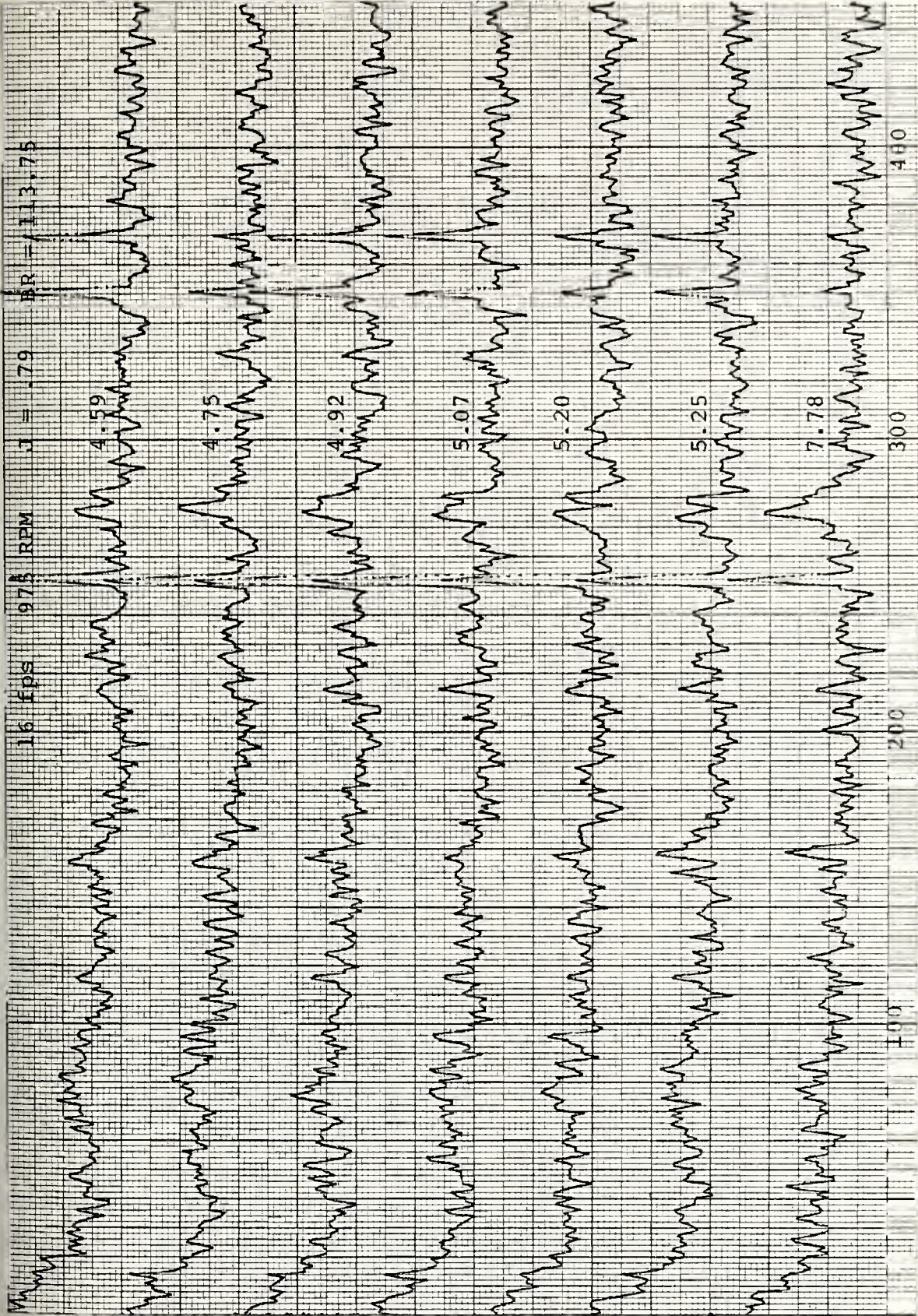
16 FPS 1070 RPM J = 72 BR = 124.83



100 200 300 400







16 fps 1040 RPM J = .74 BR = 1.21-33

4.98

5.14

5.26

5.38

5.51

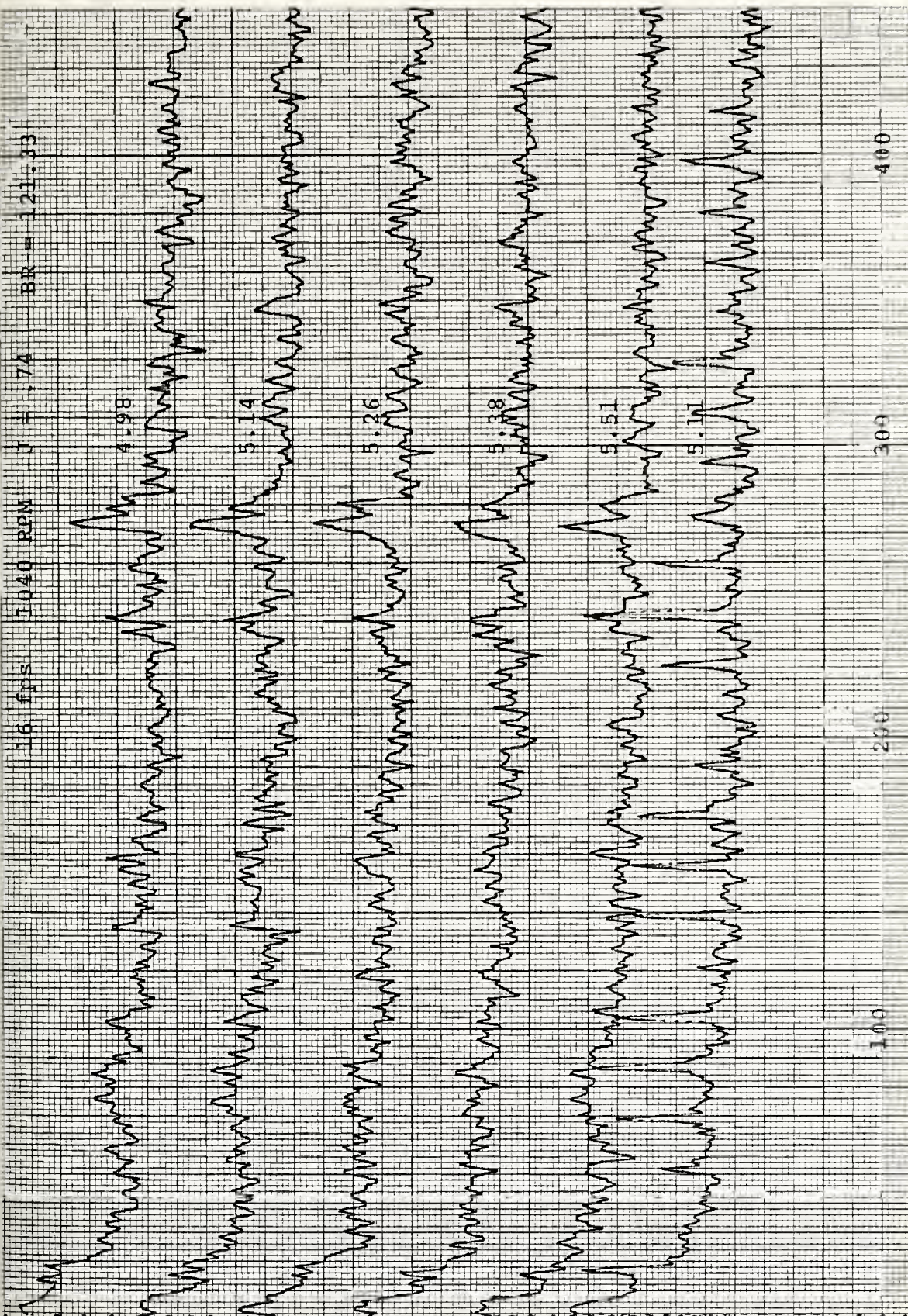
5.11

100

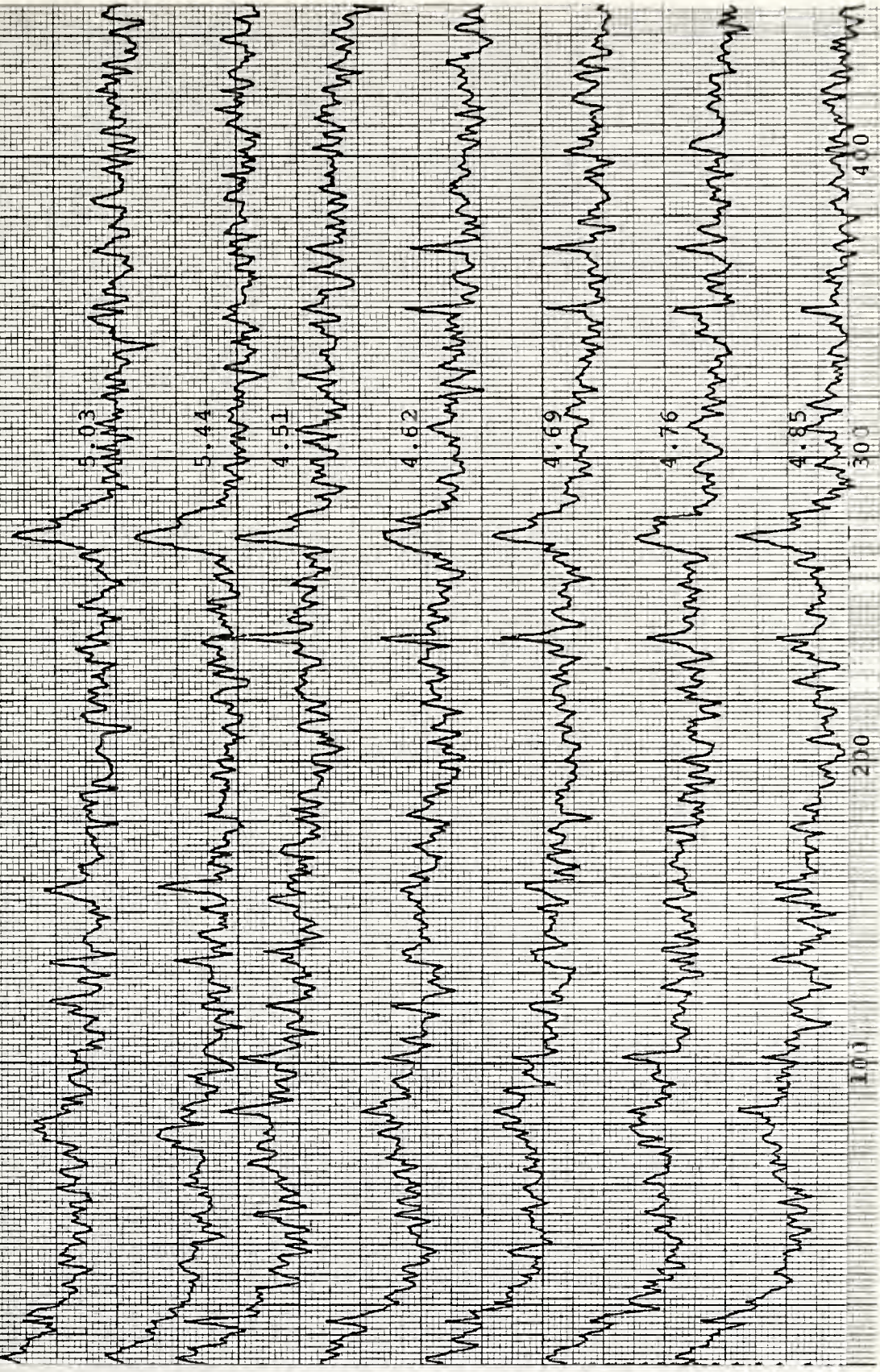
200

300

400



16 FPS 1040 RPM J = .74 BR = 121.33

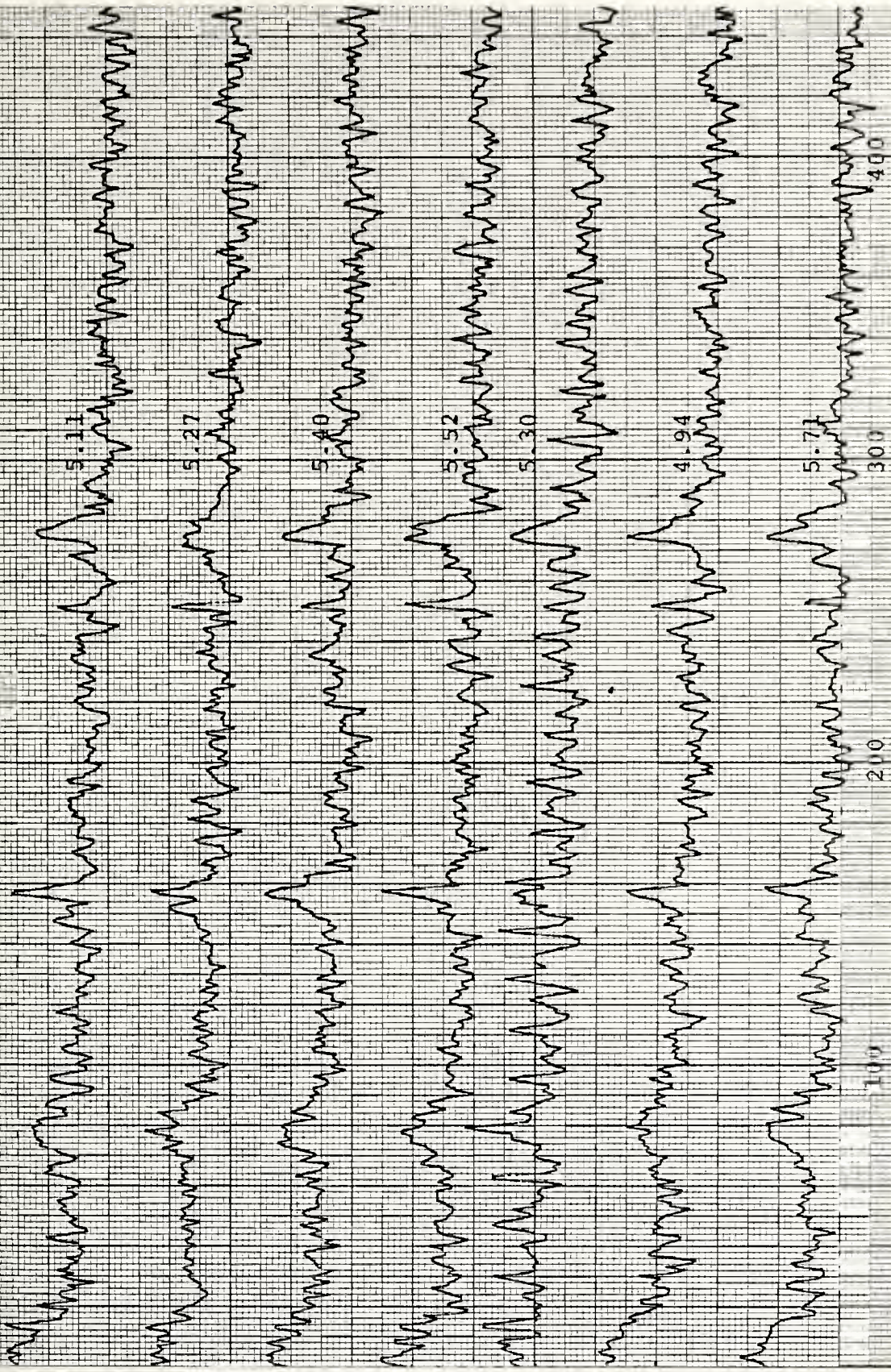


BR = 113.75

J = .79

975 RPM

16 FPS



100

200

300

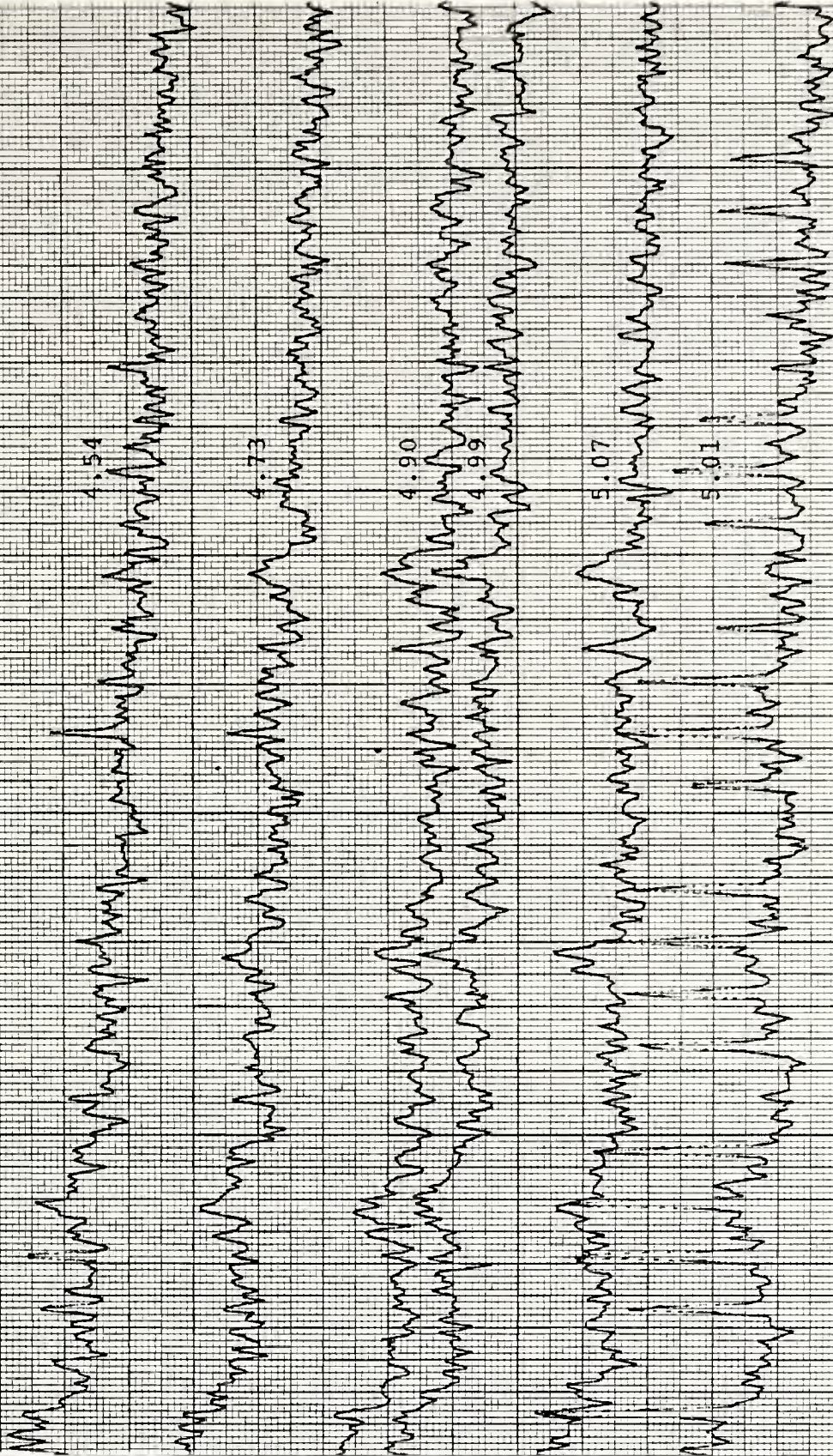
400

DR = 113.75

J = 79

975 RPM

16 FPS

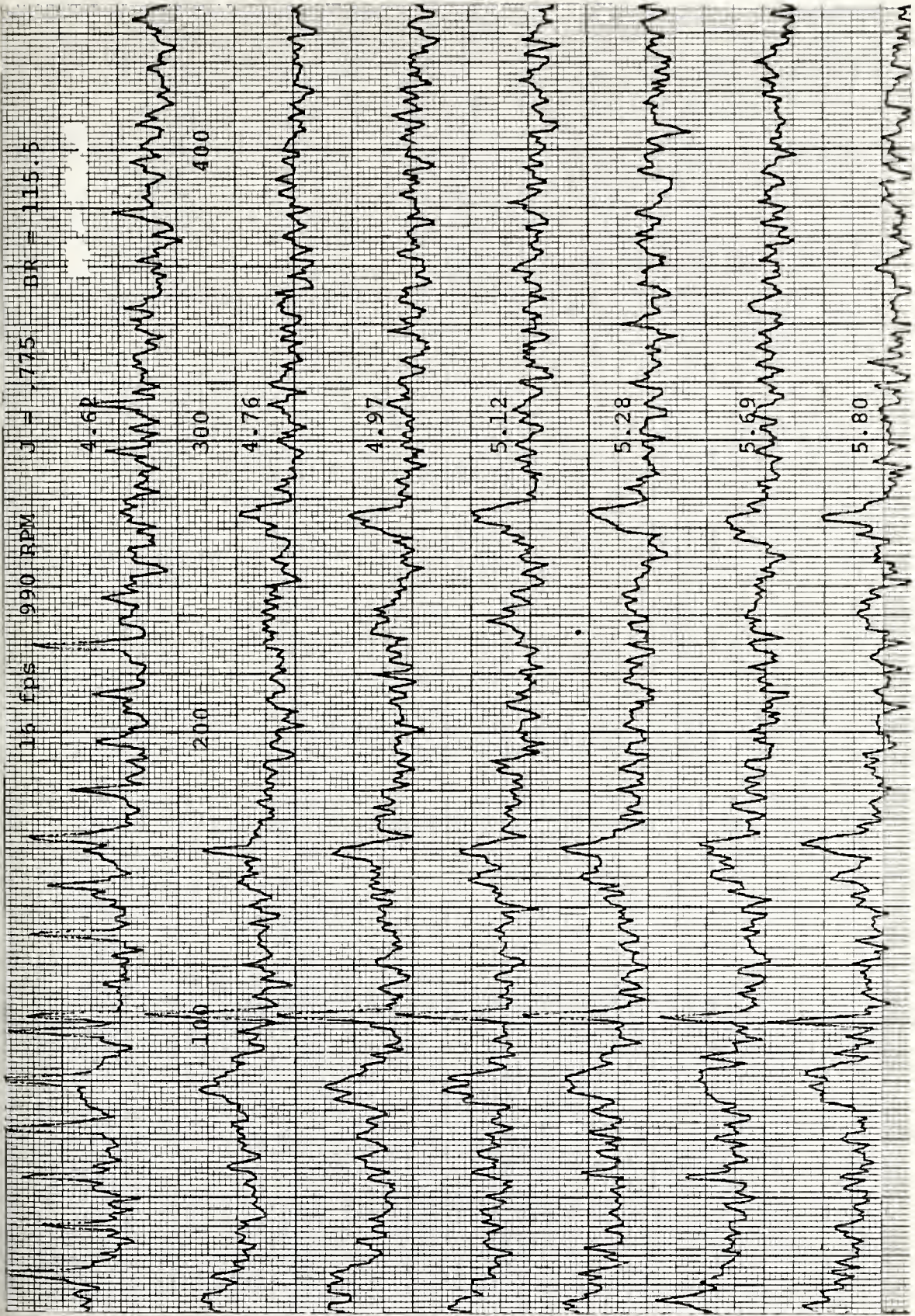


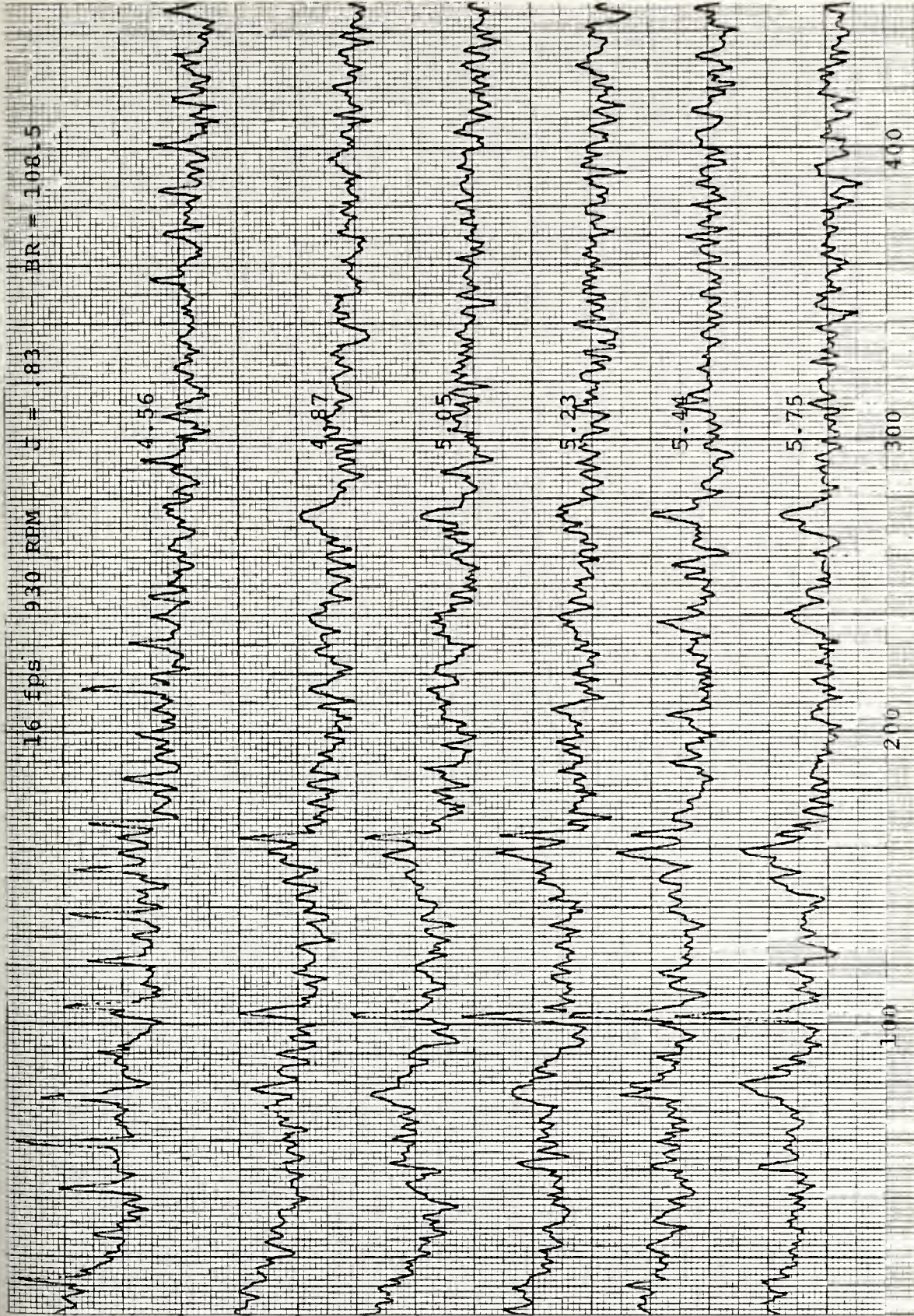
400

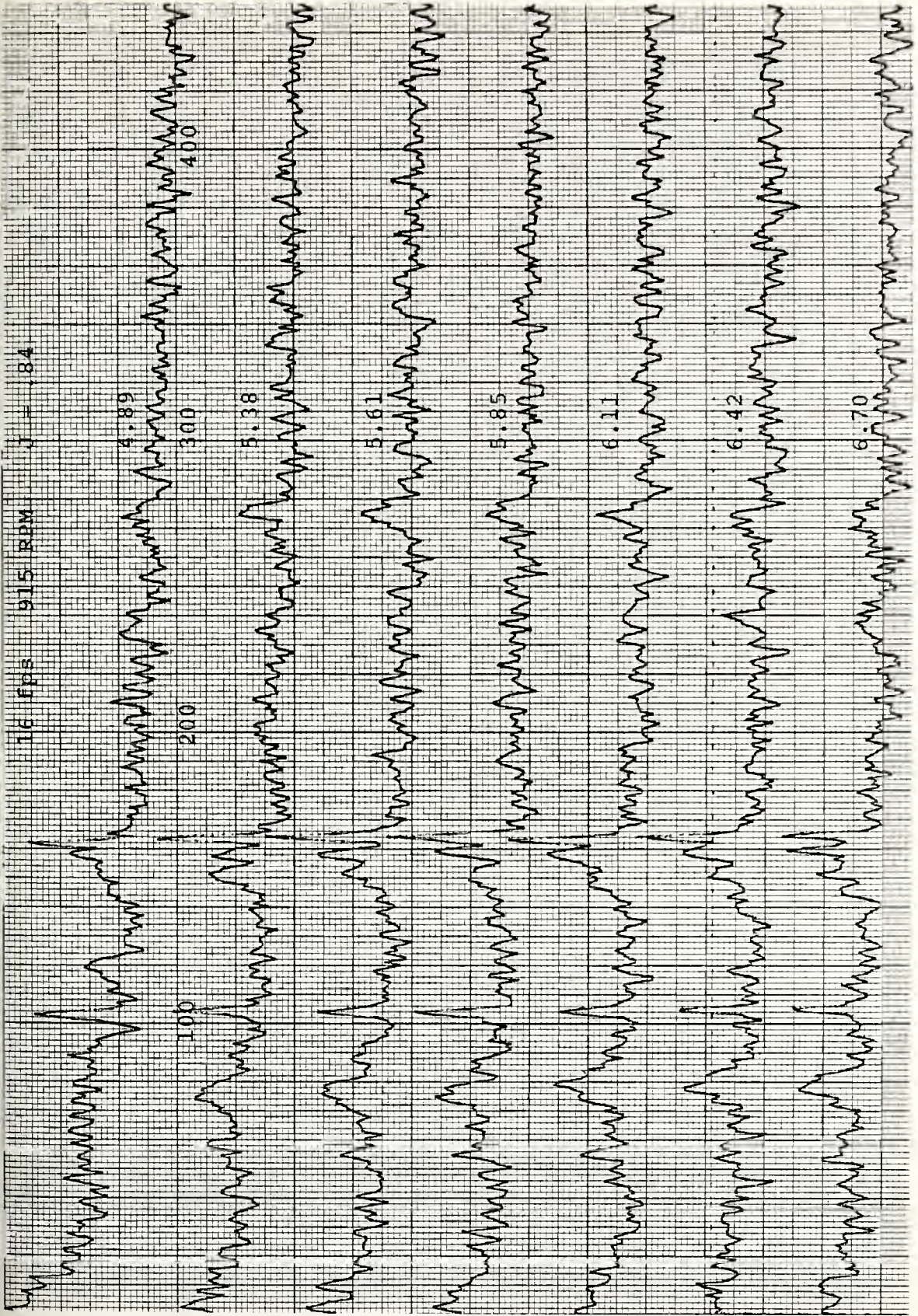
300

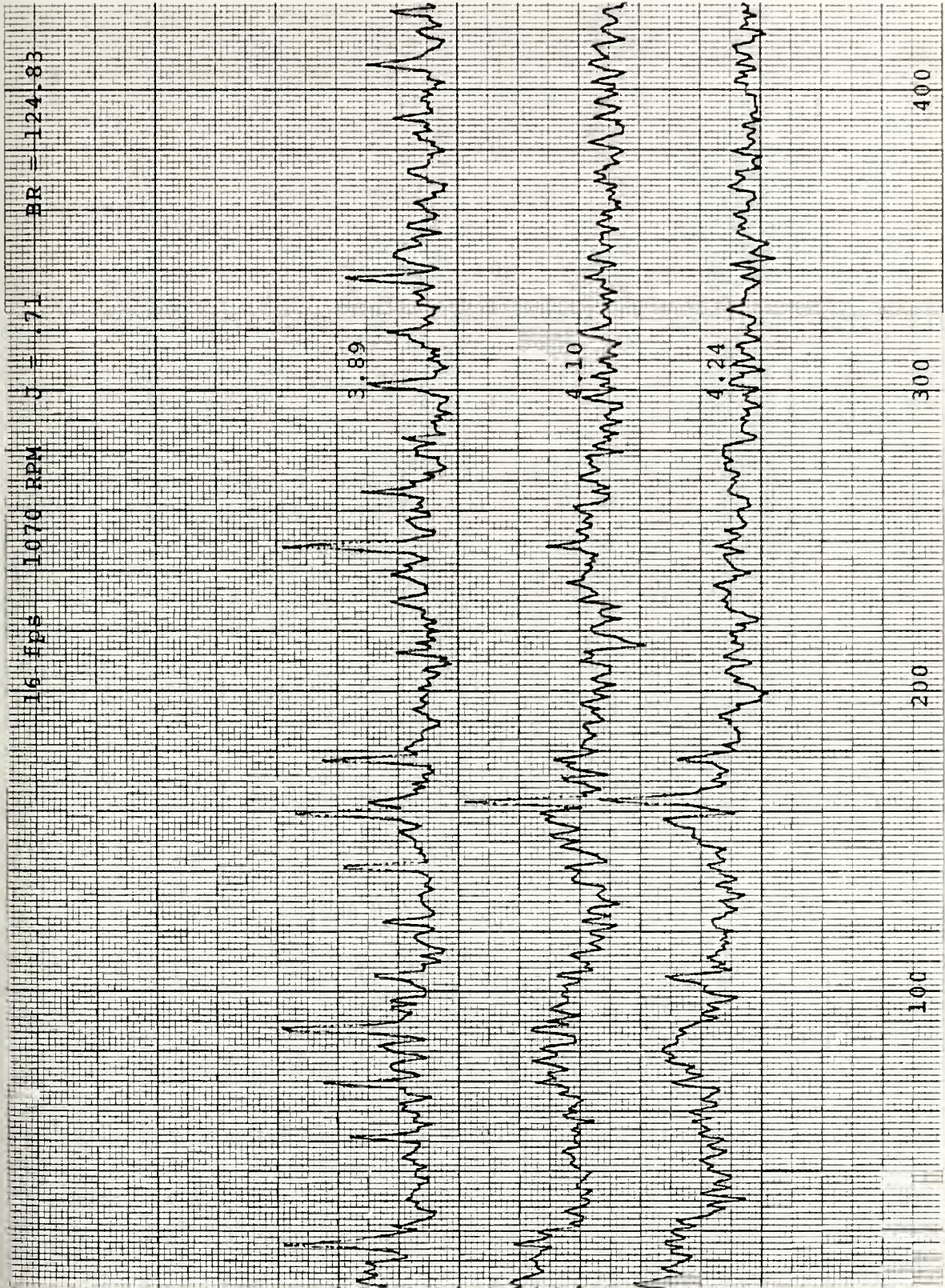
200

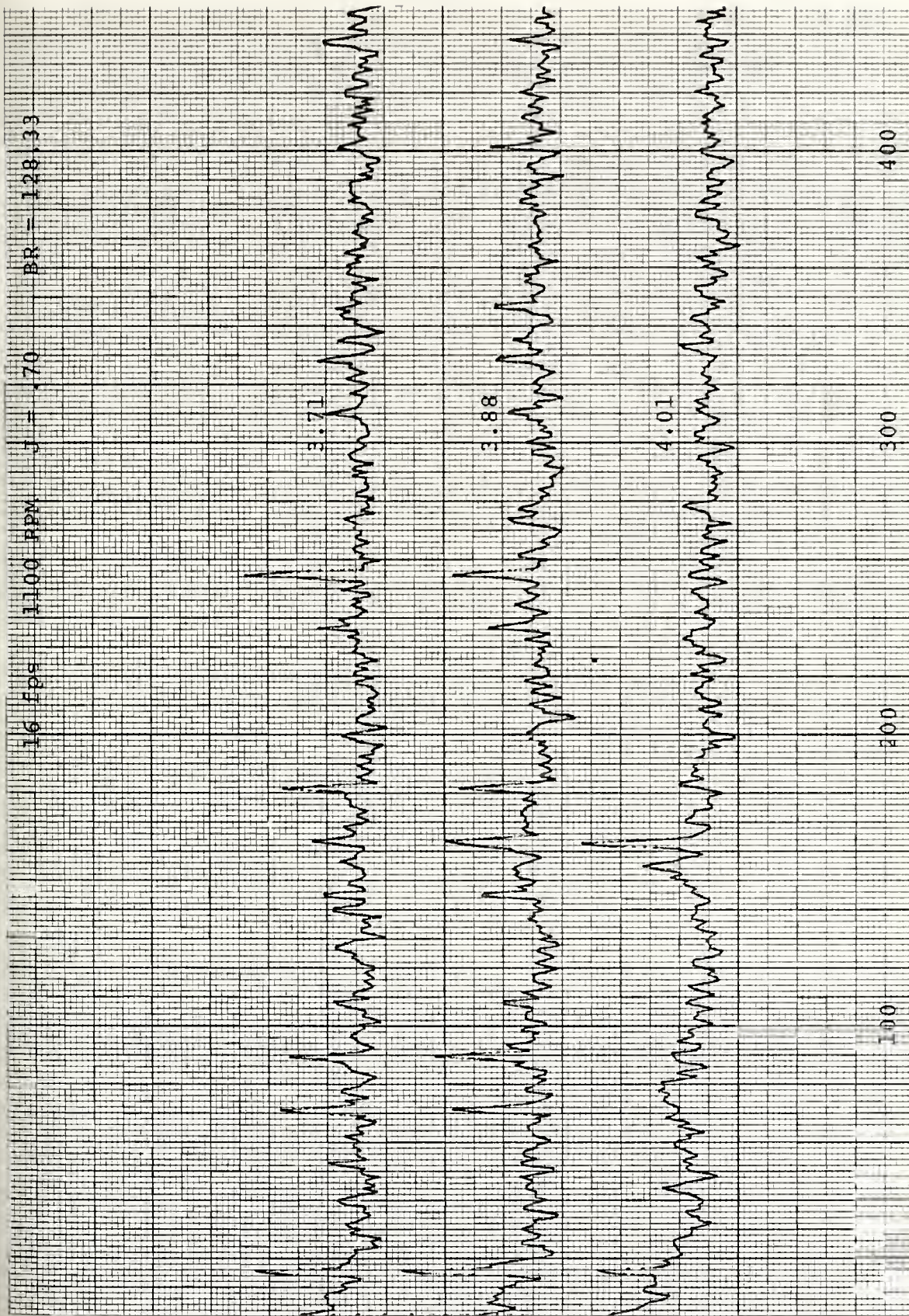
100

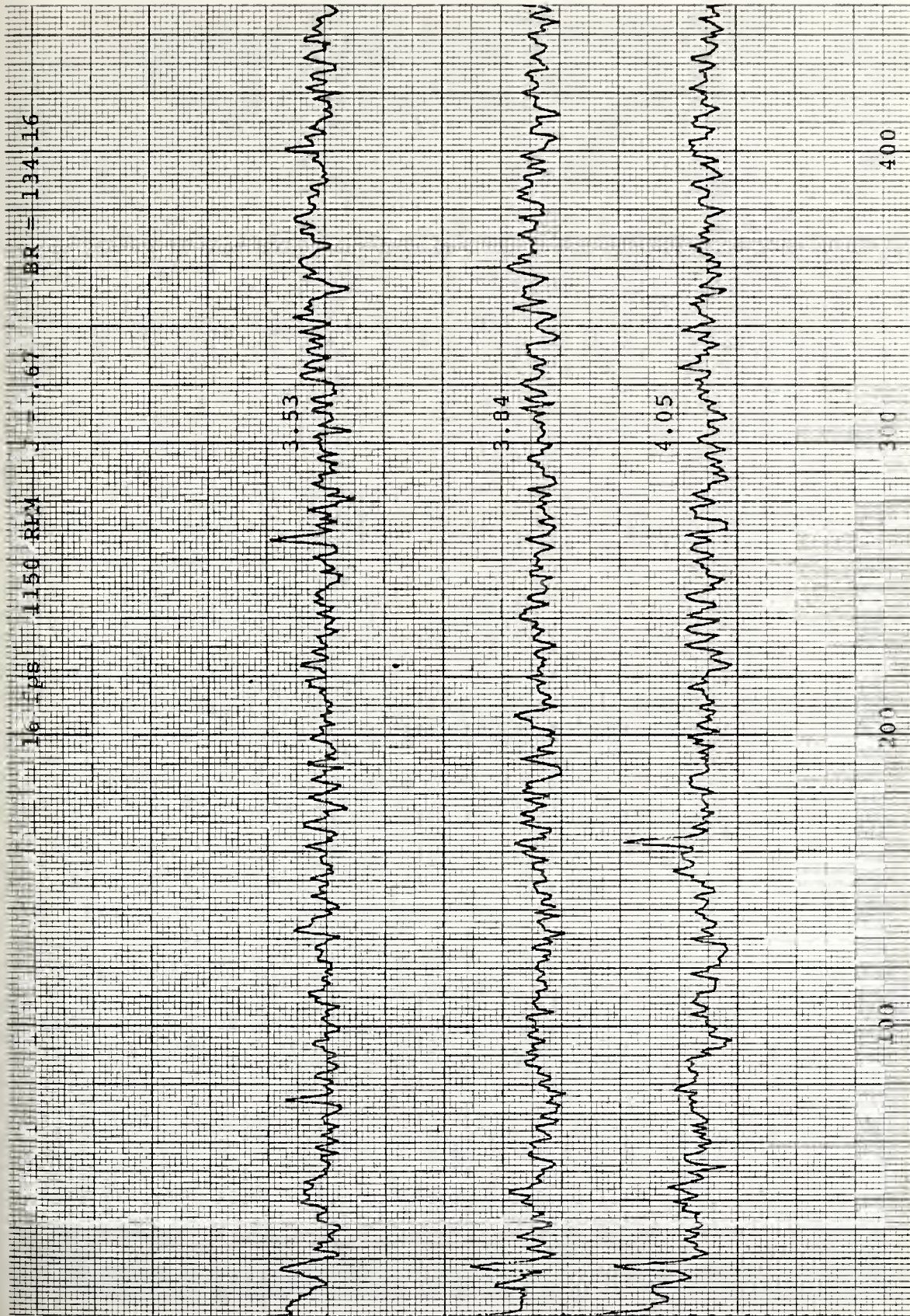


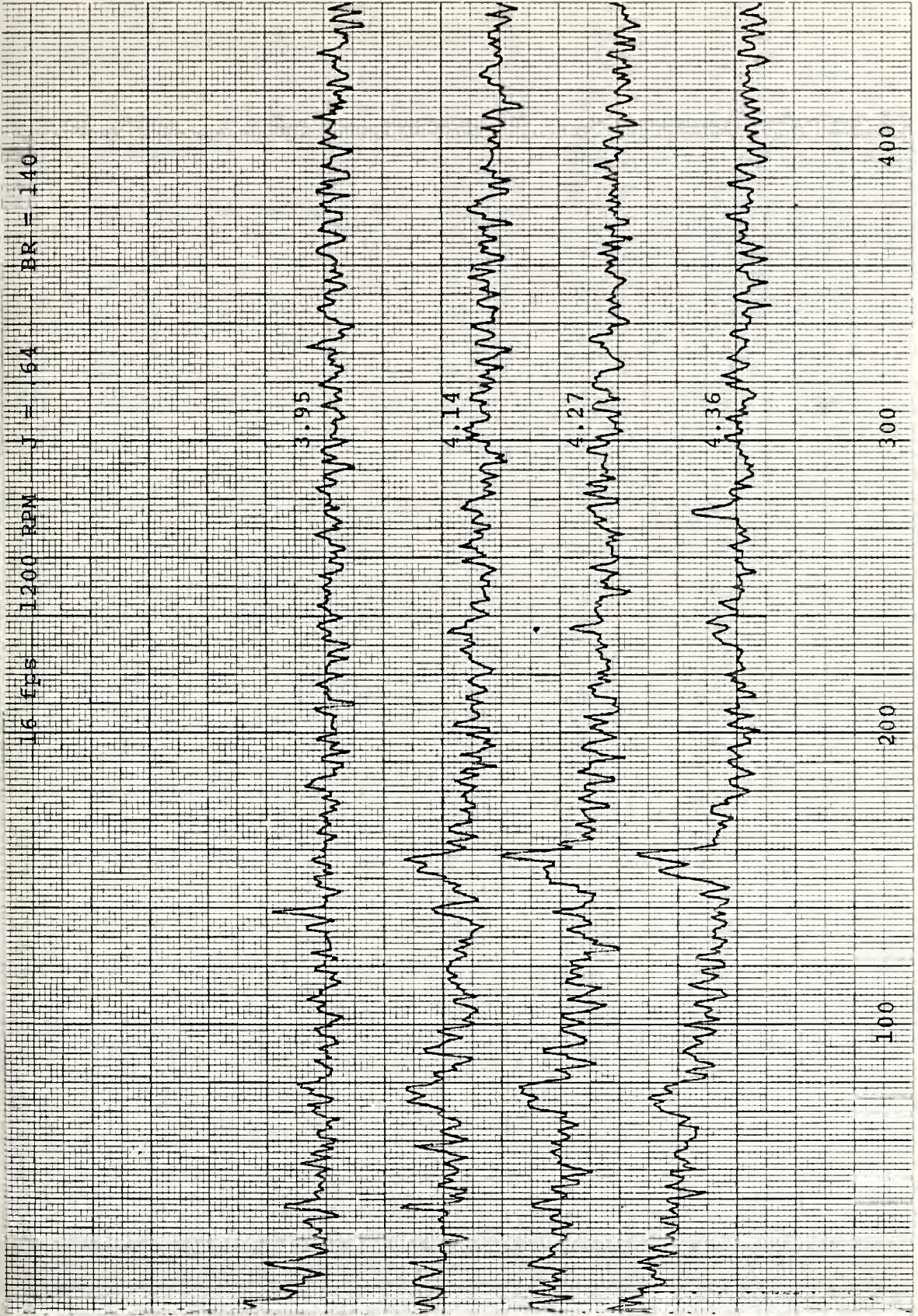


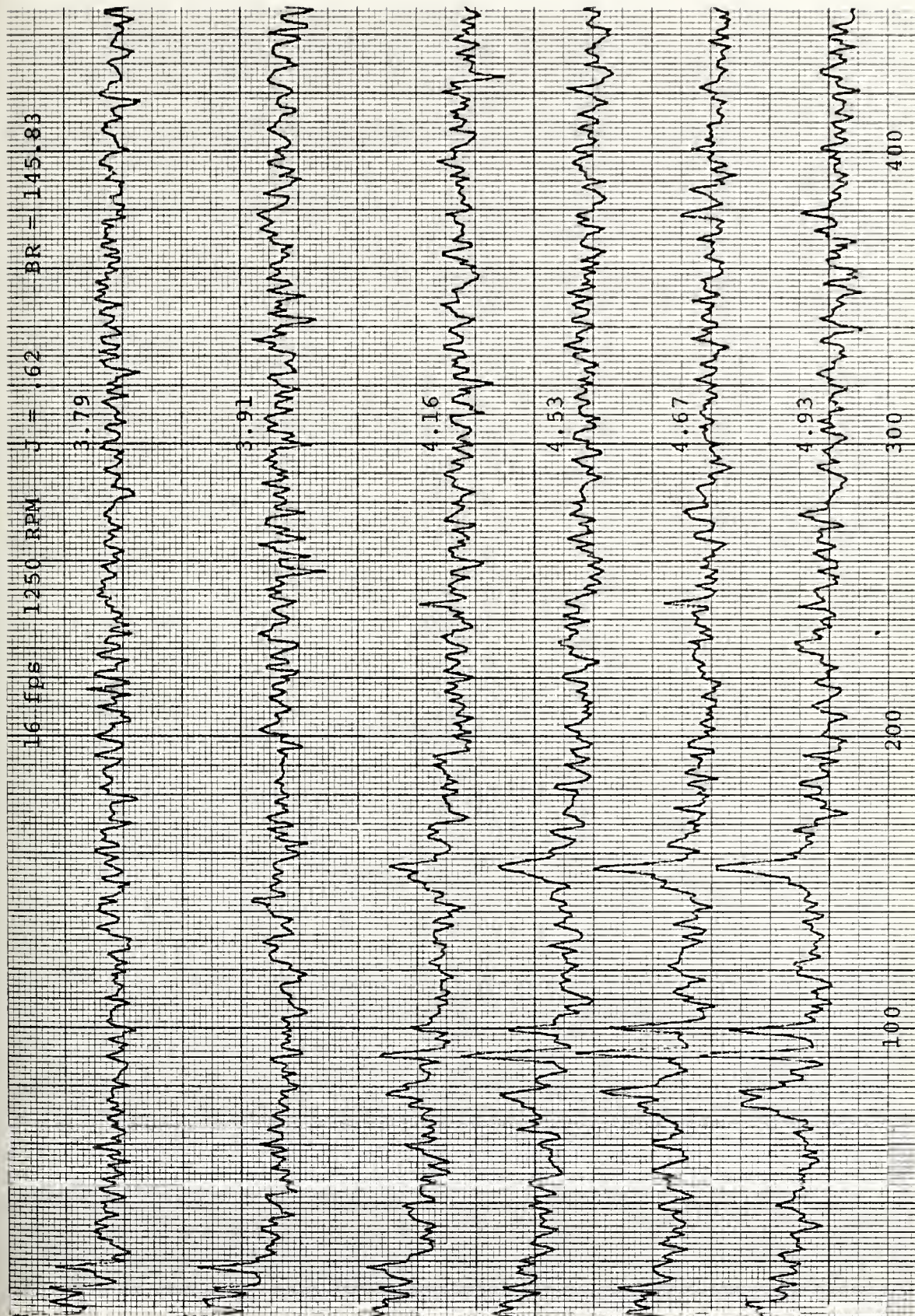


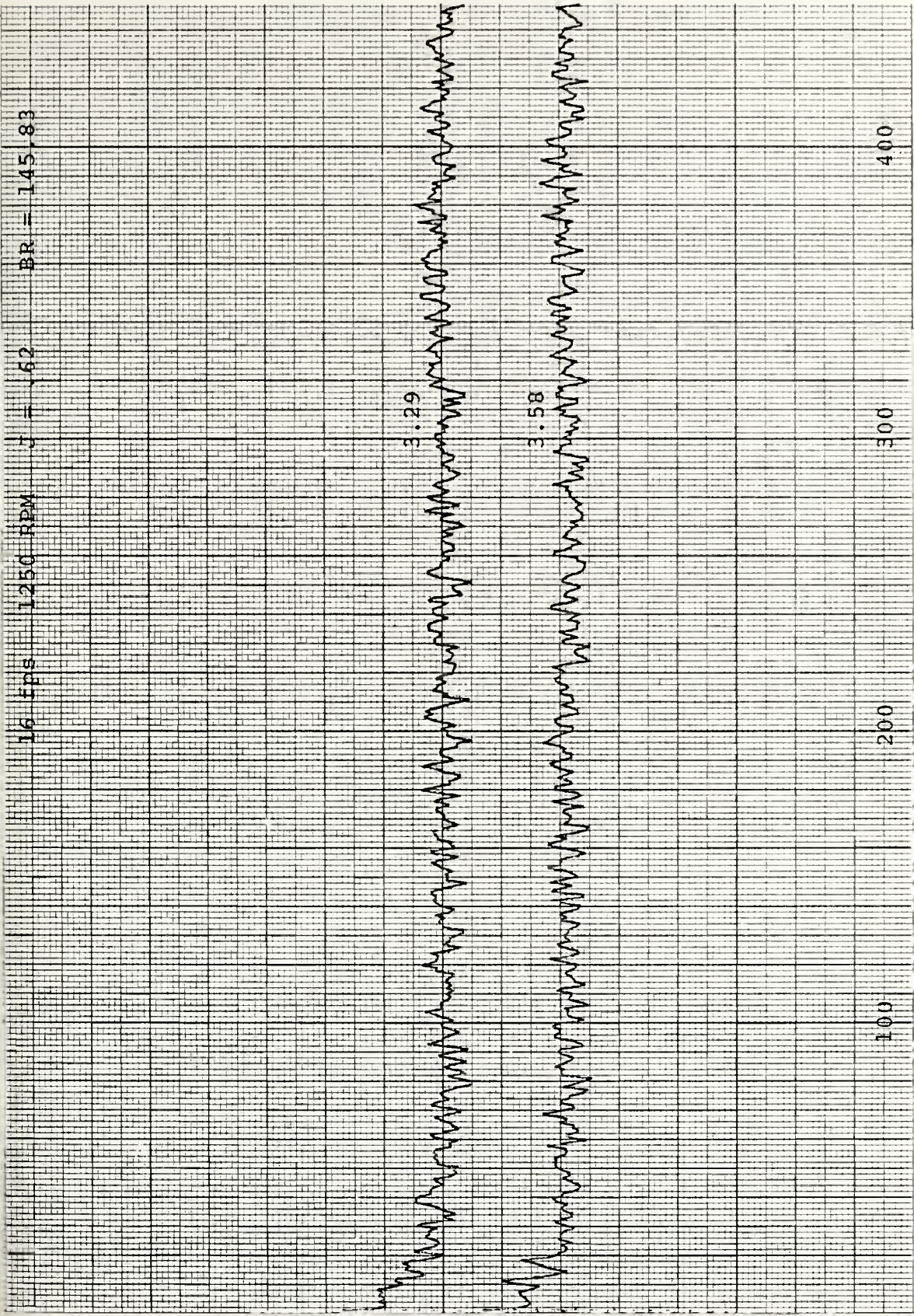


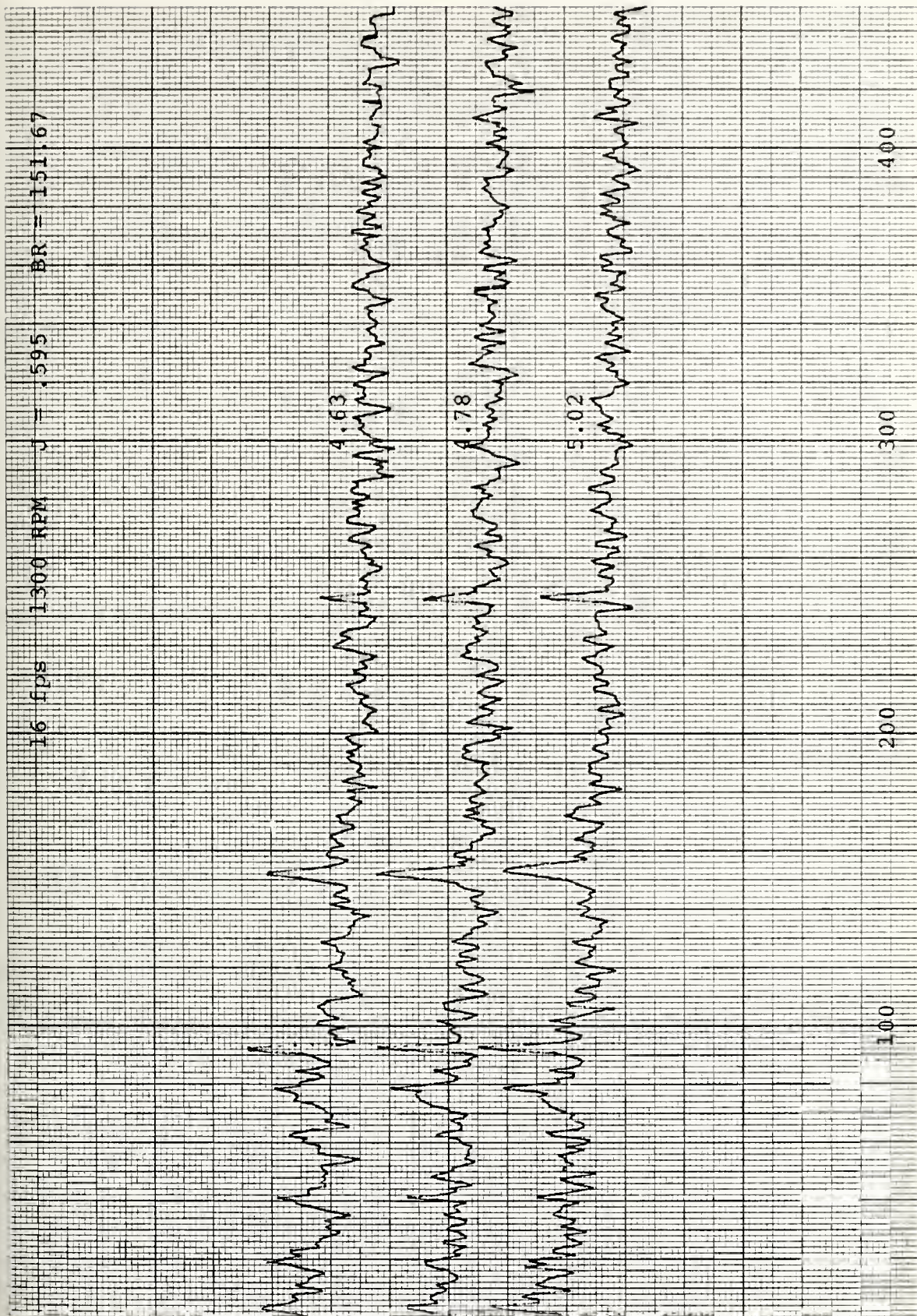


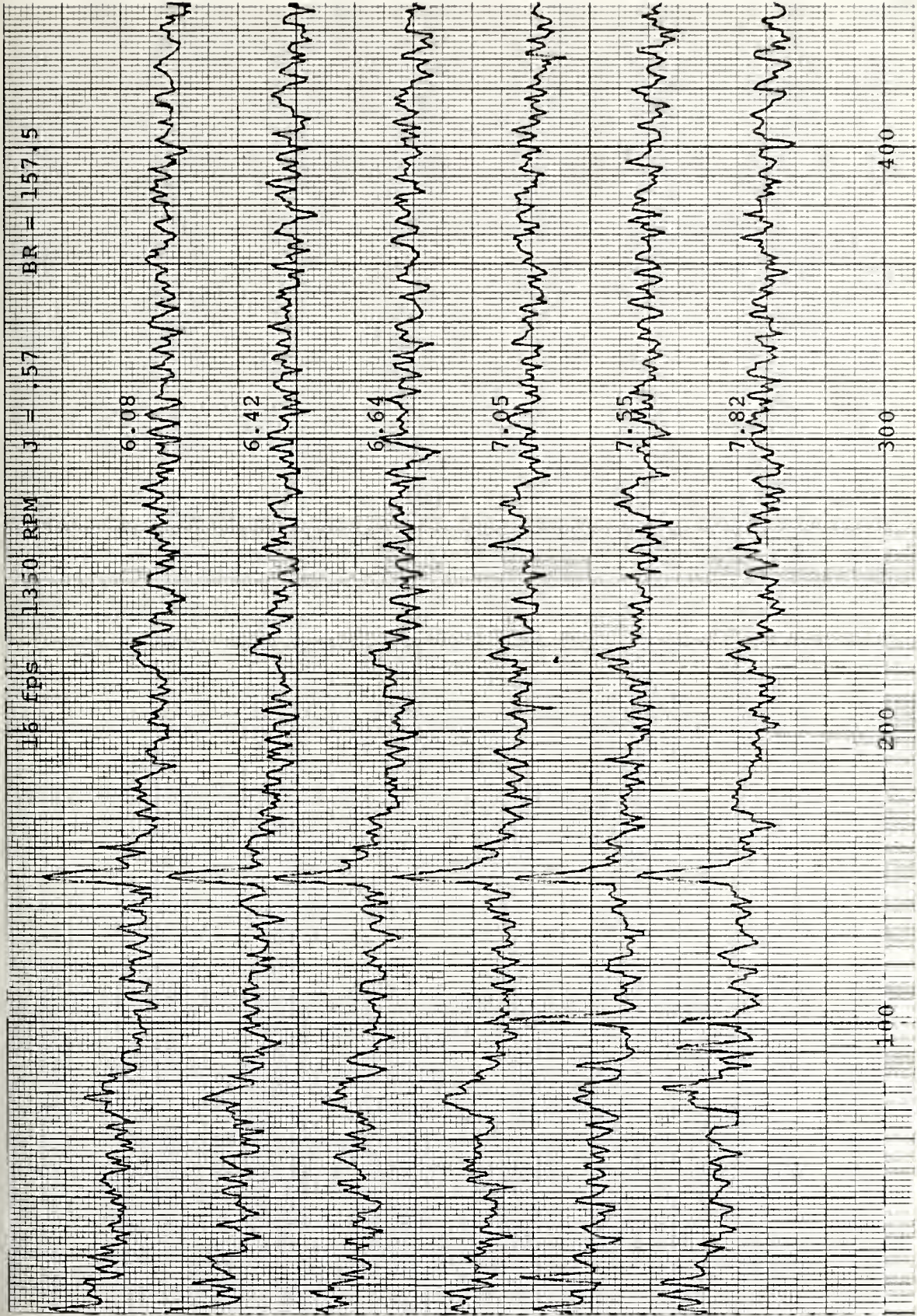


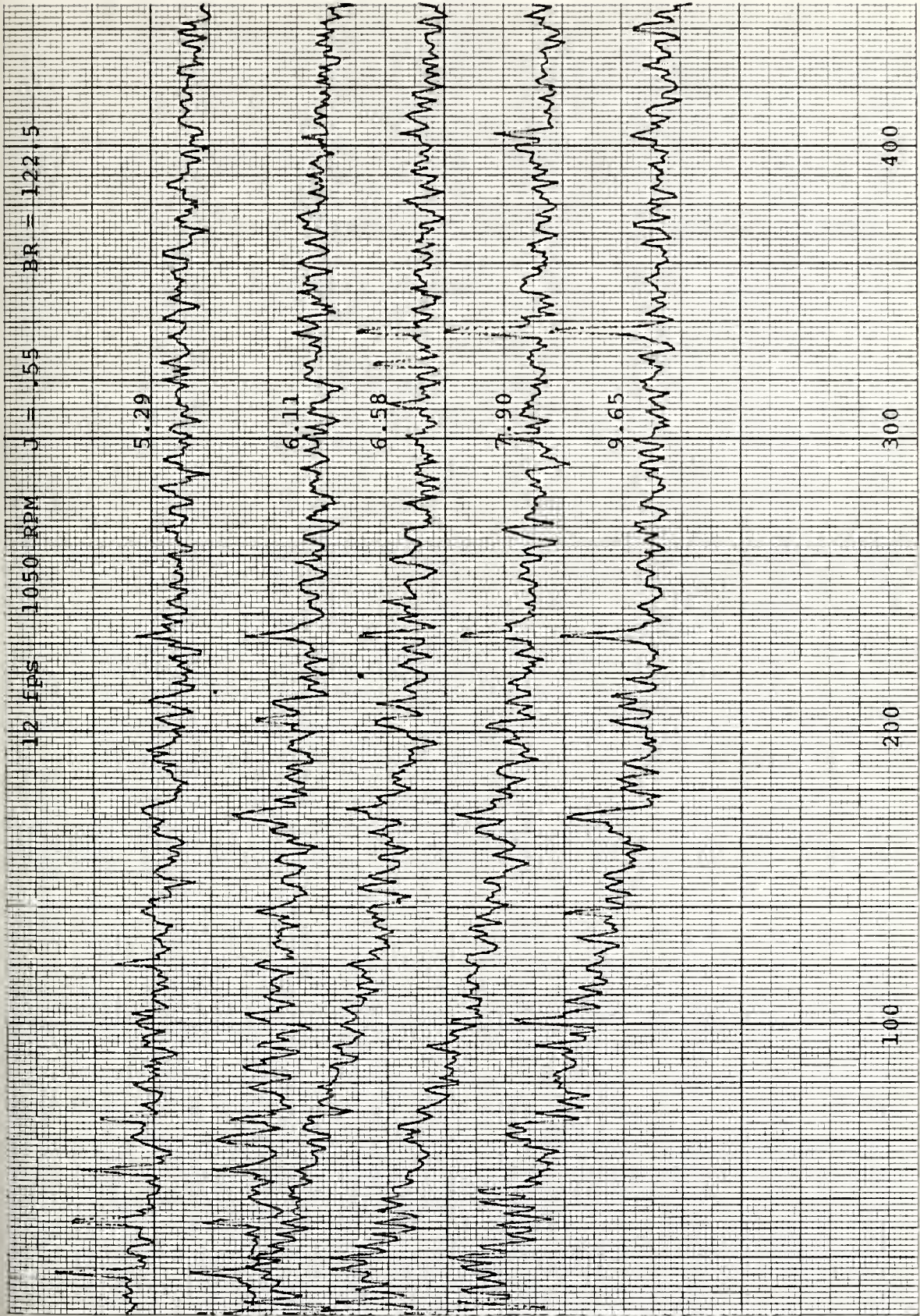


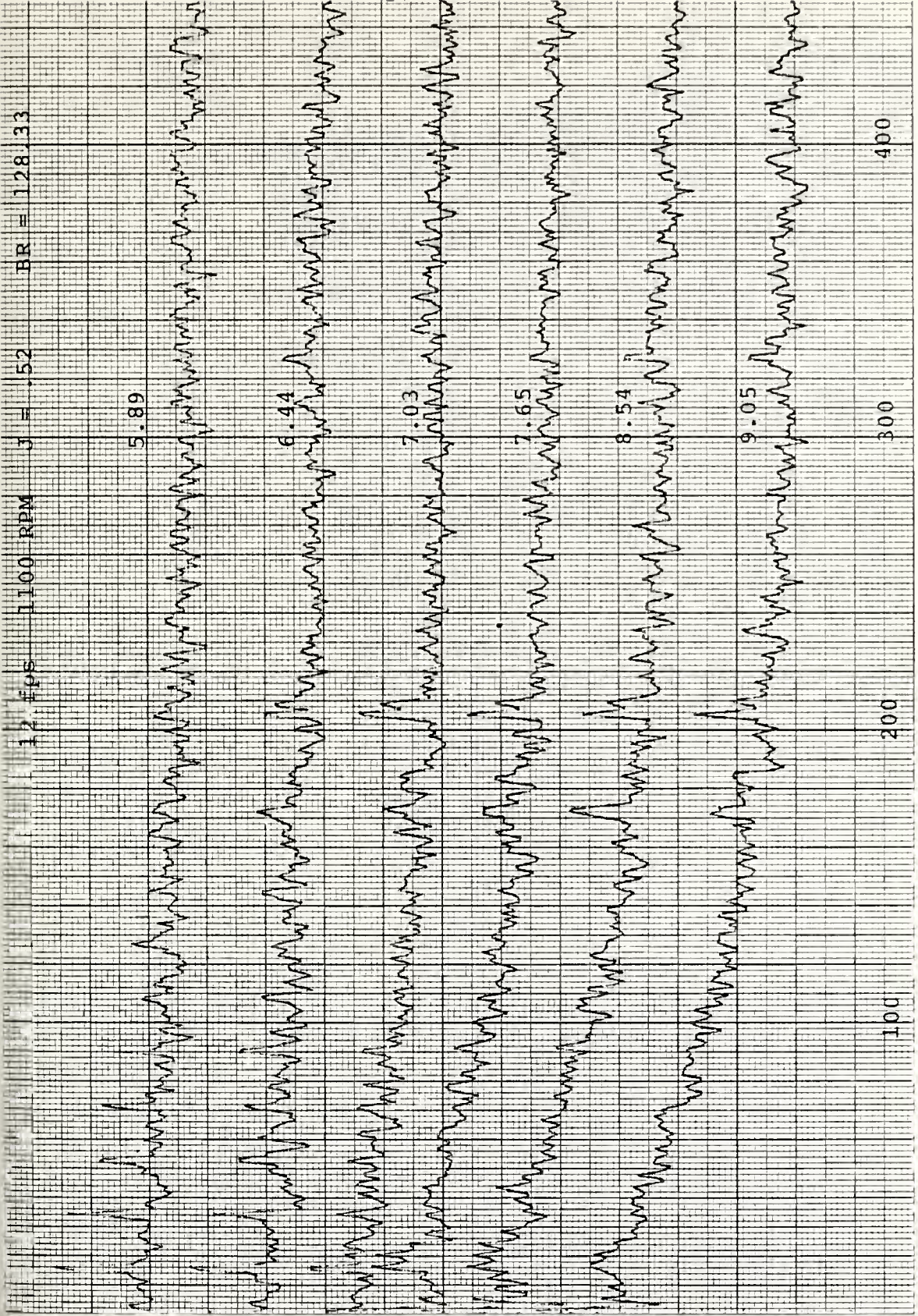


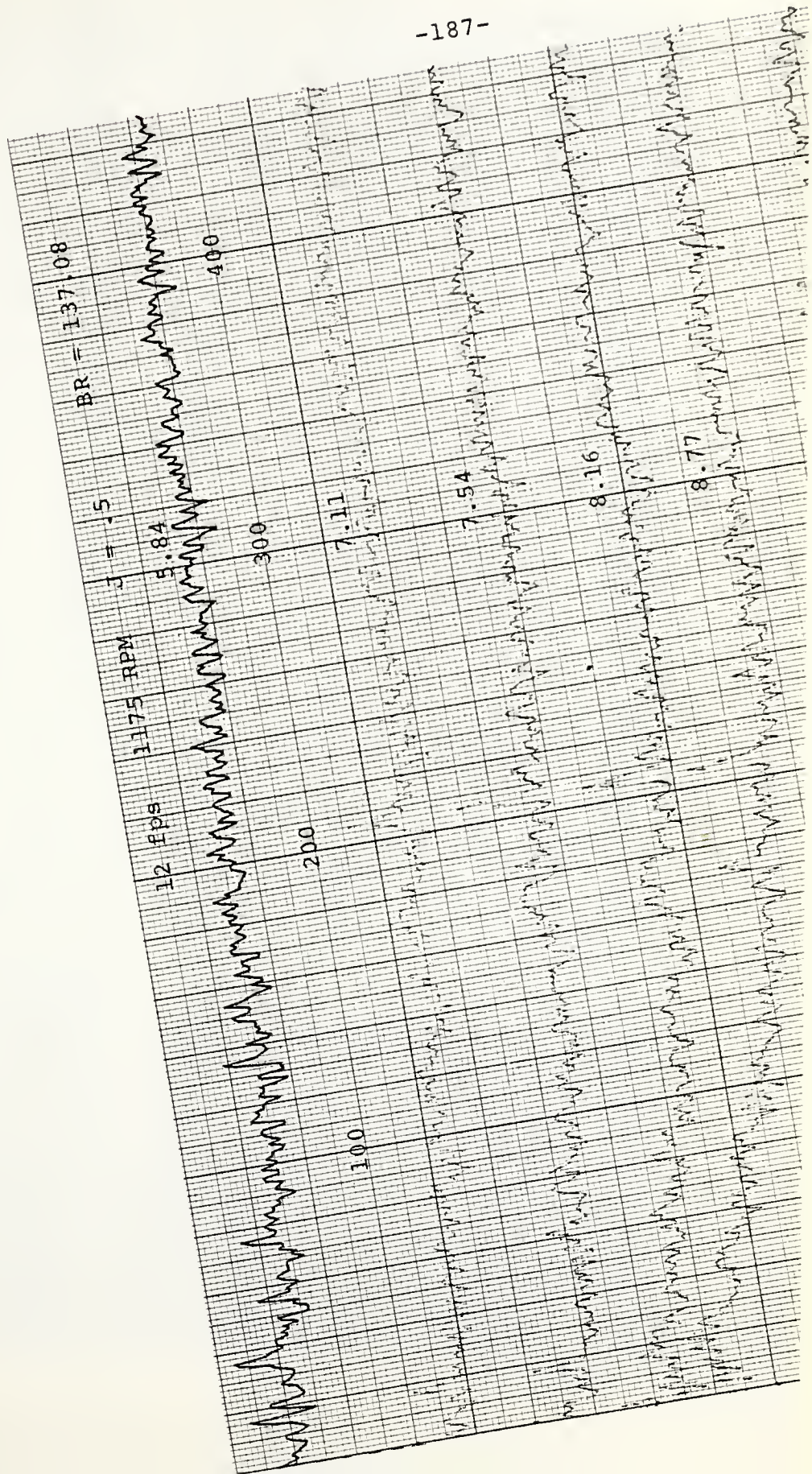


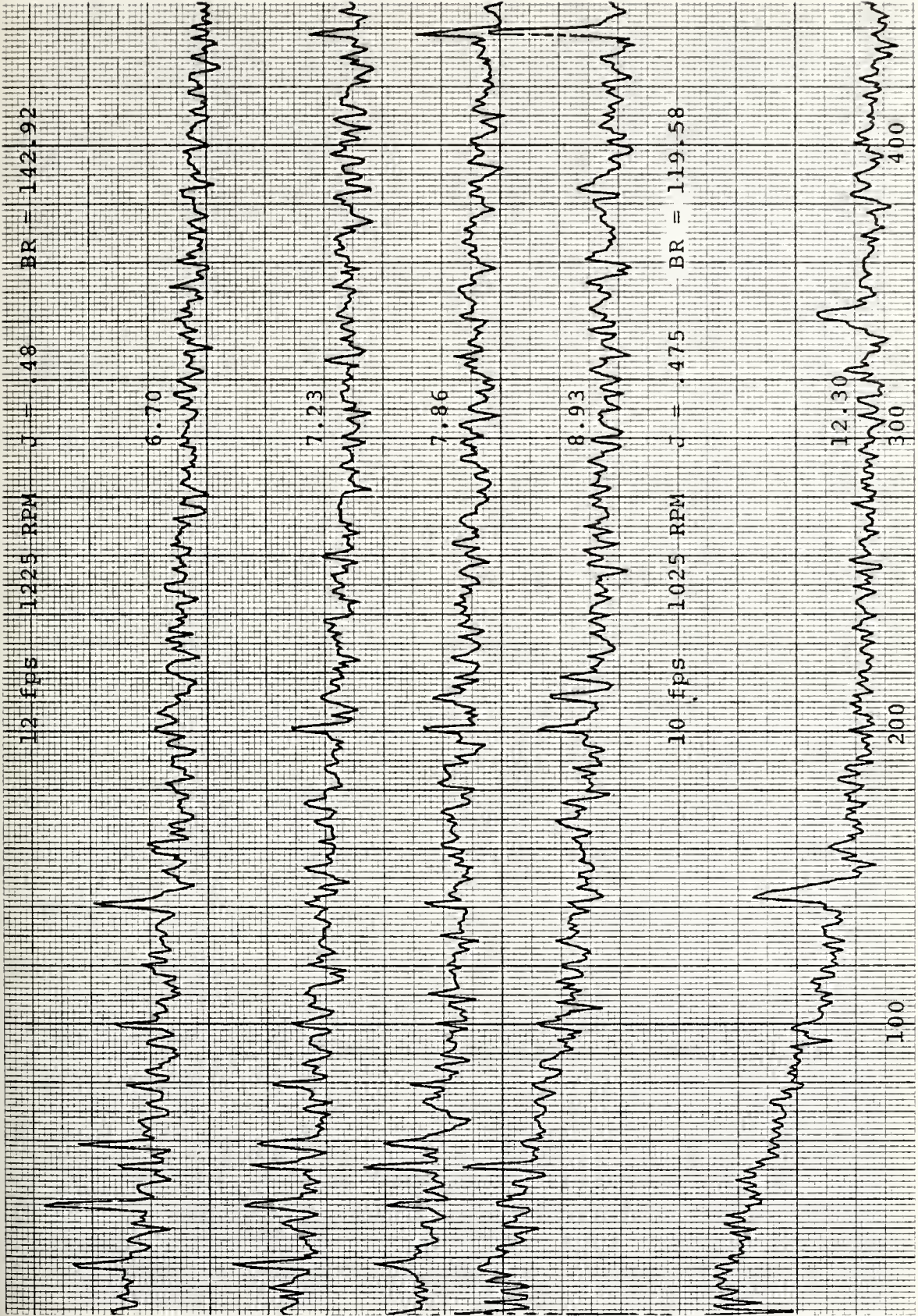


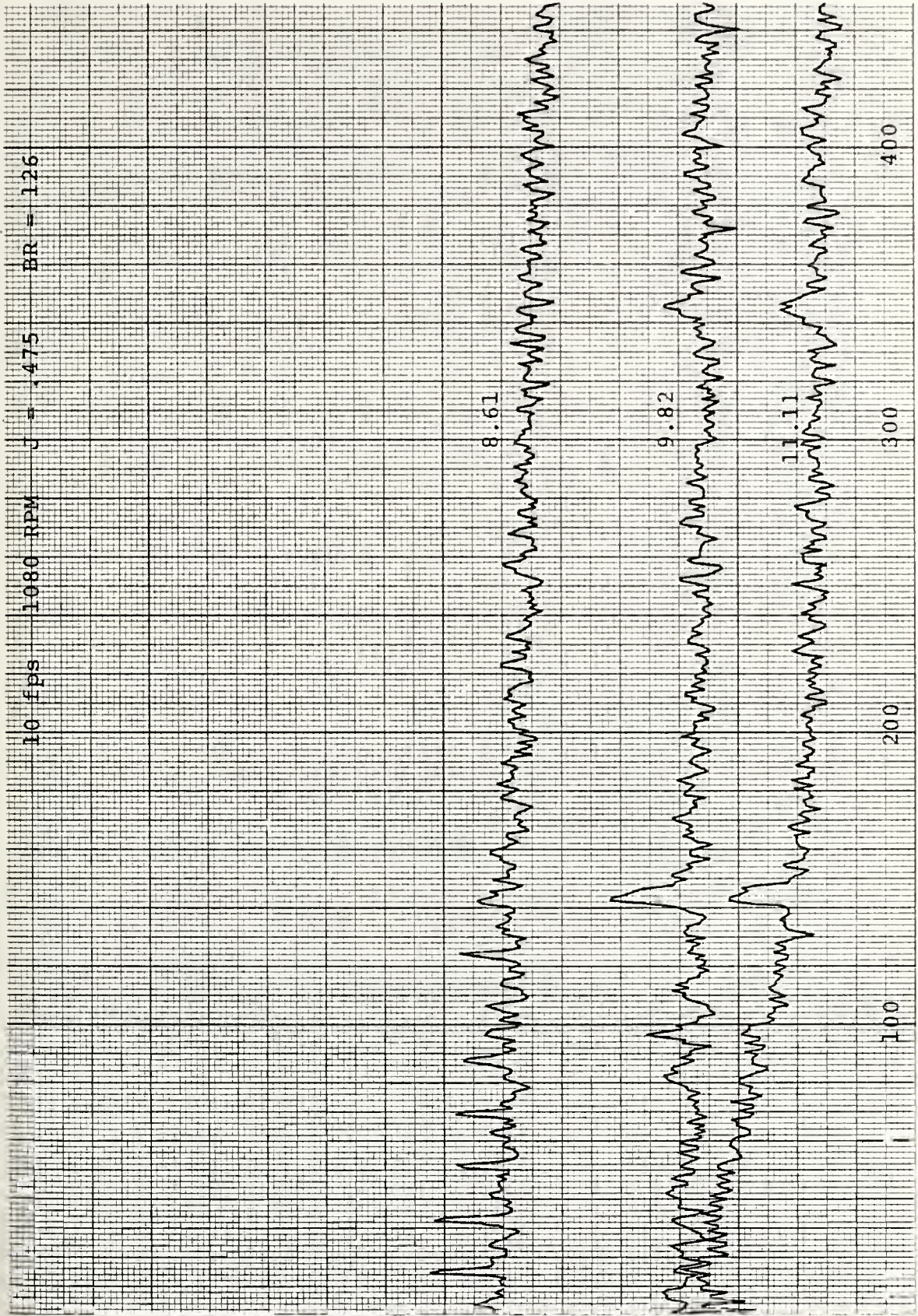


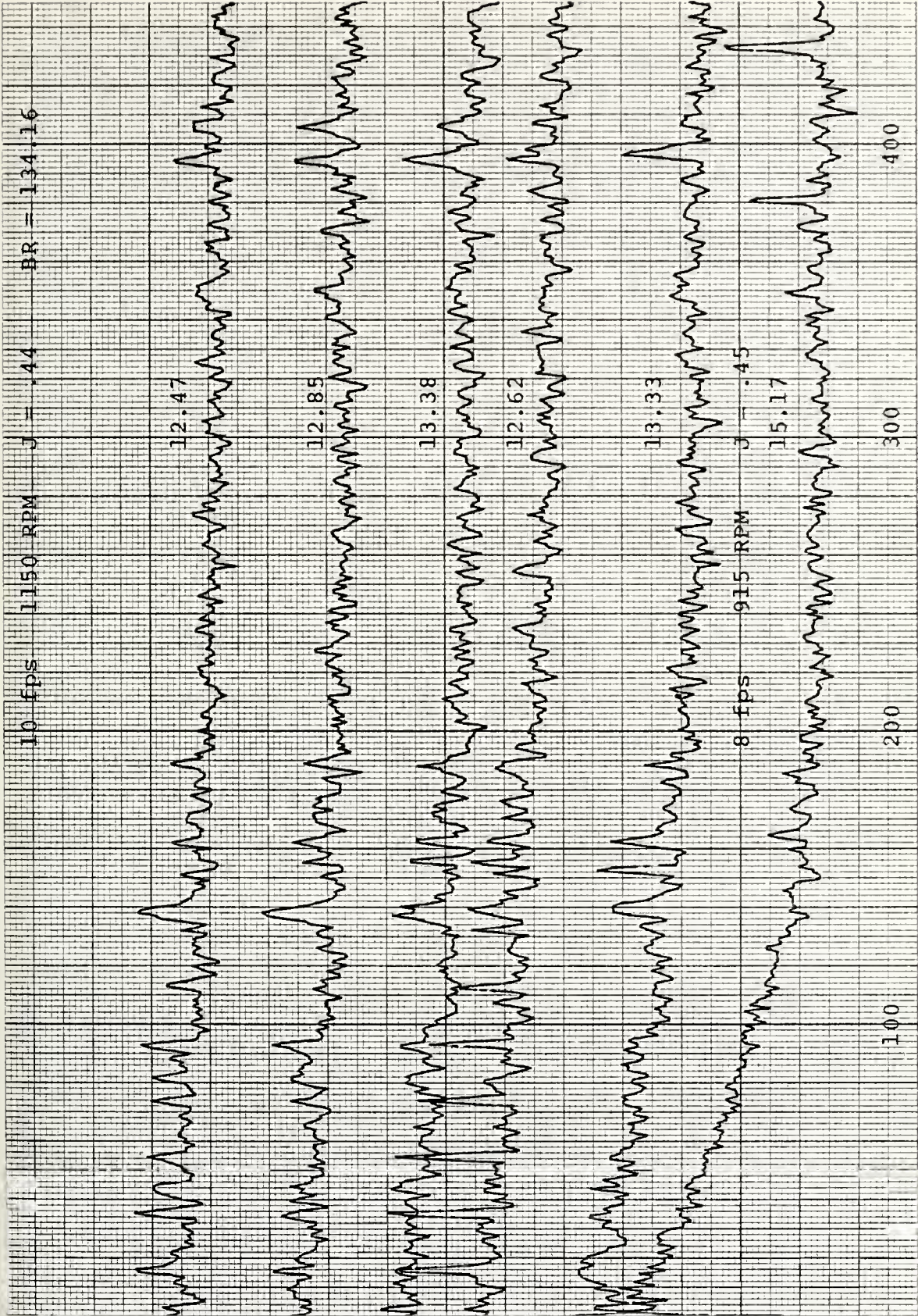


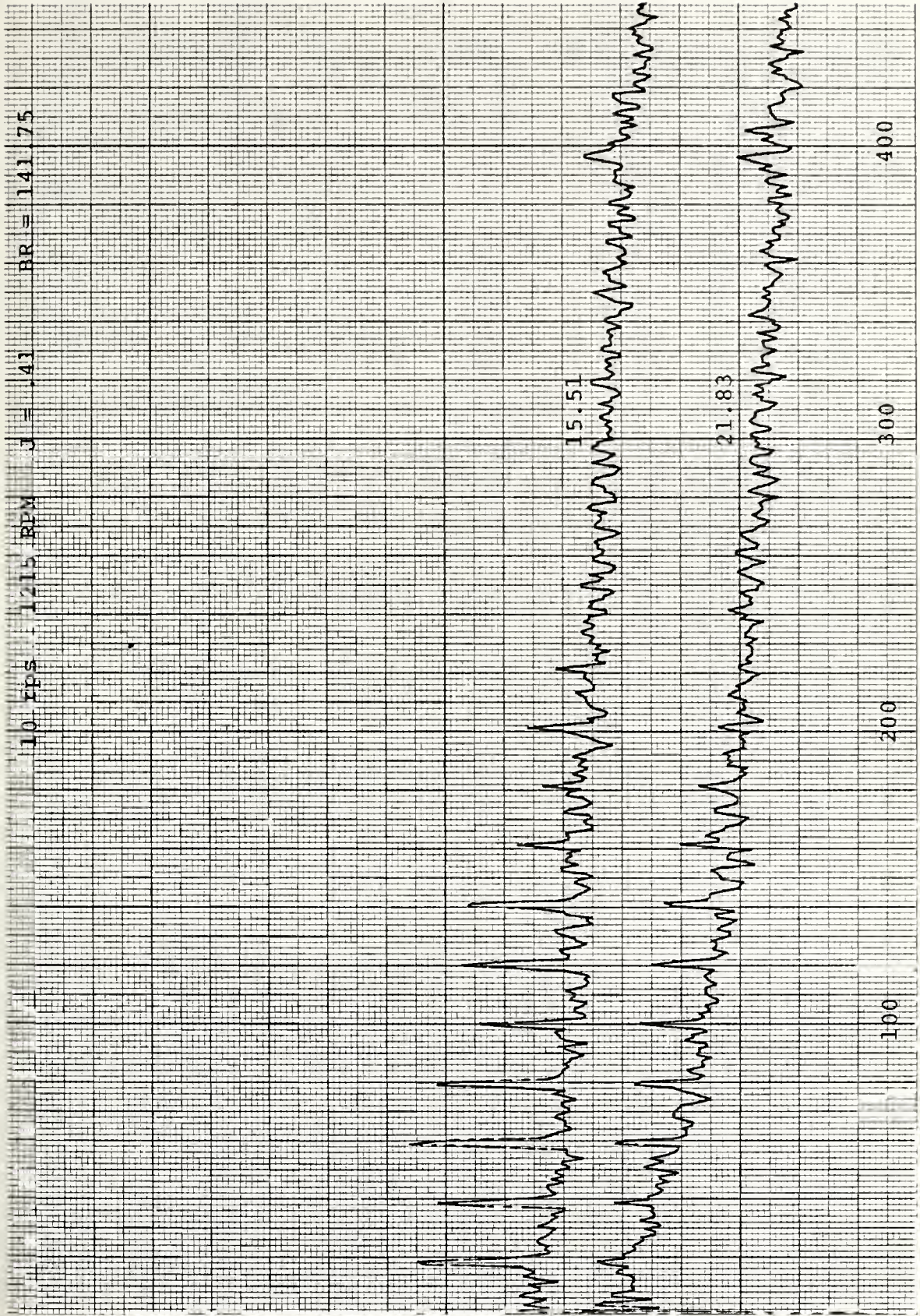


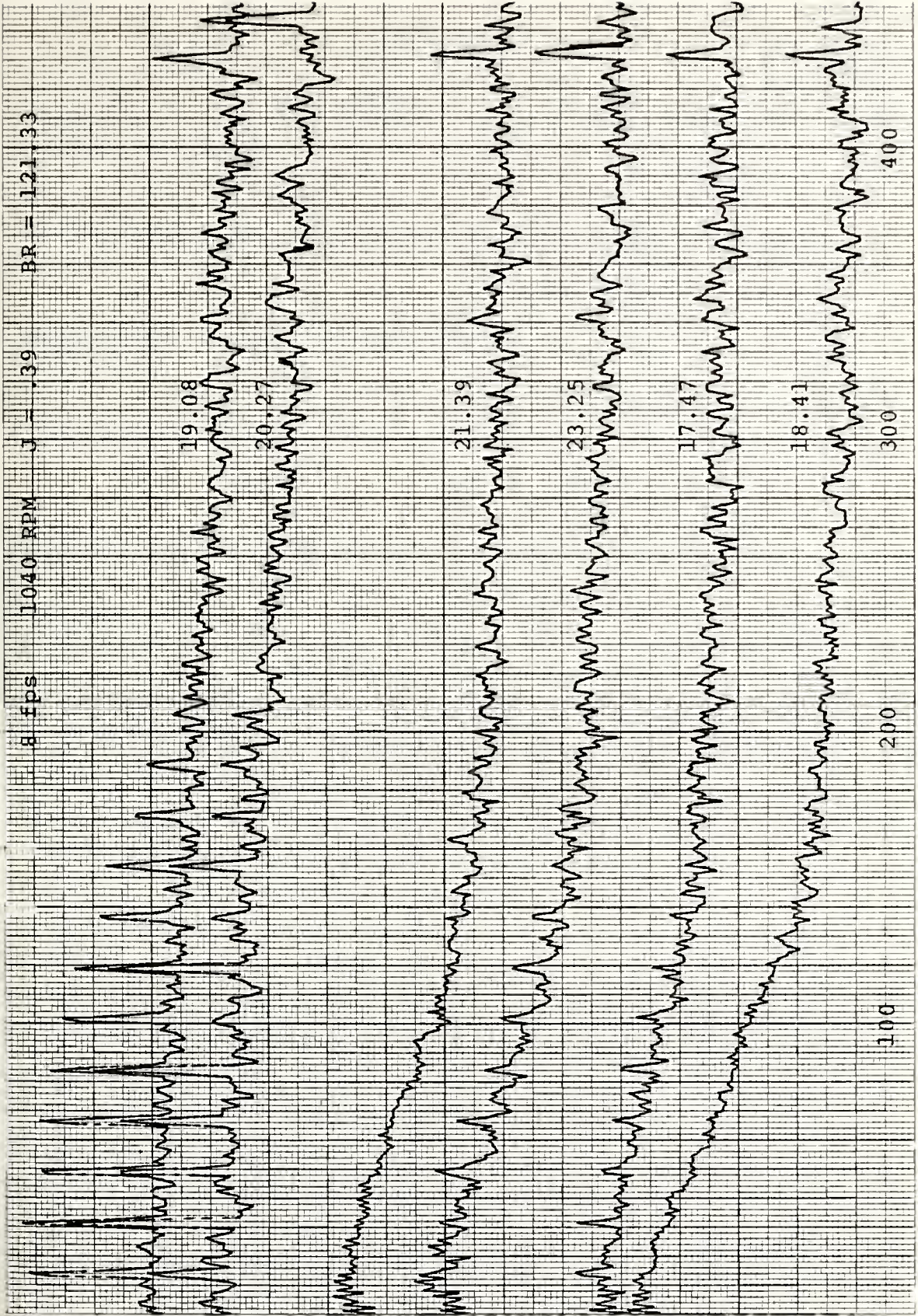


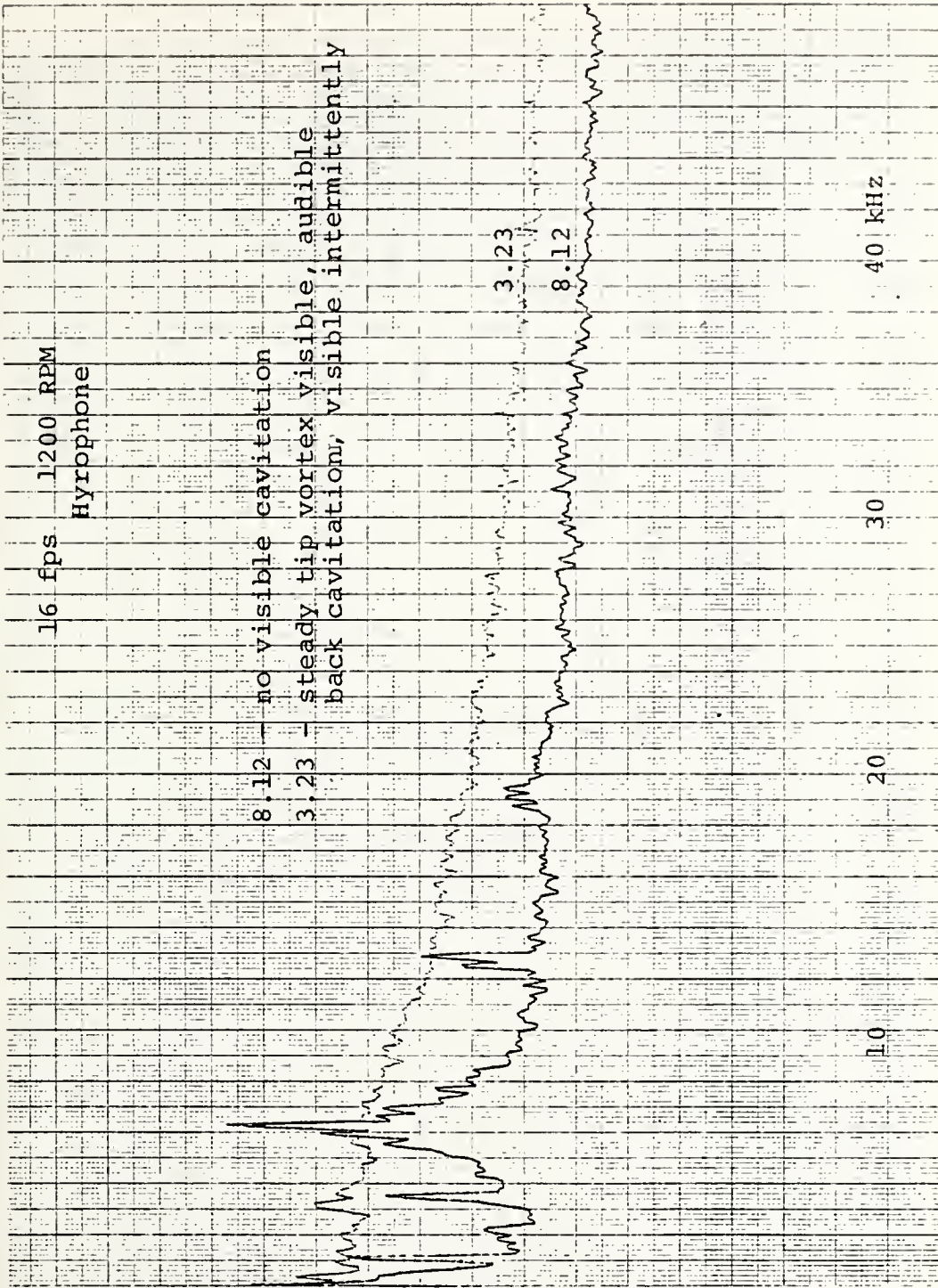


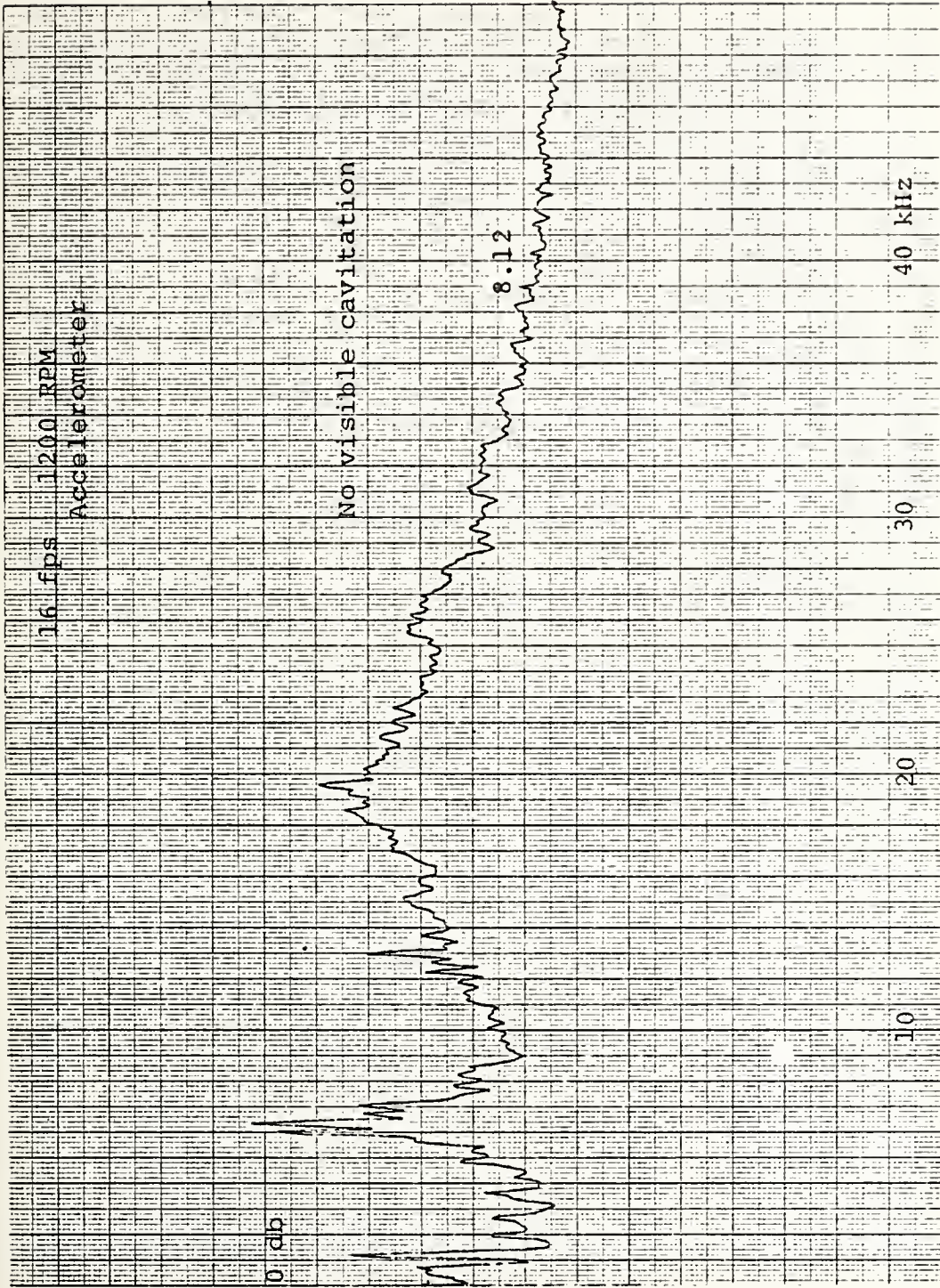


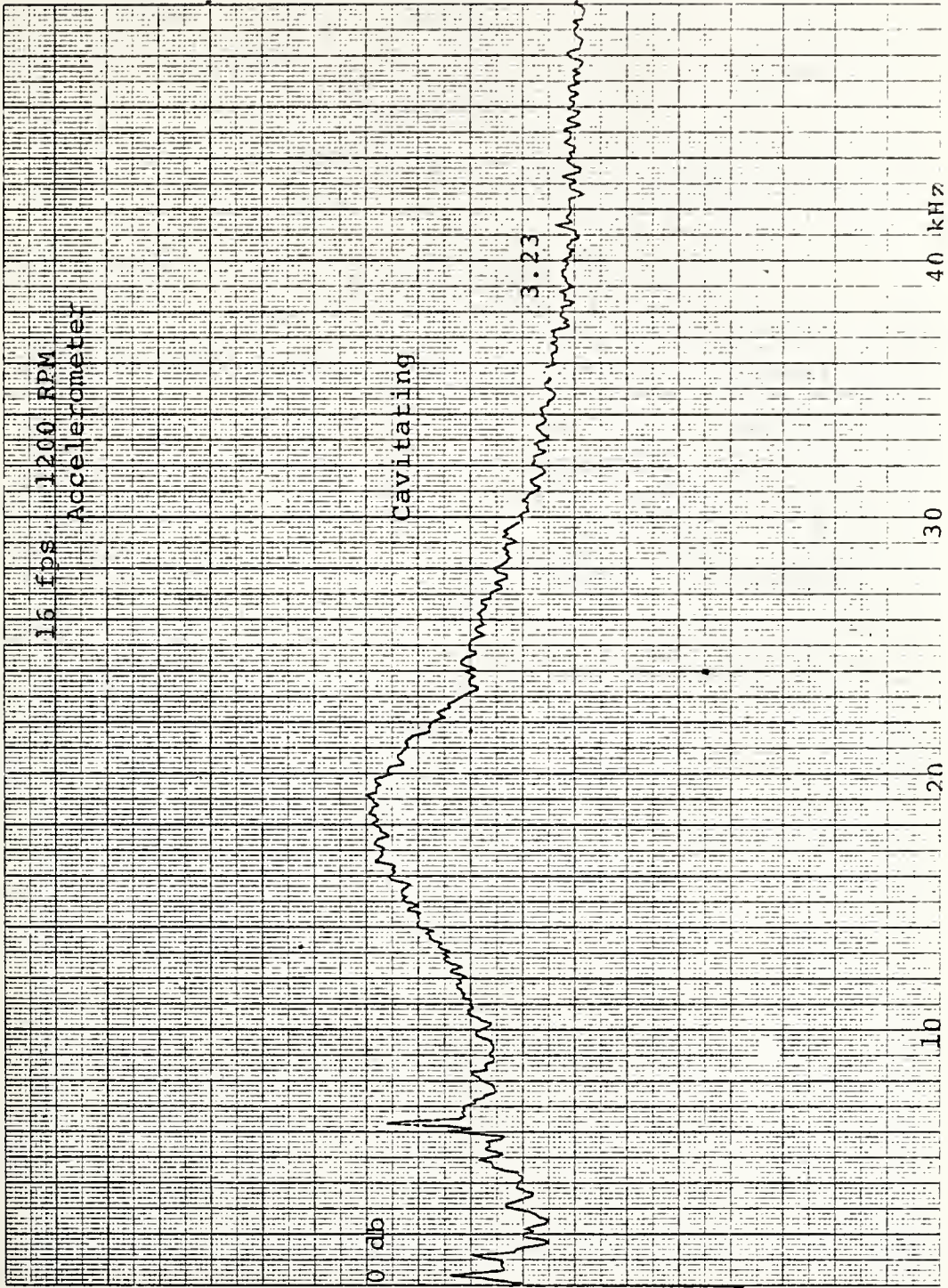












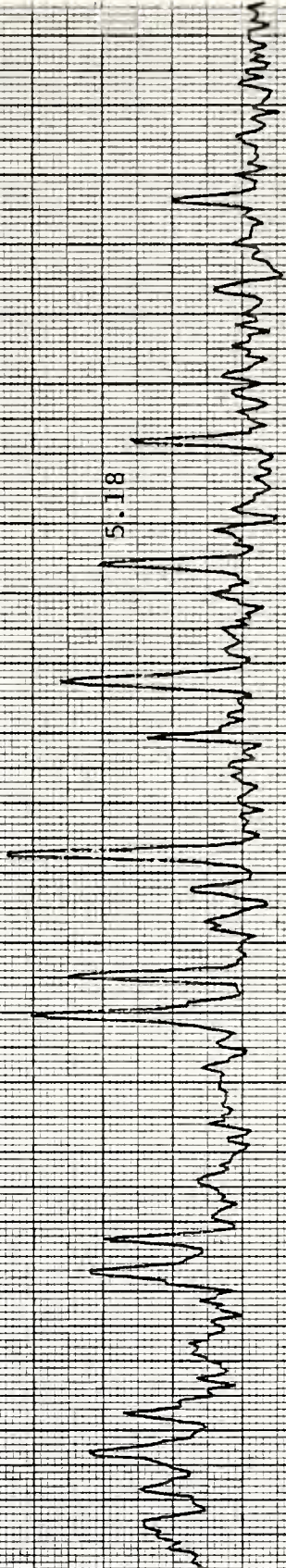
BR = 178.5

1530 RPM $\sigma = .62$

Accel.

20 fps

5.18



100

200

300

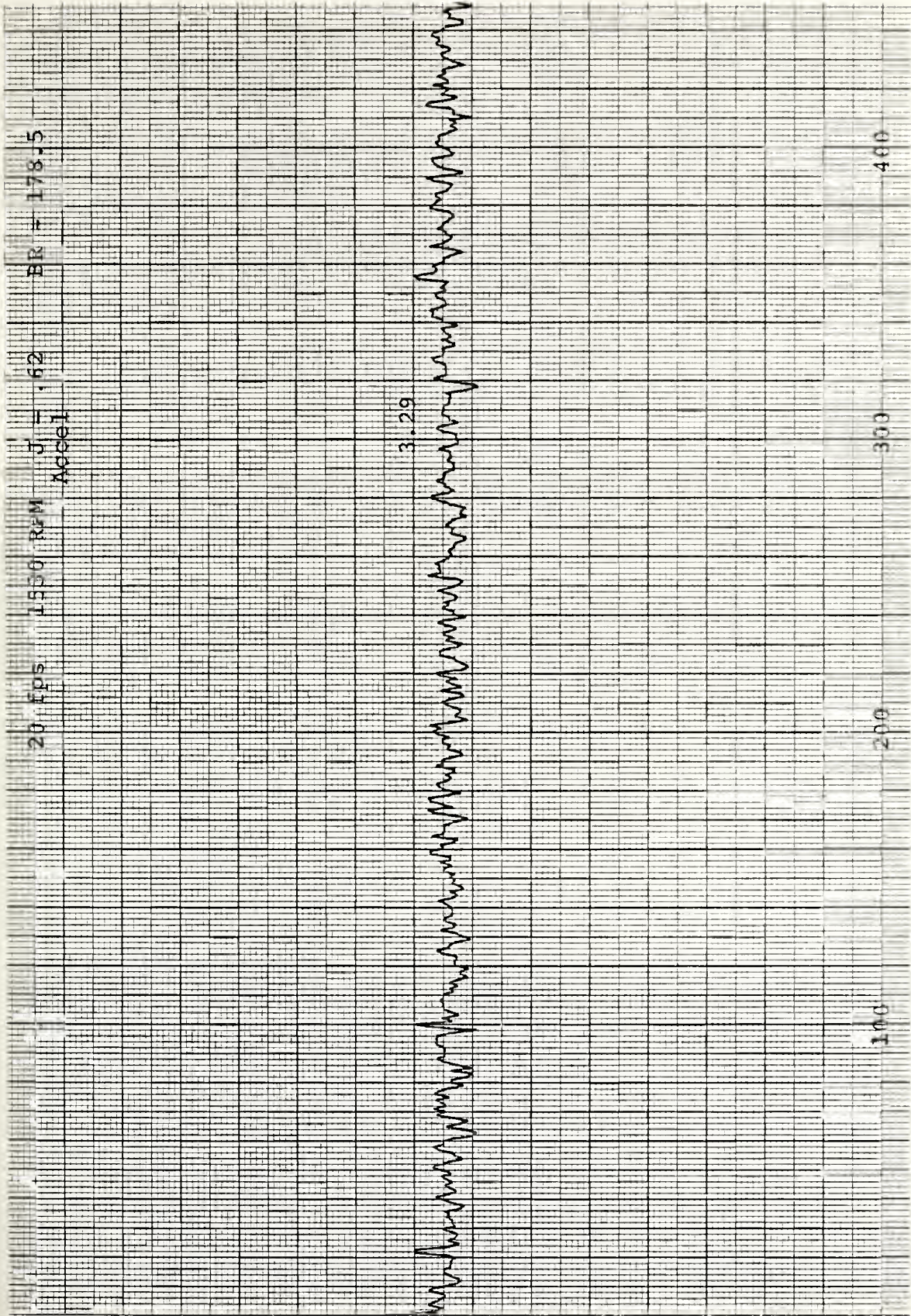
400

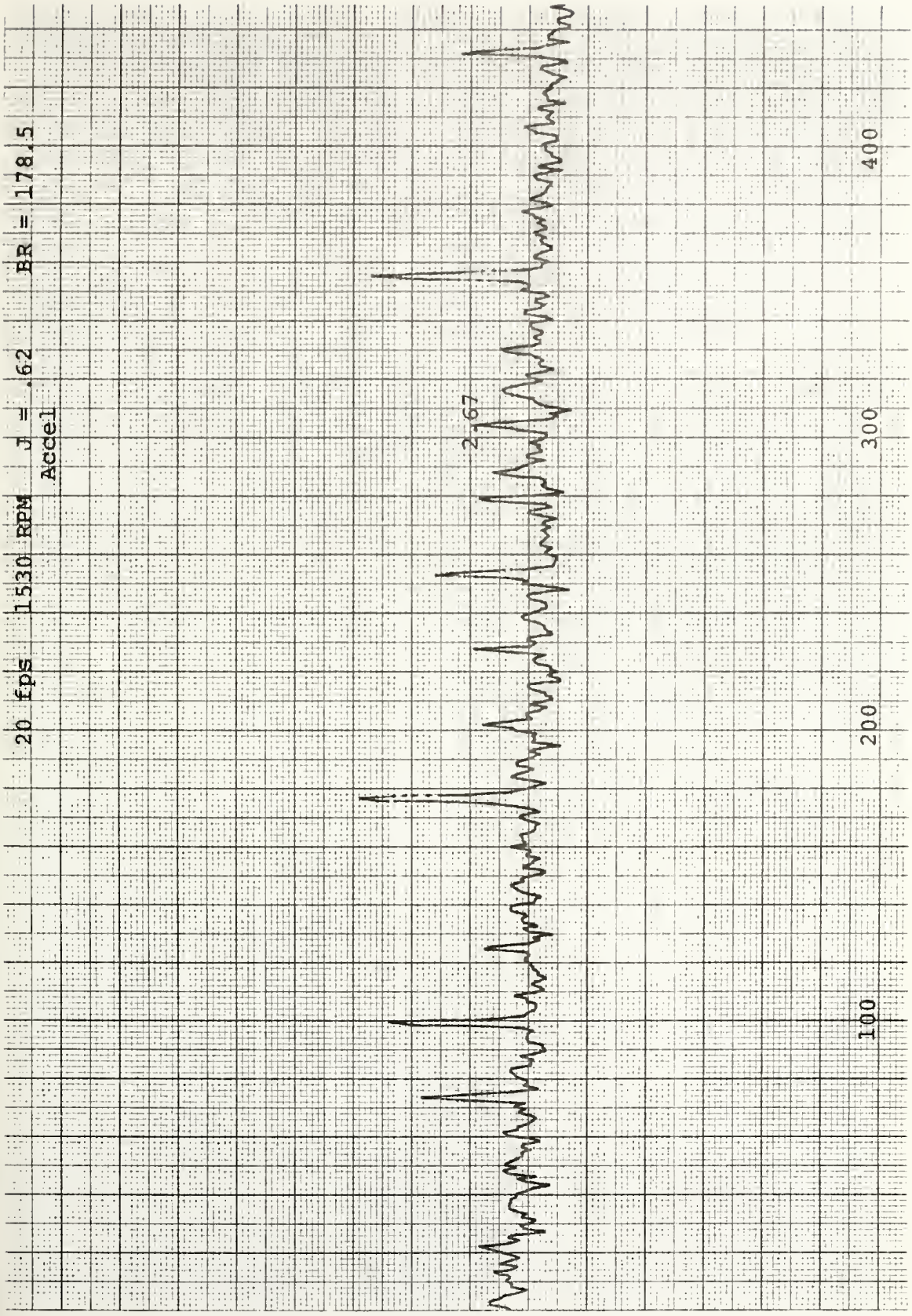
20 ipb 1530 RPM J = .62 BR = 178.5
Accel

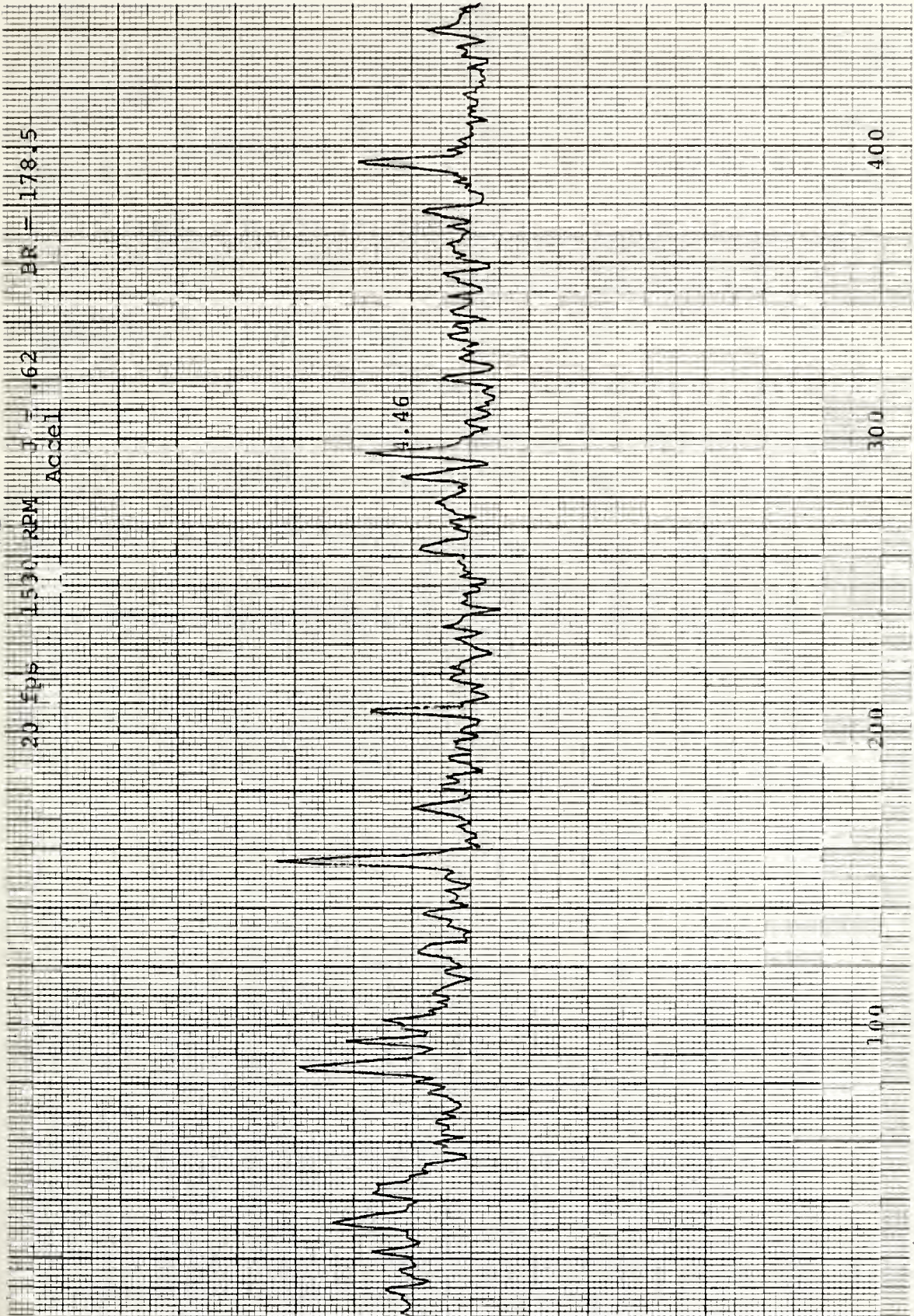
3.83

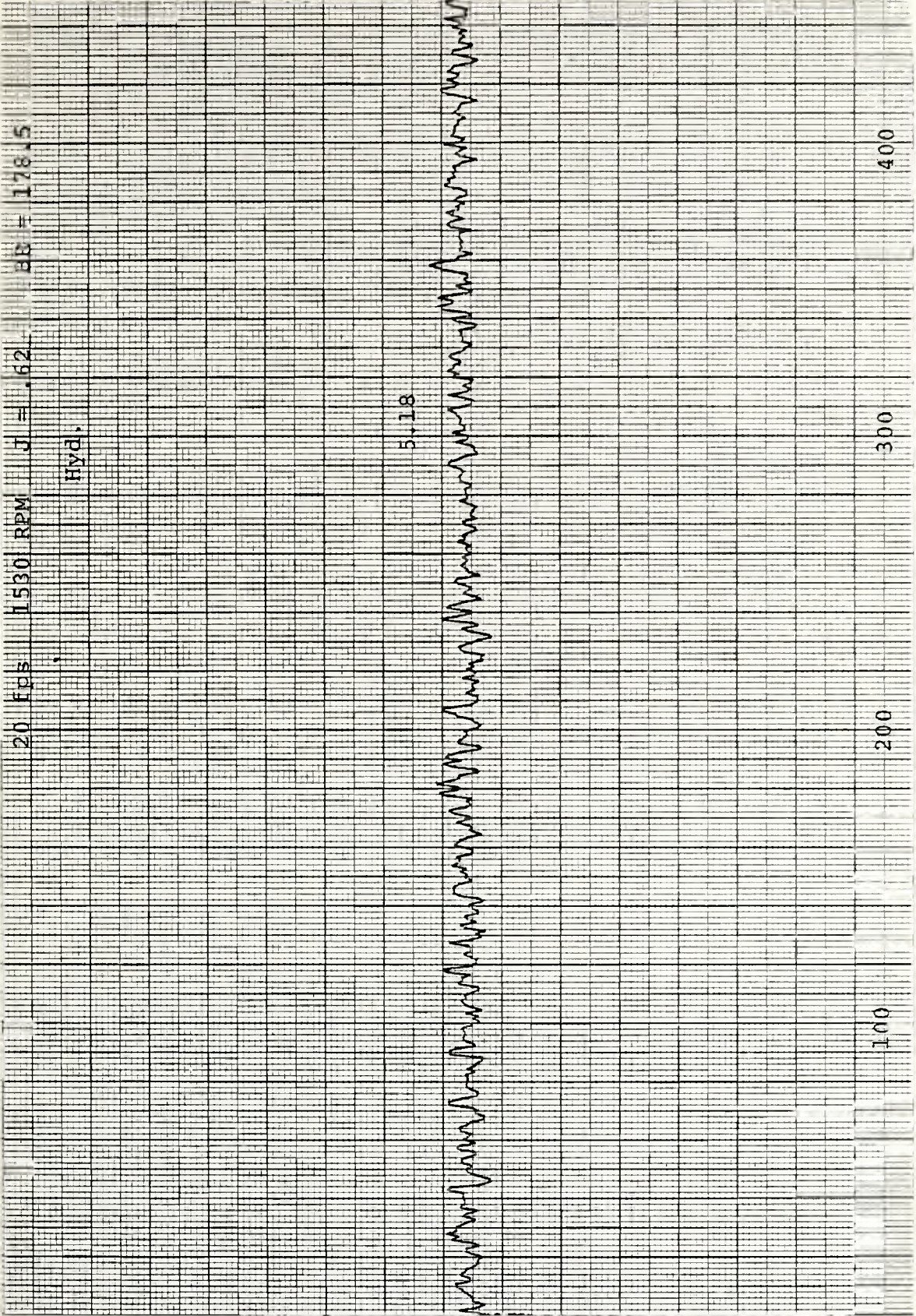


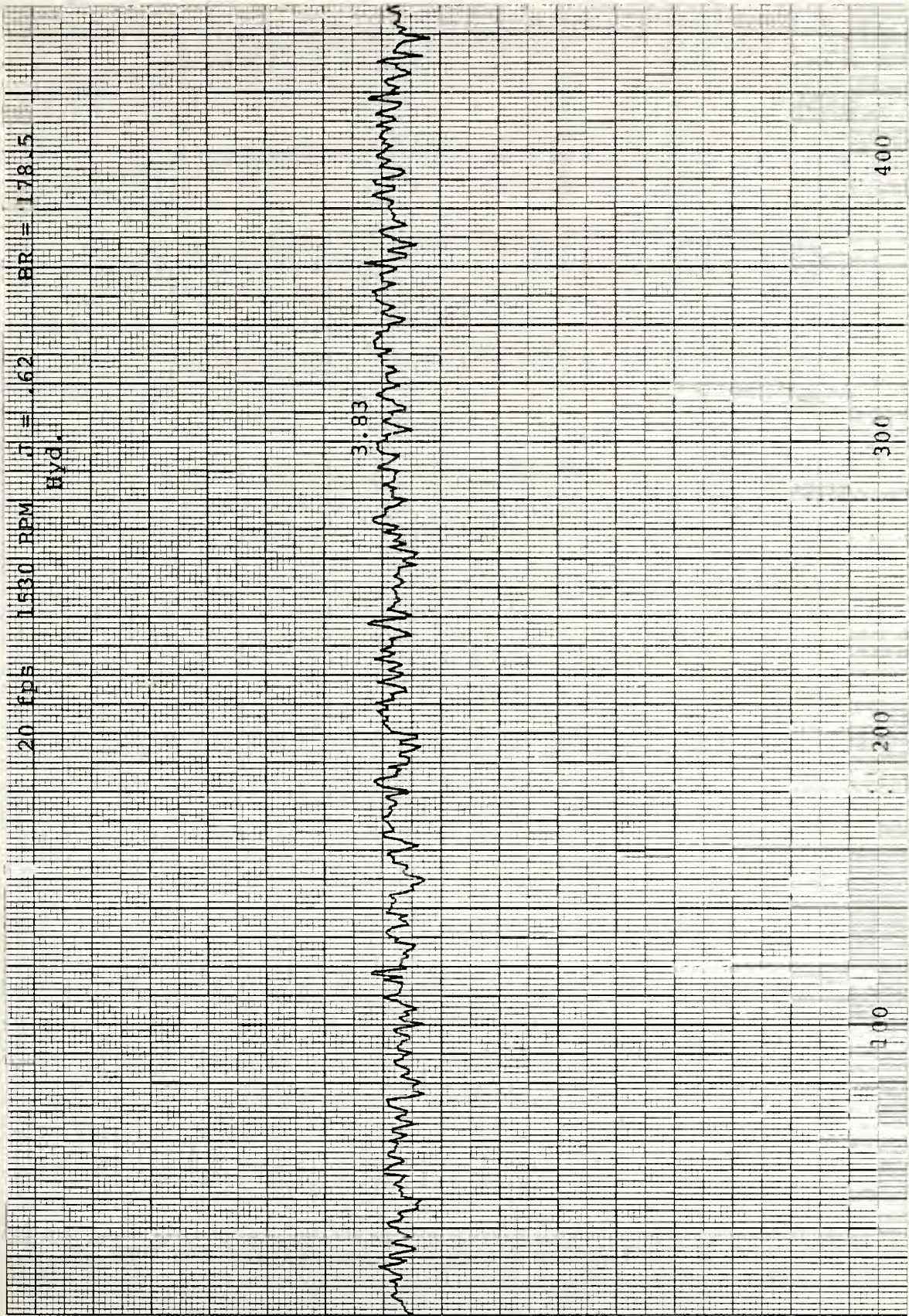
100 200 300 400

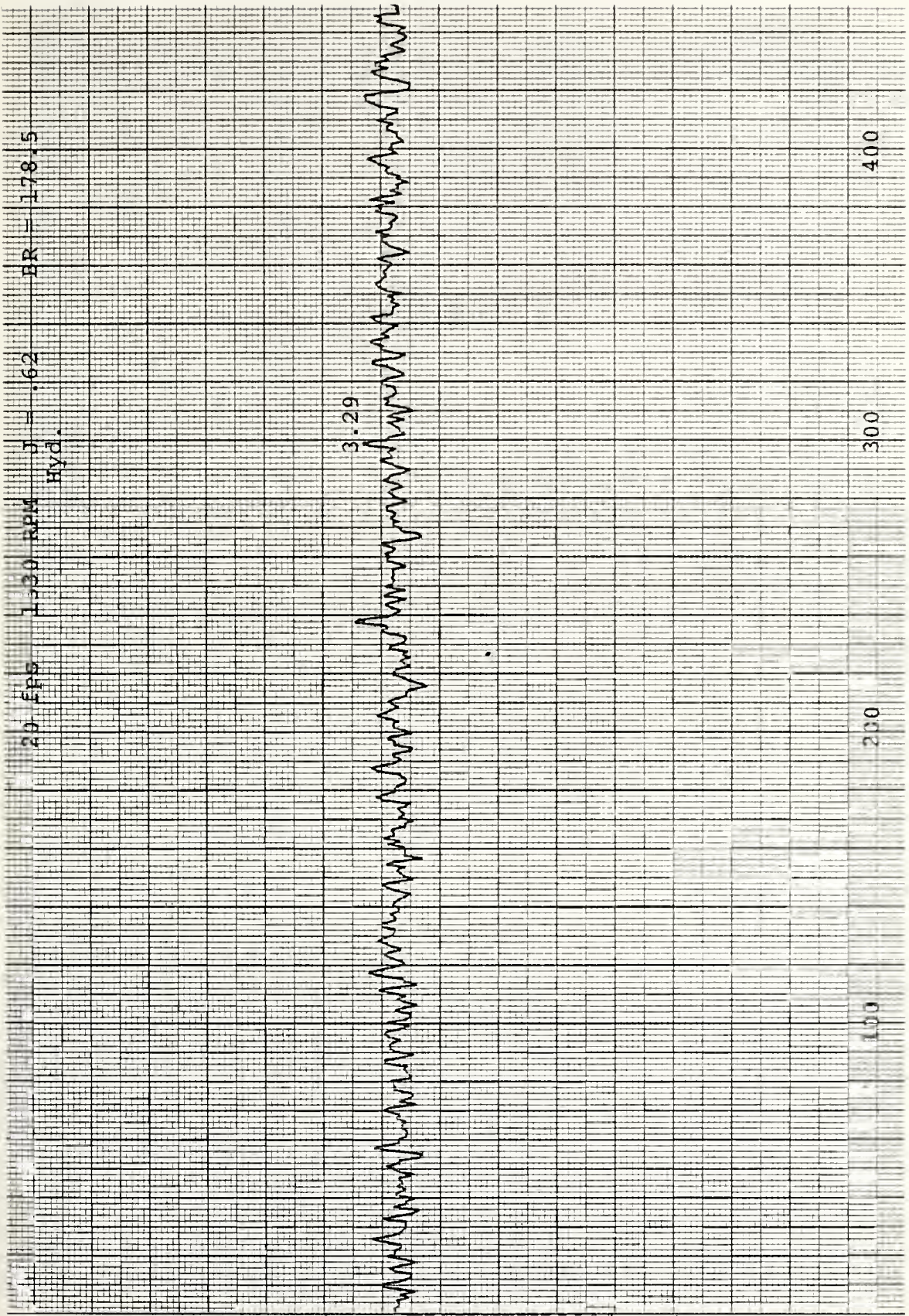


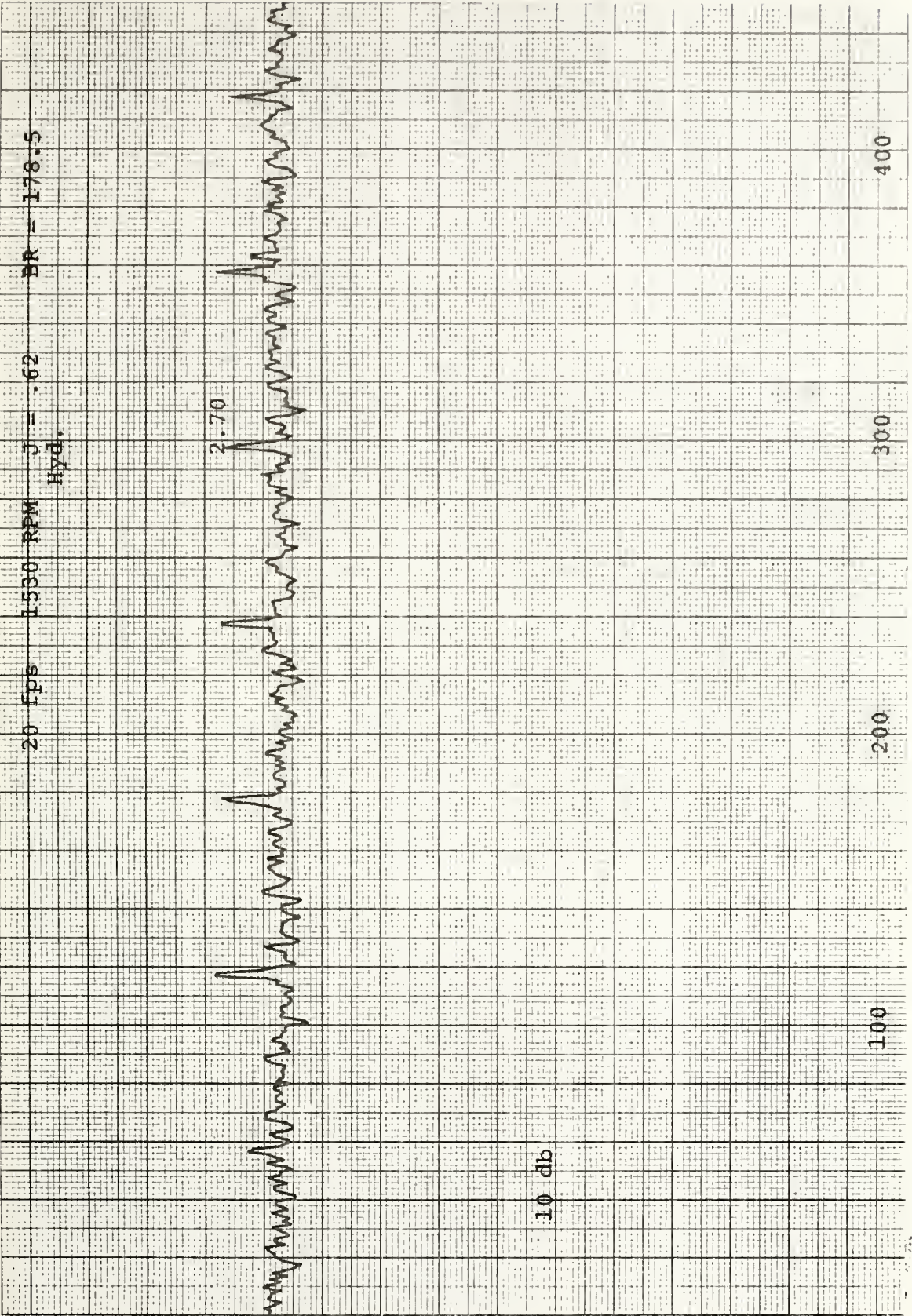


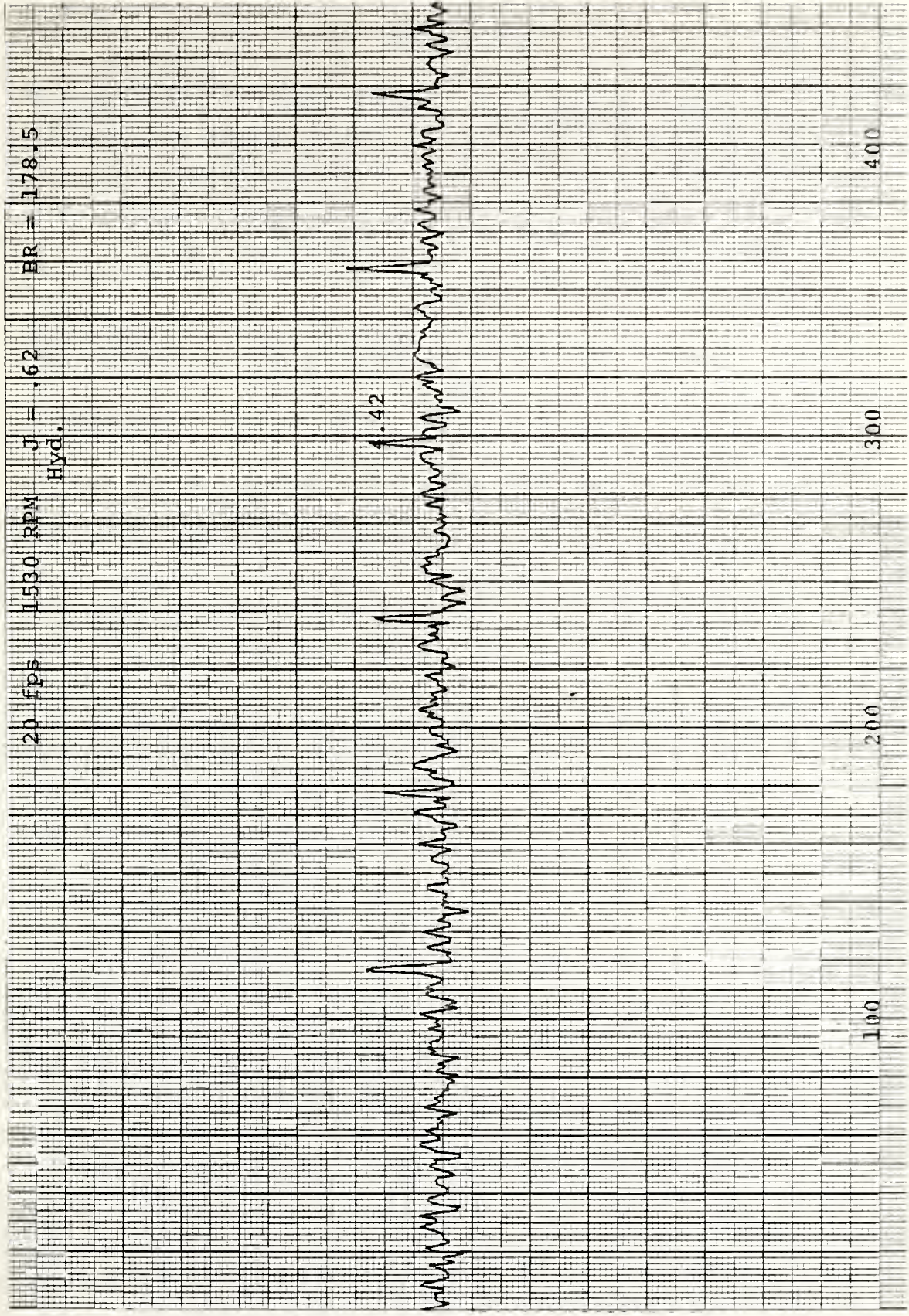


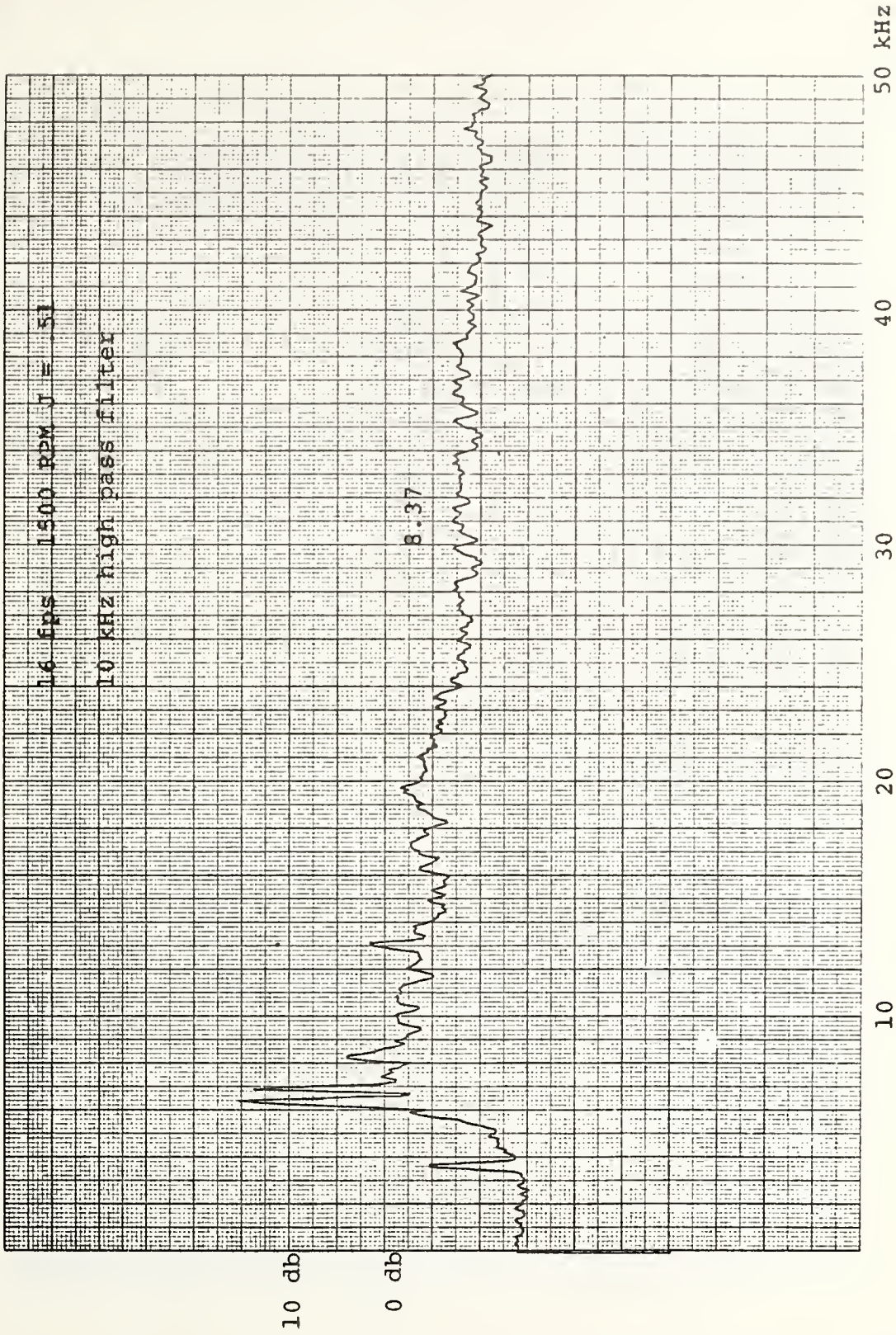








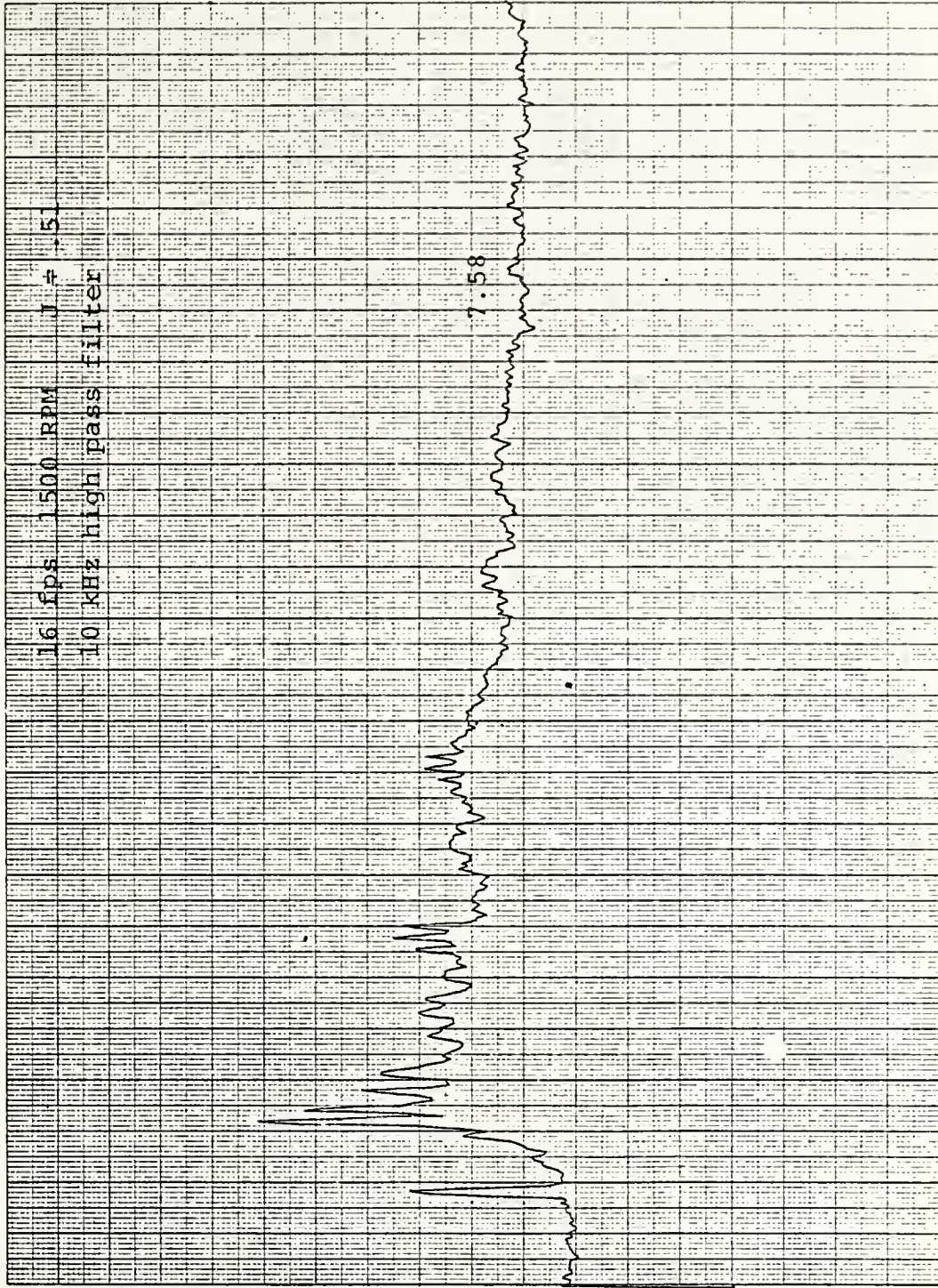




K-E 10 X 10 TO THE CENTIMETER 18 X 25 CM KEUFFEL & ESSER CO. MADE IN U.S.A.

461510

12

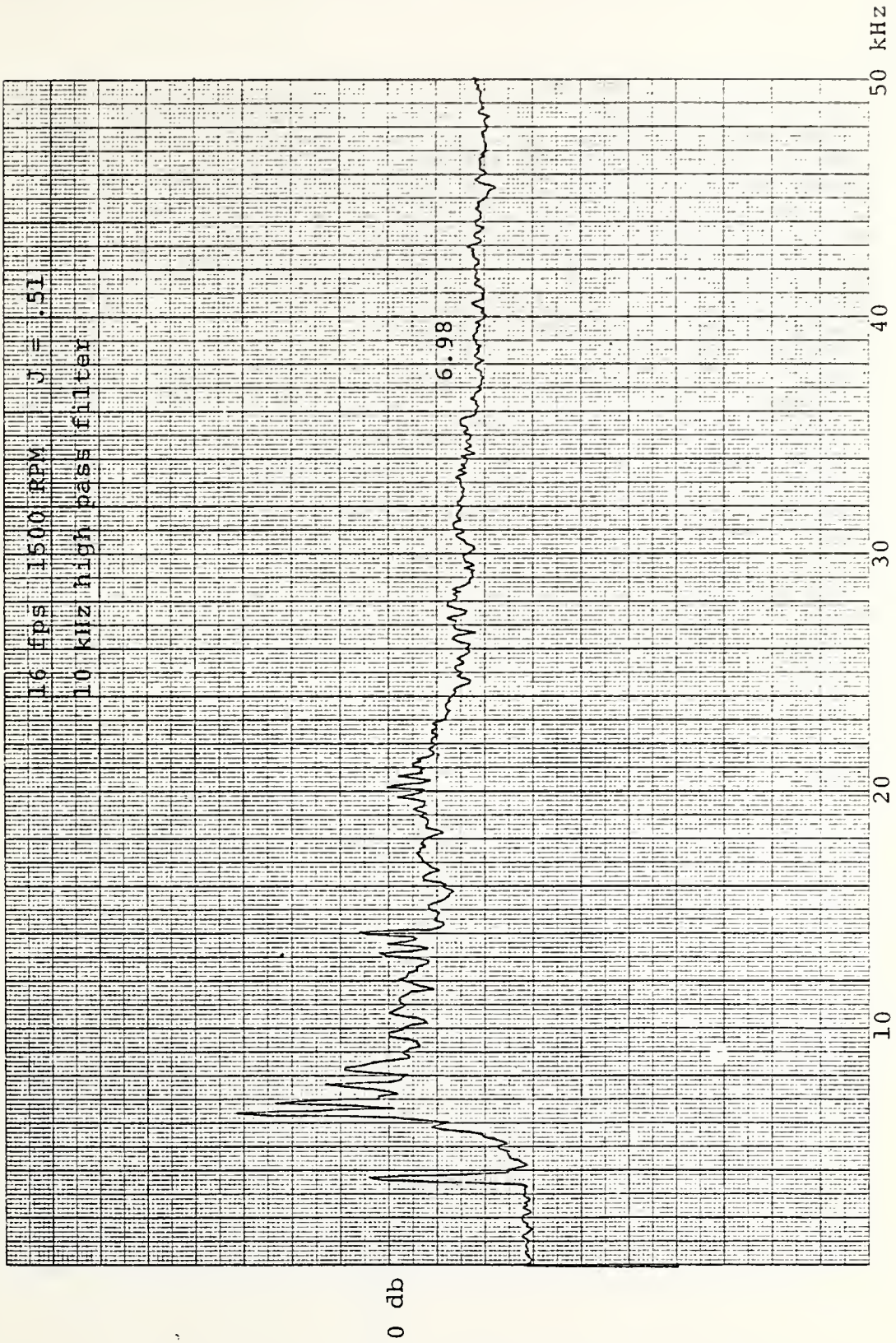


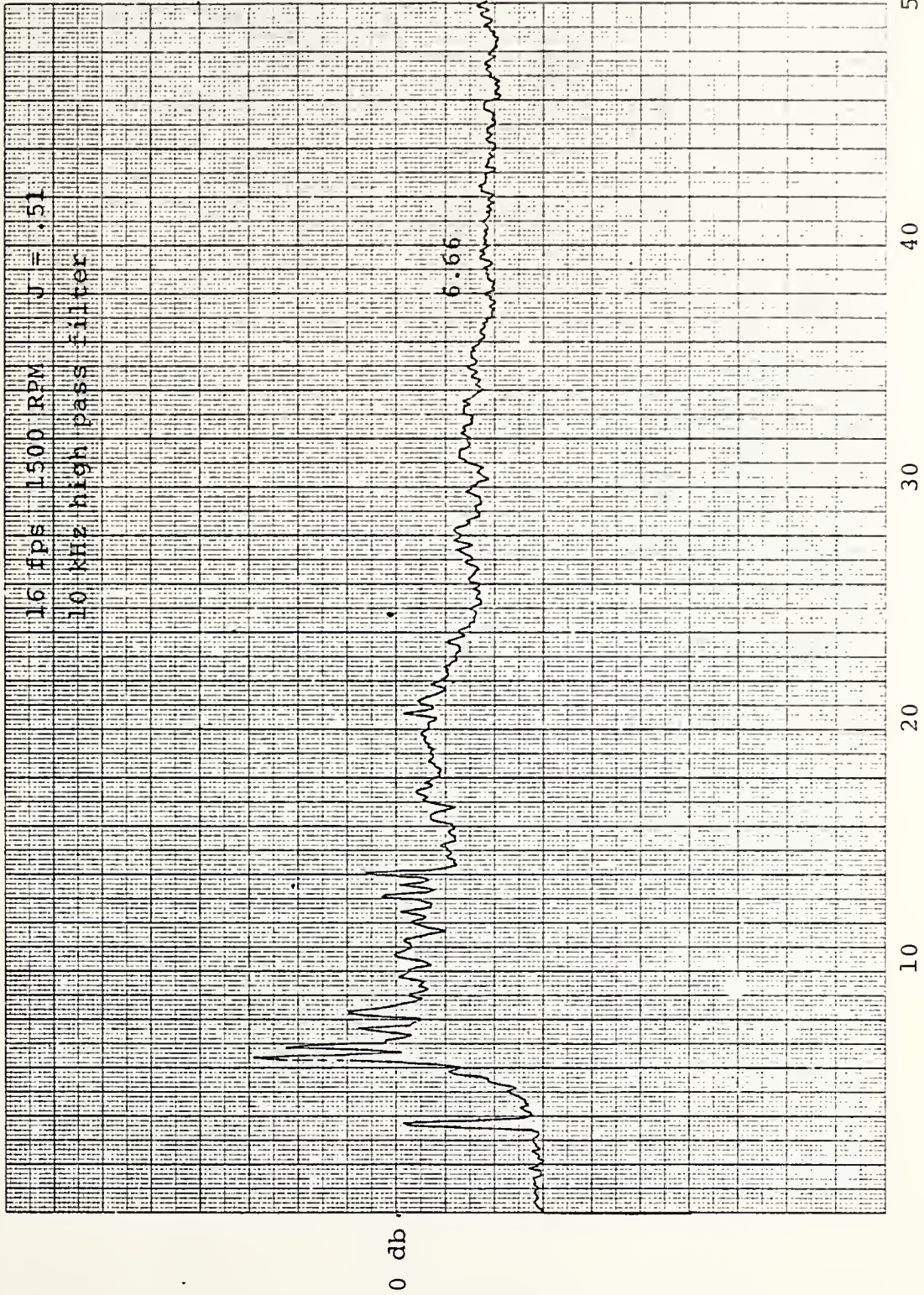
10 20 30 40 50

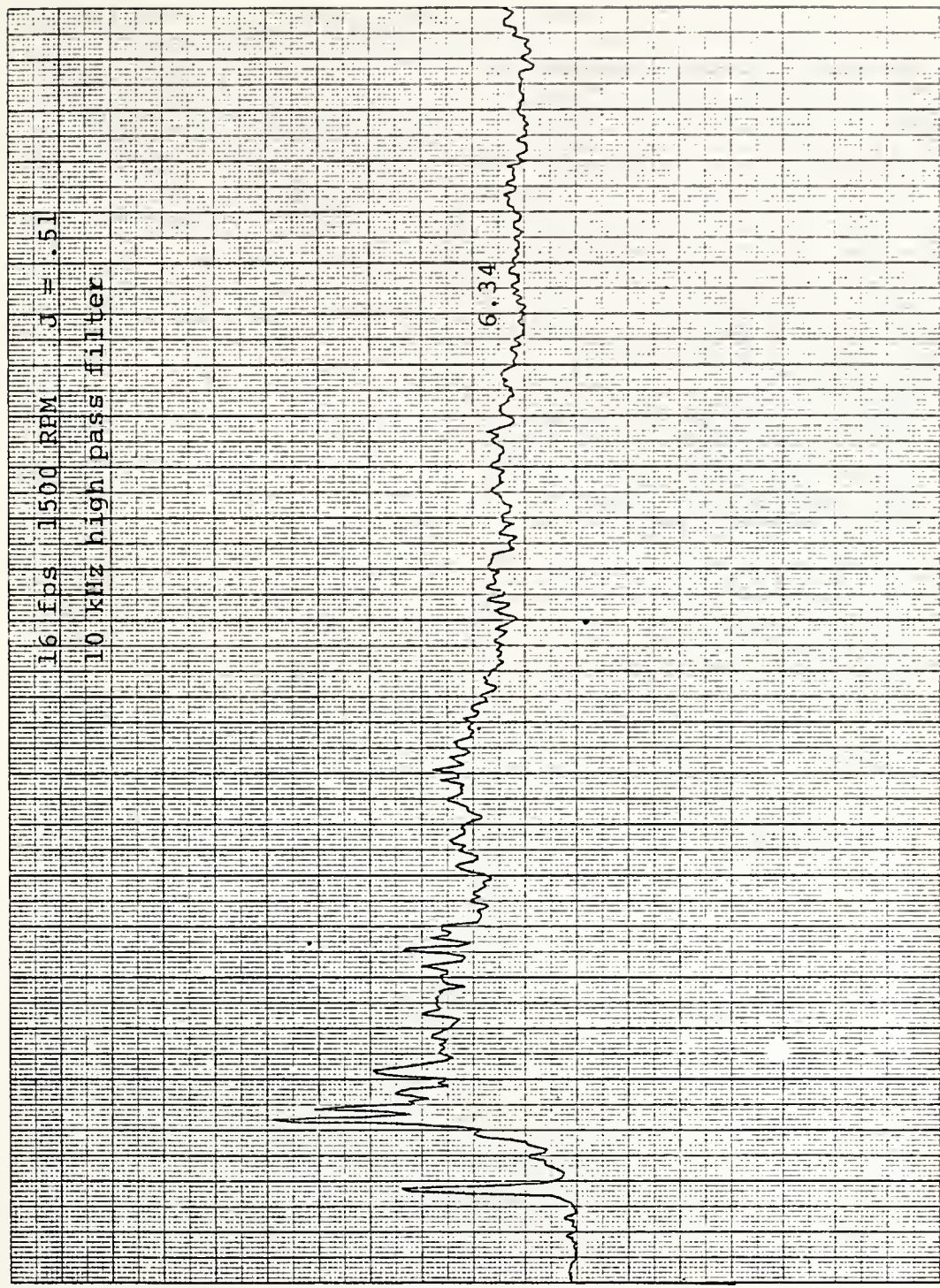
16

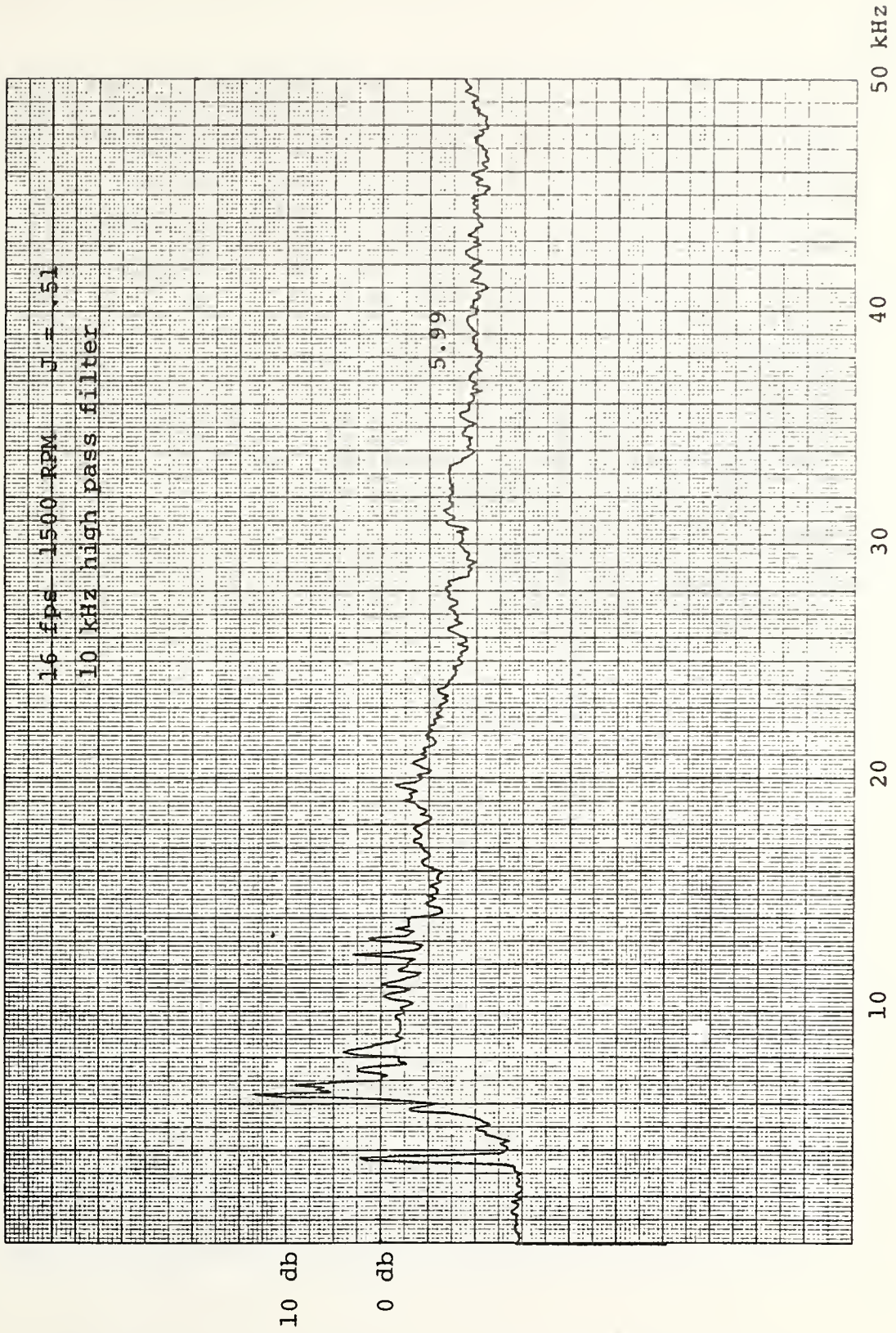
461510

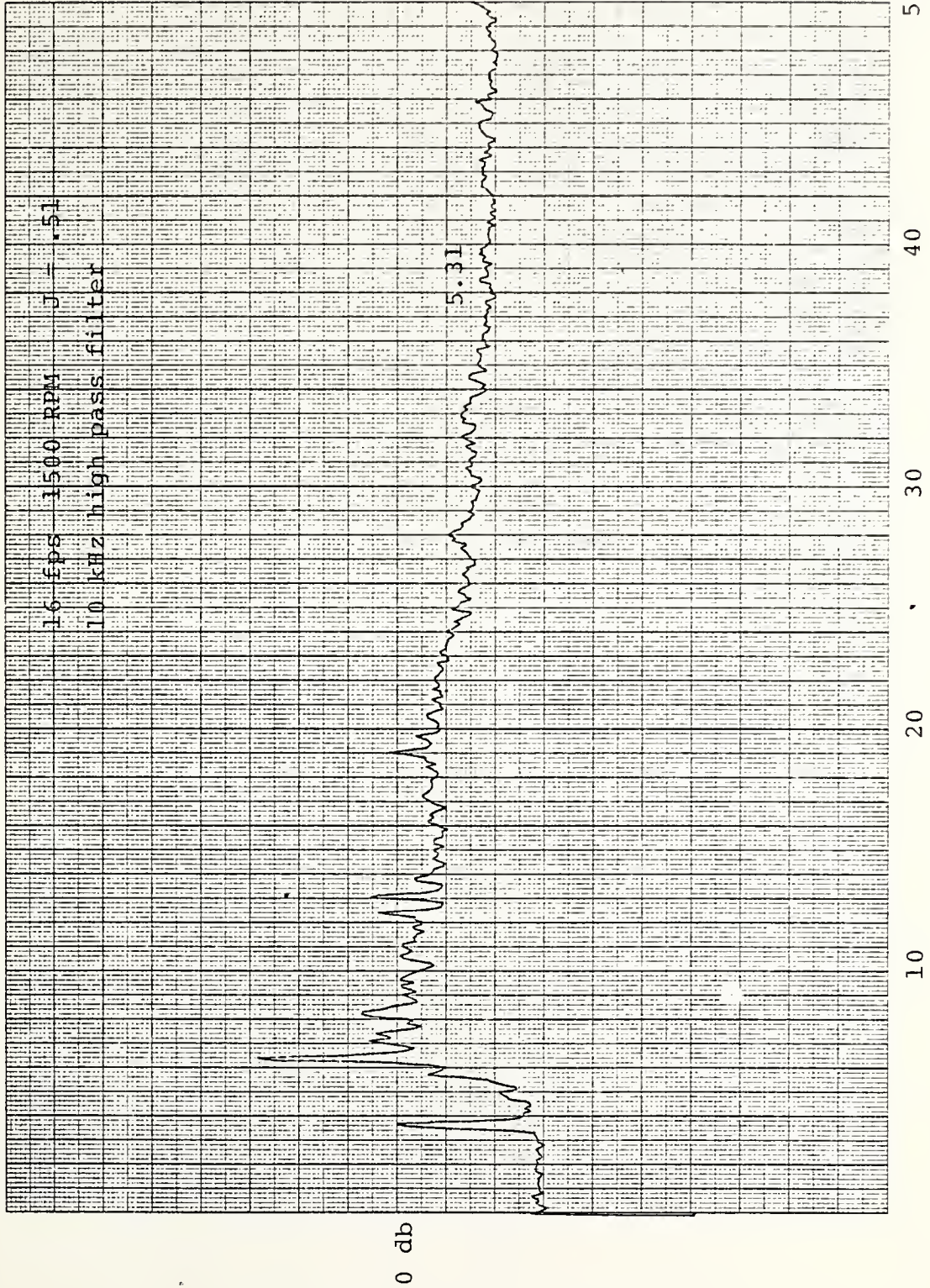
K&E 10 X 10 TO THE CENTIMETER
KEUPPEL & ESSER CO. MADE IN U.S.A.



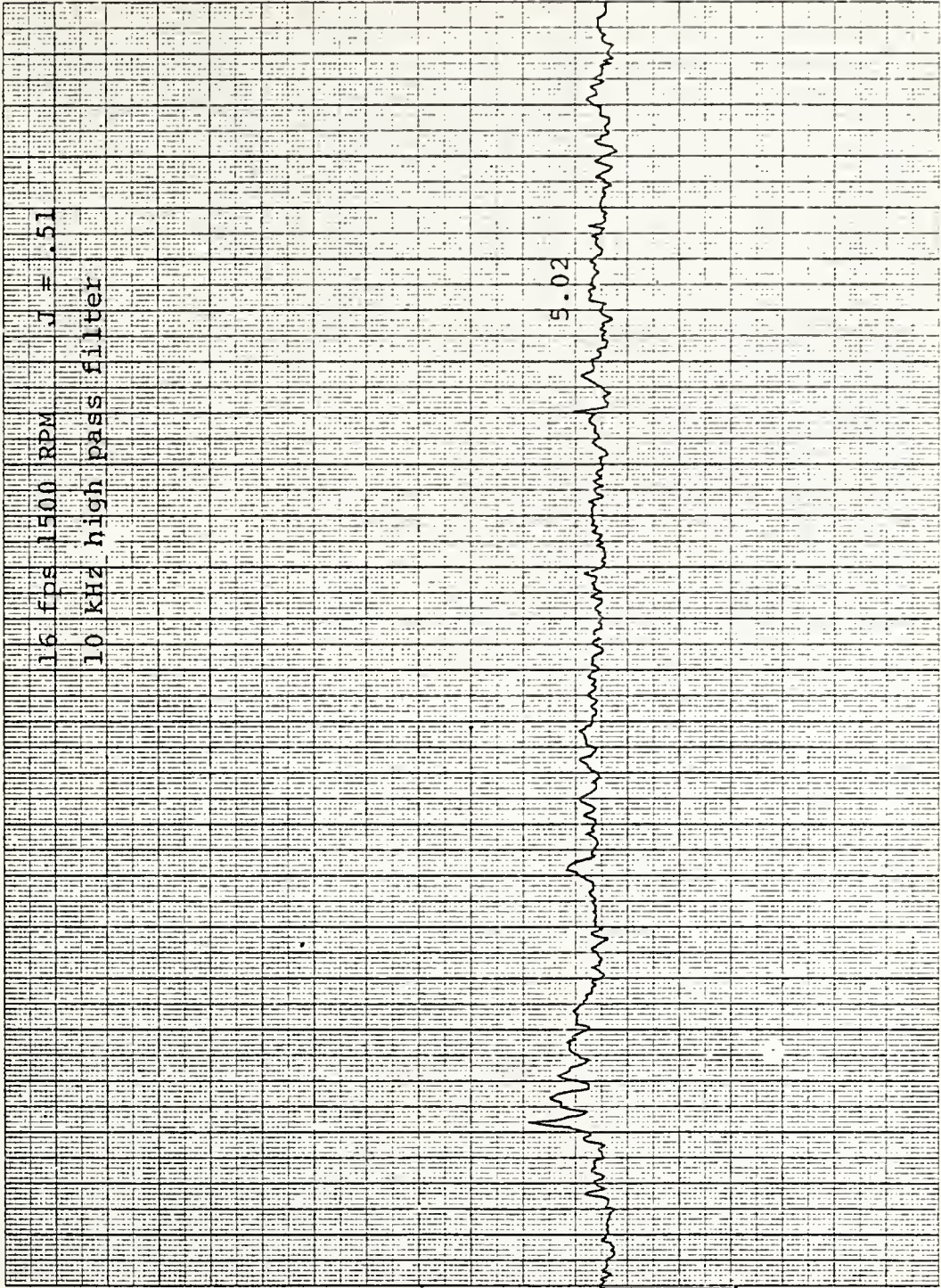








16 fps 1500 RPM J = .51
10 kHz high pass filter



0 db

50 kHz

40

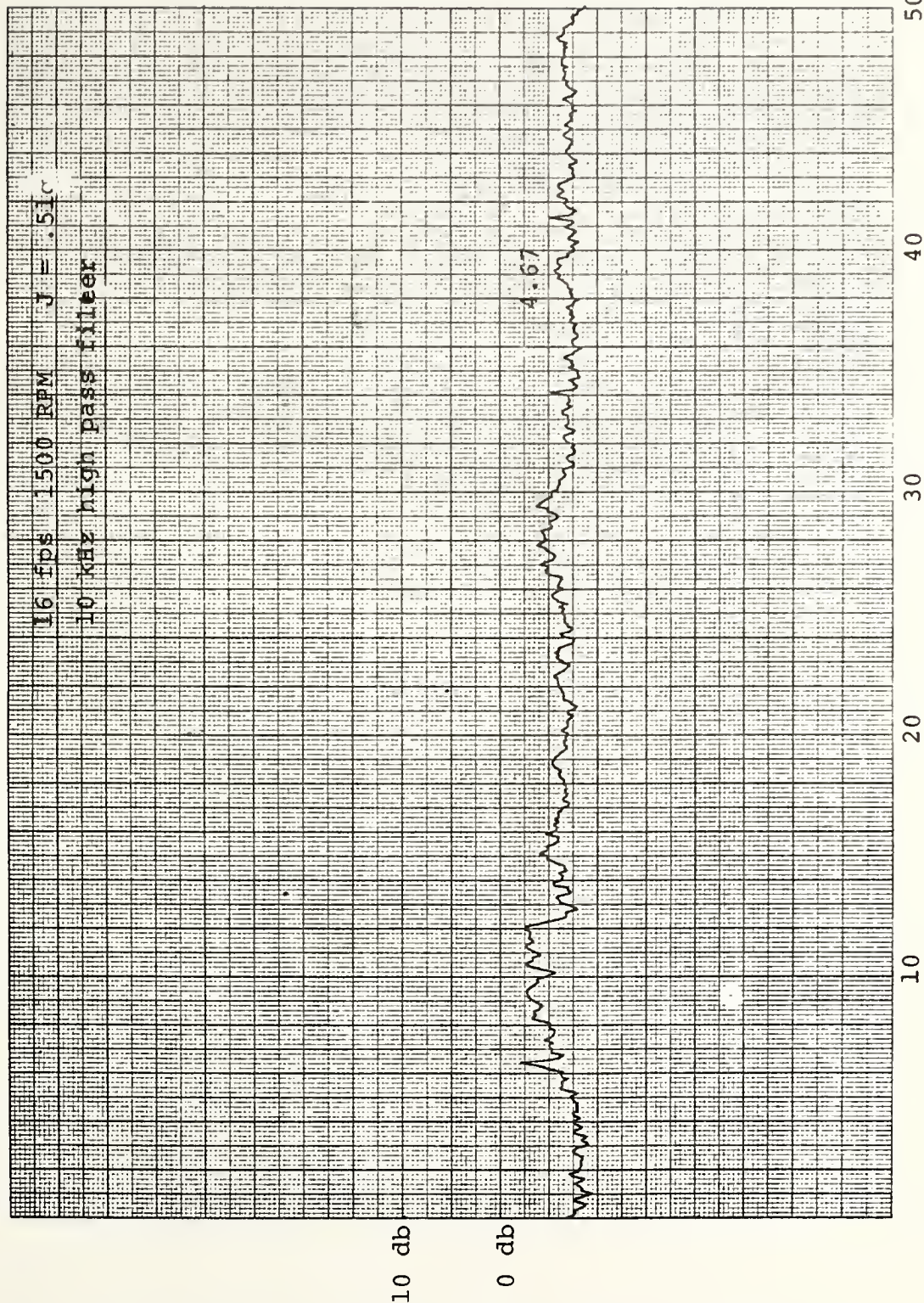
30

20

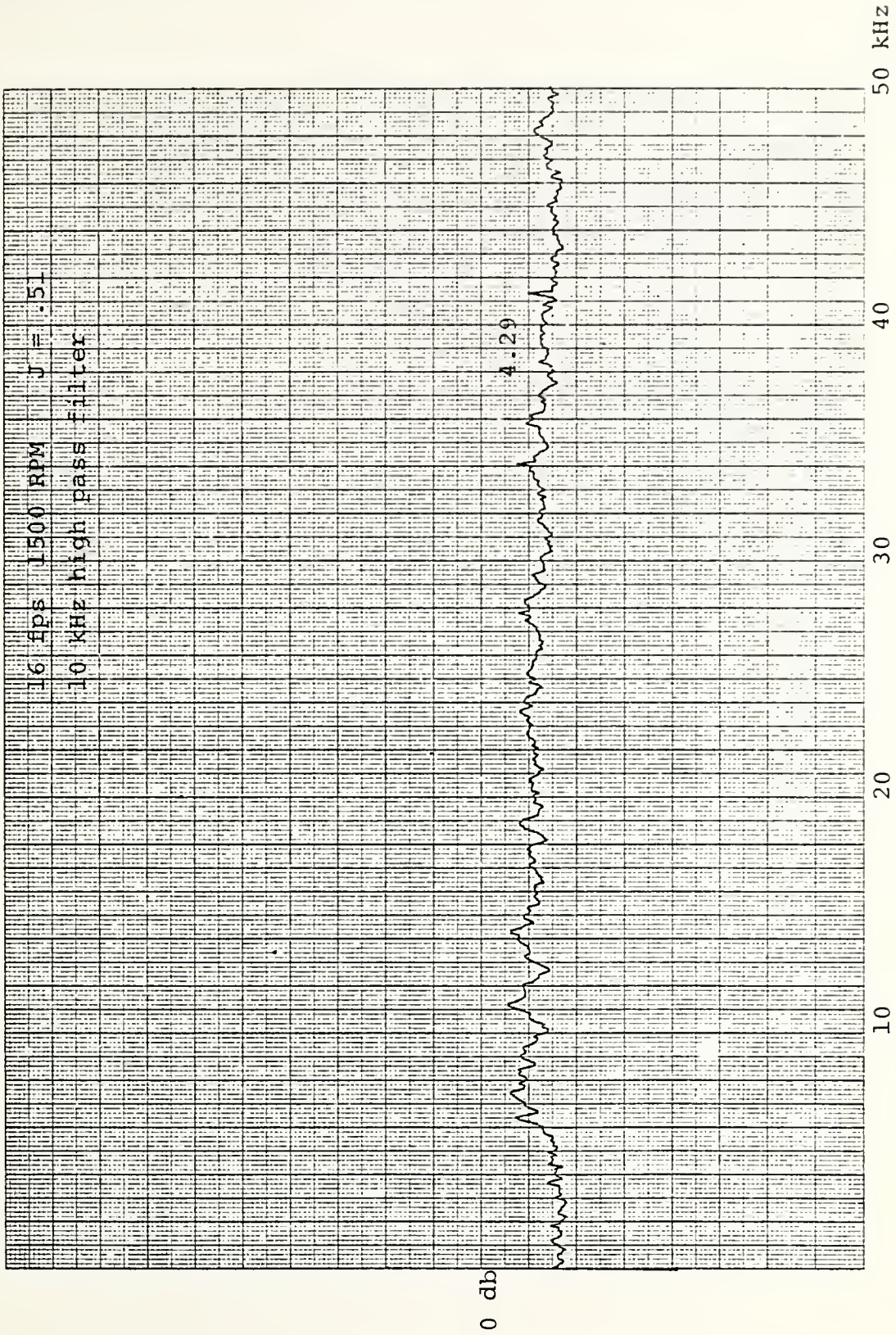
10

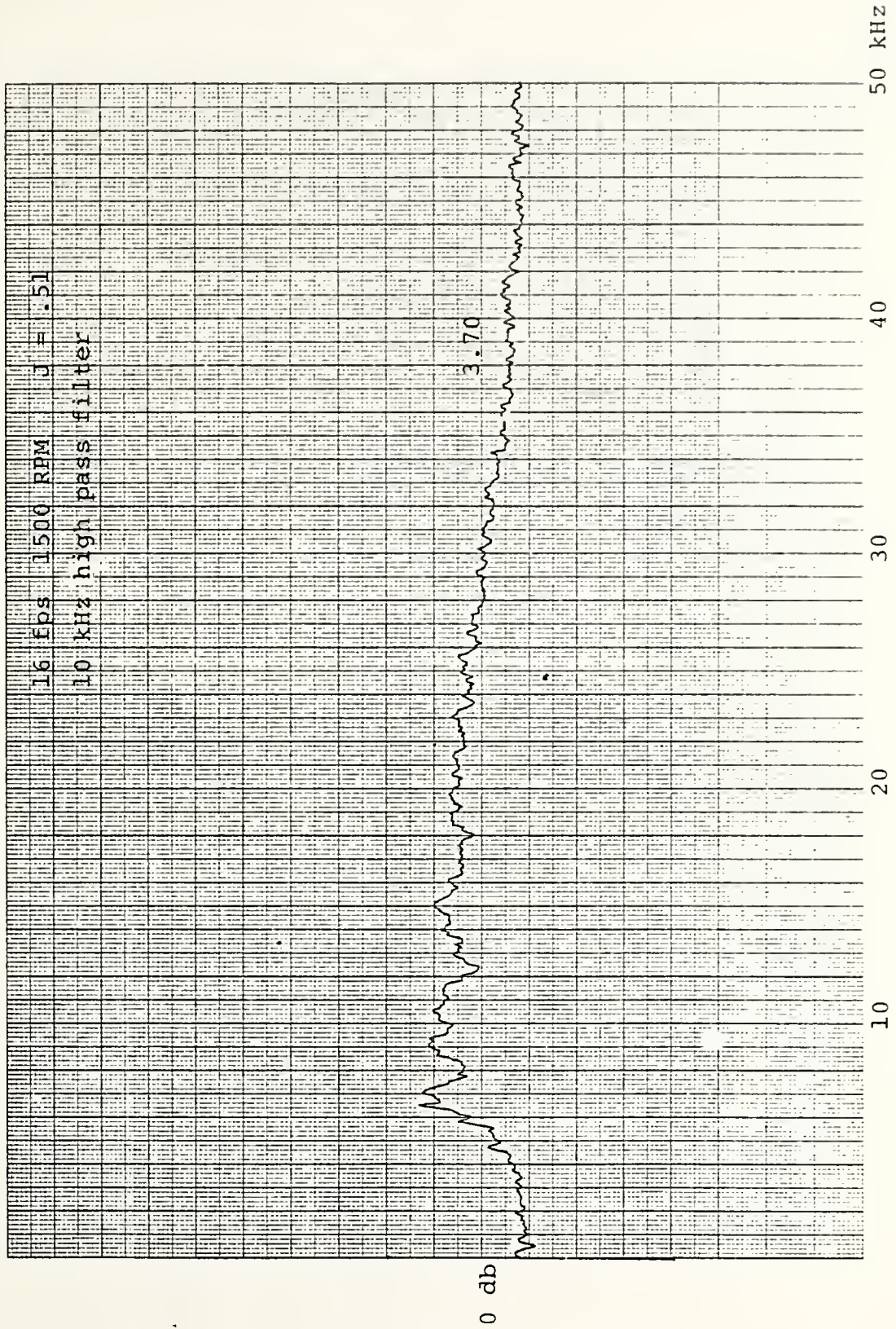
K&E 10 X 10 TO THE CENTIMETER 18 X 25 CM
KEUFFEL & ESSER CO. MADE IN U.S.A.

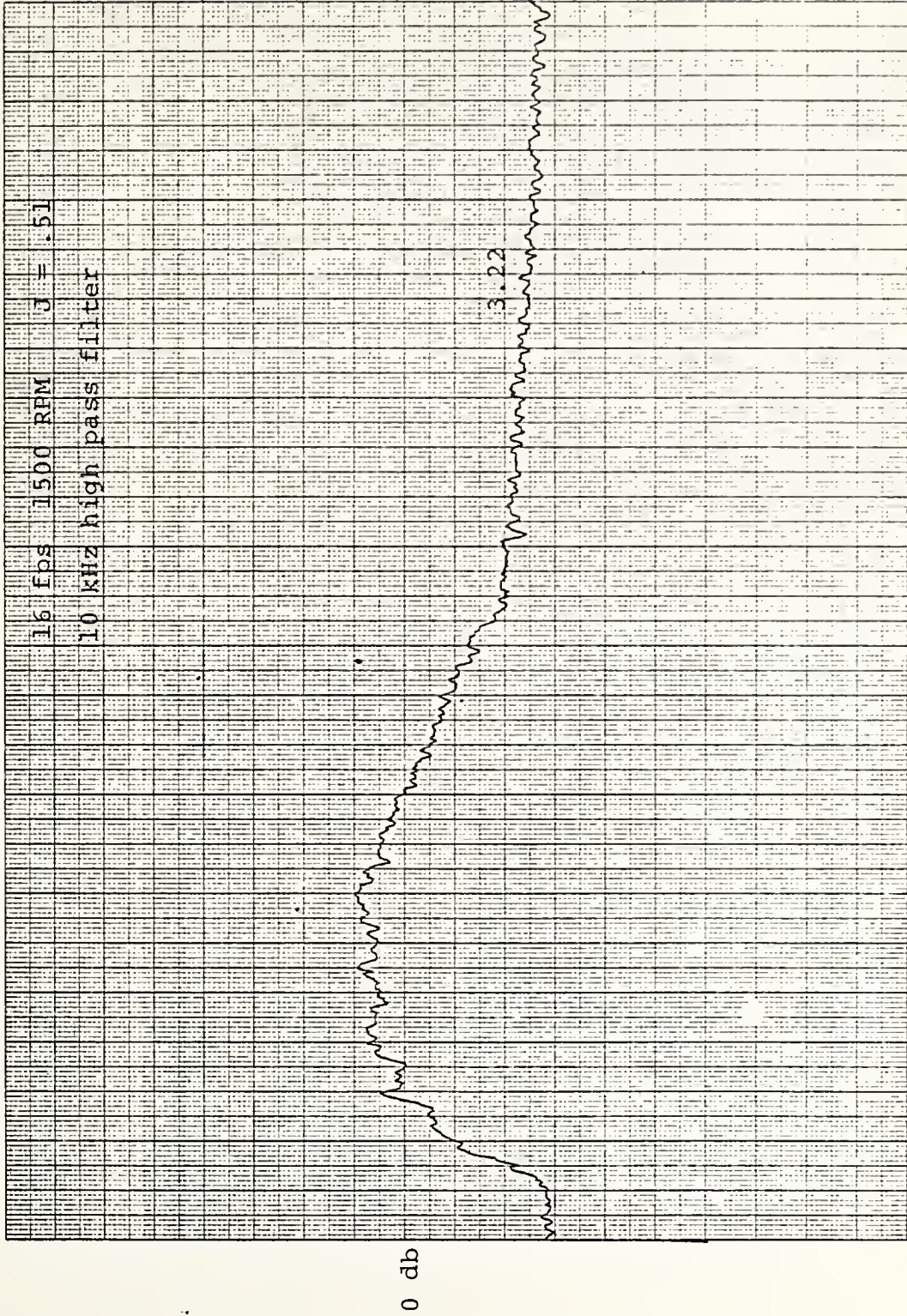
461510



32







Thesis **195541**
P9145 Prestero
c.1

A comparison of
acoustic and visual
determination of cavi-
tation inception on a
model propeller.

Thesis **195541**
P9145 Prestero

c.1 A comparison of
acoustic and visual
determination of cavi-
tation inception on a
model propeller.

thesP9145

A comparison of acoustic and visual dete



3 2768 001 93189 2

DUDLEY KNOX LIBRARY